INFORMATION TO USERS

This manuscript has been reproduced from the microfilm master. UMI films the text directly from the original or copy submitted. Thus, some thesis and dissertation copies are in typewriter face, while others may be from any type of computer printer.

The quality of this reproduction is dependent upon the quality of the copy submitted. Broken or indistinct print, colored or poor quality illustrations and photographs, print bleedthrough, substandard margins, and improper alignment can adversely affect reproduction.

In the unlikely event that the author did not send UMI a complete manuscript and there are missing pages, these will be noted. Also, if unauthorized copyright material had to be removed, a note will indicate the deletion.

Oversize materials (e.g., maps, drawings, charts) are reproduced by sectioning the original, beginning at the upper left-hand corner and continuing from left to right in equal sections with small overlaps.

Photographs included in the original manuscript have been reproduced xerographically in this copy. Higher quality 6" x 9" black and white photographic prints are available for any photographs or illustrations appearing in this copy for an additional charge. Contact UMI directly to order.

Bell & Howell Information and Learning
300 North Zeeb Road, Ann Arbor, MI 48106-1346 USA

UMI®
800-521-0600

INVESTIGATION AND MODELING OF UNSATURATED FLOW THROUGH SWELLING SOILS

Taghi Ebadi

A Thesis in

The School for Building

Civil Engineering Program

Presented in Partial Fulfillment of the Requirements
for the Degree of Doctor of Philosophy at
Concordia University
Montreal, Quebec, Canada

February 1998

ABSTRACT

INVESTIGATION AND MODELING OF UNSATURATED FLOW THROUGH SWELLING SOILS

Taghi Ebadi

Concordia University, 1998

Although the theory of water movement through an unsaturated, swelling soil has been developing for a number of years, the efficiency of the results has been limited, and the developed models have suffered from a lack of a mechanism to reliably define water flow and experimental techniques for measuring the unsaturated soil hydraulic properties. The intent of the present research is to elucidate and to investigate the theory of flow through unsaturated, swelling soil, to develop a three dimensional theoretical model based on a reliable soil swelling and unsaturated flow mechanism and, furthermore, to characterize the relationships between different soil hydraulic and swelling properties. In the first part, based on the water adsorption mechanism by the soil particles and the use of continuum theory principles, a theoretical model of unsaturated flow through swelling soil has been developed. Some new techniques were established to measure the different soil swelling and hydraulic properties and to analyze the effect of the soil's initial conditions. The reliability of the different existing empirical models, to be applied to the results obtained from hydraulics, shrinkage and swelling experiments, were investigated and modified where necessary.

A static neural network model was developed to mathematically characterize the experimental results being used in the proposed numerical solution of the mathematical

model. The neural network model works based on the back-propagation error method with adaptive learning rules by means of the neural network tool box of MATLAB software. A finite difference numerical model, based on a fully implicit method, was proposed to numerically solve the one dimensional governing equation (simplified form of 3D governing equation). For this part of the study, a computer program in C++ language was developed.

Finally, the results of the numerical method were verified using the results obtained from infiltration tests. The tests were conducted for the semi-infinite soil columns having three different confinement conditions: completely confined, semi-confined and free swelling. The results show a clear agreement between the output of the developed numerical model and the experimental data.

As one of the conclusions, the results of the numerical analysis of the developed mathematical model agreed reasonably well with those of the experiments. The study also indicated that the static neural network model, as one of the most promising models, can precisely characterize any experimental function related to the soil properties and cooperates with other numerical approaches such as finite difference method to solve a highly nonlinear partial differential equation such as unsaturated flow equation.

Acknowledgment

I take this opportunity to acknowledge with gratitude the guidance and encouragement provided by my supervisor, Professor H. Poorooshasb. The initial introduction to this problem by Dr. S.C. Cheung is also gratefully acknowledged. I also express my appreciation to Dr. A. Yazdizadeh for his guidances in developing the Static Neural Network Model.

Special thanks to the Ministry of Culture and Higher Education of Islamic Republic of IRAN for providing the financial support of the work.

The computing facilities and experimental equipments provided at the Civil Engineering Program of School for Building Department at Concordia University have been very useful in conducting my research.

Finally, my deepest gratitude and greatest appreciation go to my wife Zohre, my daughter Reyhaneh and my sons Amir and Iman for their utmost patience, endurance and understanding during my research.

DEDICATION

I would like to dedicate this thesis to my family, especially my wife, for their patience, support, understanding, and love.

TABLE OF CONTENTS

LIST OF FIGURES

LIST OF TABLES

LIST OF SYMBOLS

$\vec{q_s}$:	:	Solid Phase Flux Vector with Respect to the Spatial Coordinate
∇	:	Gradient Operator
φ:	:	an Arbitrary Scalar Function.
$\widehat{\nabla R}$	:	Gradient Deformation Matrix
ρ_{bt}	:	Soil Bulk Density
ρ_{bt}	:	Soil Bulk Density at Time t
ϑ_w	:	Soil Moisture Ratio
θ_w	:	Soil Water Content
ϑ_a	:	Adsorbed Water by Soil Particle Surface in Terms of Soil Moisture Ratio
ϑ_d	:	Mobile or Darcian Water in Soil Pores in Terms of Soil Moisture Ratio
β	:	Water Adsorbtion Coefficient in Terms of Soil Moisture Ratio
$\hat{q}_w$	:	Water Flux Vector
$\overrightarrow{q_{wR}}$	:	Water Flux Vector Relative to the Soil Particle Movement
$\vec{q_s}$	:	Soil Particle Flux Vector
$\overrightarrow{\nabla_R}$	:	Gradient Operator with Respect to the Material Coordinate
K_w	:	Unsaturated Hydraulic Permeability
Z_R	:	One Dimentional Material Coordinate (Gravitational water Potential)
K_s	:	Soil Particle Permeability (LT-1)
Ω	:	Resisting and Driving Forces Responsible for Swelling Potential

ψ	:	Soil Water Matrix Potential (Soil Suction)
P_s	:	Swelling Pressure
P_O	:	Surface Overload Pressure
ρ_t	:	Apparent Wet Soil Bulk Density
ρ_w	:	Water Density
D_s	:	Soil Particle Diffusivity Function
D_w	:	Soil Water Diffusivity Function
g	:	Gravitational Acceleration
ϑ_o	:	Soil Initial Condition in Terms of Soil Moisture Ratio
ϑ_n	:	Upper Soil Boundary Condition in Terms of Soil Moisture Ratio
t	:	Time
q_t	:	Total Water Flux
e	:	Void Ratio
m	:	Material Coordinate
D_m	:	Material Diffusivity Function
S	:	Degree of Saturation (%)
Z,z	:	Cartezian Coordinate
Ω_w	:	Water Potential Related to the Swelling Potential
θ_g	:	Gravitational Water Content
σ	:	Clay Content
K_{sat}	:	Saturated Hydraulic Conductivity
Q	:	Comulative Water Outflow
A	:	Soil Sample Section Area
L	:	Sample Length

θ_r : volumetric water content at retention point

θ_s : volumetric water content at maximum saturation

α, n, m : fitting parameters for van Genuchten model

S_e : normalized volumetric water content

λ : soil pore size distribution index

u_s : soil particle velocity

H_i : total soil water head at the soil-membrane interface in PPT apparatus

H_b : constant total water head at the bottom of the membrane in PPT apparatus

K_P : saturated hydraulic conductivity of the membrane in PPT apparatus

d : thickness of the membrane in PPT apparatus

ω : gravimetric water content

CHAPTER

1
Introduction

1.1. Introduction

The flow of water through unsaturated soil is one of the most important phenomena in soil behavior. Since the physical properties of soils, particularly clays, depend in a large degree on the amount and energy state of the water inside the soil, great attention has been focused on this phenomenon.

Many problems in civil and geo-environmental engineering as well as in agricultural science are related to the hydraulic property changes of soil due to unsaturated flow. Retaining structures, earth dams, highways, subsurface foundations, slope stability, water infiltration, migration of the pollutant through the vadose zone and water uptakes by the plant roots are some typical subjects in geotechnical, environmental and agricultural engineering involving this phenomenon.

Many attempts have been made to introduce the unsaturated flow in both swelling and non-swelling soils, through the development of the theoretical models and of the experimental techniques. So far, the studies have been mainly concerned with the rigid soil structure (i.e., no motion of the soil particles) and many mathematical models predicting

the hydraulic characteristics and water movement have been established. In addition to this, the experimental methods in both field and laboratory concerning non-swelling soils have been largely improved. Unlike non-swelling soils, however, the swelling soils exhibit additional complexities in the flow regime. Consequently, considerable differences between swelling and non-swelling soils are observed, and in spite of these efforts, there is little conclusive information on the effects of unsaturated flow on the physical and hydraulic properties of the swelling soils.

In the present study an attempt has been made to elucidate and investigate the theory of unsaturated flow through swelling soils and to study the different hydraulic and swelling characteristics of such soils.

1.2. Statement of the Problem

The major problem arising from the flow of the water through the unsaturated swelling soils is related to changes in the soil structure volume. In partially saturated swelling soils, when water is added, the gradients of the mechanical forces thereby produced and the hydrostatic pressure acting on the water in the soil, together with the swelling pressure, exert considerable control on the flow of water. This process would create some difficulties in mathematical modeling and particularly in experimental measurements of hydraulic parameters of the soil.

There are two types of unsaturated flow in swelling soil which may be classified according to the changes in the overall soil porosity and may depend on whether the boundaries of the soil specimen are confined or not. The conditions between these two lim-

its may be categorized as semi-confined, depending on the overload pressure.

After or during a construction process, a non-uniform distribution of swelling pressure is exerted on the structure due either to the moisture accumulation between the structure and soil surface or meteorological reasons which both change the moisture profile in depth as the time progresses. An accurate formulated model of the moisture distribution through the time and space, which is able to include as much as effective soil hydraulic and swelling properties, can help the construction engineers to better predict the effects of the consequences on the performance of the system.

A second problem is concerned with irrigation and root growth in agricultural engineering. The soil with a respectively high percentage of clay particles on the surface may, in some instances, be desirable (higher residual water and low permeability), but may also influence its capability for holding water (a most important factor in synchronizing irrigation time). In such a soil, the variation of soil moisture within a given depth and through a certain span of time can significantly change the soil volume, particularly in the top layer. Therefore, the moisture profile and the hydraulic properties of the soil must be determined to minimize the irrigation time and to increase the engineers' knowledge of soil water retention.

From geo-environmental point of view, a problem arises when the swelling soil is subjected to the infiltration of contaminated water. A second problem would be the flow of contaminated water from a disposal site (e.g. landfills) or from deeply buried radioactive materials, in which the swelling soils are used as the sealing layer. If the surface layer has a highly swelling potential, the upward flow due to swelling exceeds the downward flow due

to gravity (Smiles, 1976). Therefore; polluted water does not properly infiltrate and creates an undesirable environmental impact on the soil surface. In the aforementioned cases, there is a need for an effective predicting model to properly evaluate the soil moisture profile and hydraulic properties of the swelling soils. The model must be applicable for both the free swelling (surface layer) and completely confined (underground seal layer) conditions.

1.3. Objectives

Specifically the following tasks were performed in the present study:

1) Identifying the mechanism of unsaturated flow through swelling soil and introducing the essential differences between the flow regime through swelling and non-swelling soils.

2) Development of a new three dimensional governing mathematical expression for moisture profile in the soil, based on the defined mechanism and simplifying the governing equation in one direction (vertical), to express the unsaturated flow through swelling soil.

3) Introducing new methodology for measuring the hydraulic and swelling properties of soil (water retention, saturated and unsaturated permeability, swelling pressure, shrinkage characteristic, particle permeability and water adsorption coefficient)

4) Establishing the empirical equations for some of the measured hydraulic and swelling properties of the soil.

5) Using the neural network method, to estimate the different hydraulic and swelling parameters of the soil, to be used in the numerical analysis of the governing equation with different initial conditions.

6) Developing a finite difference numerical method and writing the corresponding computer code in C++ language to solve the governing equation numerically.

7) Designing an apparatus to identify the water profile and bulk density of the soil column by means of the slice method, in order to verify the results of the numerical method in three different conditions: completely confined, semi-confined and free swelling.

1.4. Literature Review

Over the years, a lot of work has been done towards the development of mathematical and numerical modeling for describing the unsaturated flow through the soil. These efforts may be categorized in two major groups: one is related to the studies already done on the unsaturated flow through the non-swelling soils with no soil expansion during the flow, and the other considers the mechanism of the unsaturated flow through swelling soil.

In the following, a brief account of these studies is presented, discussing the capabilities of the various models in expressing the mechanism of unsaturated flow through non-swelling and swelling soils.

1.4.1. Water Flow through Non-Swelling Soils

Slichter (1898) used Darcy's equation (1856) in conjunction with the concept of mass balance in porous media to describe the saturated flow. The balance in vertical direction was presented by:

$$\frac{\partial q_w}{\partial z} = \frac{\partial \theta}{\partial t} \qquad \text{Eq. 1.1}$$

where q_w is the volumetric flux of the water in the vertical direction, θ is the volumetric water content, t is the time, and z is the vertical direction of cartesian coordinate. Bucking-

ham (1907) modified the Darcy equation, (valid only for saturated conditions) and established an equation for the flow through unsaturated soils. Buckingham made two important modifications to Darcy's equation: first assuming that the soil hydraulic conductivity is a function of water content ($k_w = k(\theta)$) and secondly he described the total soil water potential as:

$$\Phi = z - \psi \qquad \text{Eq. 1.2}$$

where ψ represents matrix suction and is a function of the soil water content. Considering these modifications, the simple form of the unsaturated flow equation for a non-deformable soil was written as:

$$q = k(\theta)\frac{\partial \psi}{\partial z} - k(\theta) \qquad \text{Eq. 1.3}$$

By assuming:

$$\frac{\partial \psi}{\partial z} = \frac{d\psi \partial \theta}{d\theta \partial z} \qquad \text{Eq. 1.4}$$

and substituting in Eq. 1.3:

$$q = k(\theta)\frac{d\psi \partial \theta}{d\theta \partial z} - k(\theta) \qquad \text{Eq. 1.5}$$

defining soil-water diffusity function as:

$$D(\theta) = k(\theta)\left[\frac{d\psi}{d\theta}\right] \qquad \text{Eq. 1.6}$$

and substituting this into Eq. 1.5 yields:

$$q = -D(\theta)\frac{\partial \theta}{\partial z} - k(\theta) \qquad \text{Eq. 1.7}$$

equation Eq. 1.7 is known as the Buckingham-Darcy equation.

Richards (1931) presented the governing partial differential equation of unsatur-

ated flow problem by use of the mass balance principle. Substituting Eq.1.7 into Eq. 1.1 results in:

$$\frac{\partial}{\partial z}\left[D(\theta)\frac{\partial \theta}{\partial z}\right]+\frac{\partial k}{\partial z}=\frac{\partial \theta}{\partial t} \qquad \text{Eq. 1.8}$$

Childs (1936) studied this equation, assuming the diffusity constant, but this approach did not agree well with the experimental results. Philip (1957) modified equation Eq. 1.8. This modification shows infiltration into a homogenous semi-infinite porous medium with the constant initial moisture content, θ_o, at z=0 (surface) and the initial water content, θ_n, for $z \geq 0$. Thus Eq. 1.8 becomes:

$$\frac{\partial \theta}{\partial t}=\frac{\partial}{\partial z}\left(D\frac{\partial \theta}{\partial z}\right)-\frac{\partial k}{\partial z} \qquad \text{Eq. 1.9}$$

This equation is known as a basic model for the infiltration process through a vertical soil column. Further attempts deal mainly with the use and verification of the Philip model in different conditions and different soil types. (Groenevelt and Bolt,1974; Touma et al.,1986; Feddes et al.,1988; Warrick et. al.,1993; Ross and Paralange, 1994). The development of the constitutive relationships (i.e., unsaturated hydraulic conductivity and moisture retention curve) have become the most important part of these studies in unsaturated flow through non-swelling soils. Some studies attempted to establish the rationality of these relationships theoretically (Van Genuchten, 1980; Ross et. al.,1993; Rossic et. al.,1994; Ross,1994), and others expressed them experimentally (Wosten et. al. 1988; Warrick,1993; Tamari, 1993; Van Dam et. al., 1994; Salehzadeh, 1994).

It seems that the mechanism of unsaturated flow through non-swelling soils has been well studied and the proposed models describe this mechanism satisfactorily. How-

ever, further studies are required to establish more accurate constitutive equations for the flow parameters in the different soils.

1.4.2. Water Flow through Swelling Soils

The efforts mentioned above were concerned with the modeling of water flow through the stable porous medium (non-swelling soils). The studies on the behavior of swelling soils began with the investigation of the influences of moisture content on the soil bulk density (Haines 1923, Lauritzen and Stewart 1941, Fox 1964; Snethen, 1981).The study of flow effects on the behavior of swelling soils was initiated by Zaslavsky (1964). He introduced the notion of "relative velocity of water flow" and argued that Darcy's equation and hydraulic permeability are meaningless unless the flux of water, q, is measured relative to the movement of soil particles. According to this argument, and considering an elementary box in a fixed coordinate system, he introduced the total flux of water as a summation of the specific flux q and the flux related to the soil particle movement, $q_s \cdot \theta$:

$$q_t = q + q_s \cdot \theta \qquad \text{Eq. 1.10}$$

where q_t is the total water flux and q_s is the velocity of the soil particles. He derived the general differential equation in the vertical direction for saturated and unsaturated soil as follows:

$$\frac{\partial}{\partial Z}\left[k(\theta)\cdot\left(-\frac{\partial \psi}{\partial Z}\right)\right] + \frac{\partial k}{\partial Z} = \frac{\partial \theta}{\partial t} + \frac{\theta}{1-n}\frac{\partial n}{\partial t} + q_s\frac{\partial \theta}{\partial Z} \qquad \text{Eq. 1.11}$$

For the specific case of saturated swelling soil, Eq. 1.11 becomes:

$$\nabla\bullet[k(e)\nabla\Phi] = \frac{1}{1+e}\left[\frac{\partial e}{\partial t} + q_s \cdot \nabla ln(1+e)\right] \qquad \text{Eq. 1.12}$$

where e is the void ratio and n is soil porosity. The last two components of the right side of Eq 1.11 show the movement of the particles, which would not be present in the case of non-expansive soil. Since in this equation the fixed cartesian coordinate was used, it is more difficult to define the boundary condition and establish the unsaturated hydraulic conductivity relationship. Consequently, there might be no practical solution to Eq. 1.11, unless we assume a very simple and unrealistic boundary condition. Smiles and Rosenthal (1968) assumed a one dimensional infiltration of water through a vertical saturated sample and free to swell only in the flow direction. Instead of fixed coordinates, they defined the material coordinate, m, as follows:

$$\frac{\partial m}{\partial z} = (1+e)^{-1} \qquad \text{Eq. 1.13}$$

the most important feature of choosing such a coordinate was that the mass balance equation for saturated flow becomes:

$$\frac{\partial e}{\partial t} = -\frac{\partial q}{\partial m} \qquad \text{Eq. 1.14}$$

Also they assumed that the potential gradient component of the gravity can be negligible; therefore, the term dk/dz in the governing equation is ignored. Finally they derived the equation:

$$\frac{\partial e}{\partial t} = \frac{\partial}{\partial m}\left[\frac{k}{1+e}\left(-\frac{\partial \psi}{\partial e}\frac{\partial e}{\partial m}\right)\right] \qquad \text{Eq. 1.15}$$

In simplifying this equation, they assumed the diffusity coefficient as follows:

$$D_m = \frac{k}{1+e}\left(-\frac{\partial \psi}{\partial e}\right) \qquad \text{Eq. 1.16}$$

and derived the following equation:

$$\frac{\partial e}{\partial t} = \frac{\partial}{\partial m}\left(D_m \frac{\partial e}{\partial m}\right) \qquad \text{Eq. 1.17}$$

Comparing Eq. 1.9 with the gravity term ignored and Eq. 1.17 shows that the z and D of an unsaturated non-swelling soil are respectively comparable with the m and D_m for the saturated unstable soil. Since the dependent variable employed in Eq. 1.17 cannot express the saturation conditions ($0 < S < 1$), this model may only be applied to the saturated condition of swelling soils.

Philip (1968) offered a formulation for theoretical treatment of the one dimensional saturated solution of flow through swelling clay-colloid pastes. He proceeded with his analysis in terms of the normal cartesian space coordinate Z and volumetric water content rather than material coordinate m and void ratio e. The following governing differential equation is the result of his work:

$$\frac{\partial \theta}{\partial t} = \frac{\partial}{\partial Z}\left[(1-\theta)D\frac{\partial \theta}{\partial Z}\right] + \left(D\frac{\partial \theta}{\partial Z}\right)\Big|_{Z=0}\frac{\partial \theta}{\partial z} \qquad \text{Eq. 1.18}$$

where $-D\frac{\partial \theta}{\partial Z}\Big|_{Z=0}$ is the rate of volume change of the soil column, called "drift velocity". The definition of the boundary condition with respect to a fixed co-ordinate for this equation is very difficult, and as a consequence, finding a practical solution to the equation is also difficult.

At the same time, Raats and Klute (1968a,1968b,1969) developed the application of continuum mechanics to the motion of a fluid in the soil. From the macroscopic point of view, they proceeded with the kinematics and mass balance of emulative flow. They pointed out that each phase can be assumed to be a non-rigid phase but the solid phase is

regarded as a reference coordinate. At the end of the first paper they came out with a very general mass balance equation of a multiphase system as follows:

$$\rho^s \cdot \left.\frac{\partial\left(\frac{\theta^\alpha}{\rho^s}\right)}{\partial t}\right|_{\bar{R}_s} = -\left(\frac{\partial \bar{R}_s}{\partial \bar{r}}\right)\frac{\partial}{\partial \bar{R}_s}\{\theta_a(\bar{v}_a - \bar{v}_s)\} \qquad \text{Eq. 1.19}$$

where ρ^s is the mass of the solid phase per unit bulk volume, θ^α is the volume of the aqueous phase, t is the time, v_a is the velocity vector for the aqueous phase, v_s is the velocity vector for the solid phase, $\bar{R}_s$ is the position vector of the material particles, i.e., the material coordinate of the solid phase, and $\bar{r}$ is the position vector in a rectangular cartesian coordinate, i.e., the spatial coordinate of the solid phase. In the case of a one-dimensional flow, the governing differential equation concluded from Eq. 1.19 in diffusity form becomes:

$$\left.\frac{\partial\left(\frac{\theta}{\rho^d}\right)}{\partial t}\right|_{R_1} = \frac{\partial}{\partial R_1}\left[D\left(\frac{\theta}{\rho^d}\right)\cdot\frac{\partial\left(\frac{\theta}{\rho^d}\right)}{\partial R_1}\right] \qquad \text{Eq. 1.20}$$

where R_1 presents the material coordinate in the flow direction (horizontal). The diffusity function is given as:

$$D\left[\frac{\theta}{\rho^d}\right] = k\cdot\frac{1}{\rho_\circ^d}\cdot\frac{\rho^d}{\rho_\circ^d}\cdot\frac{d\psi}{d\left(\frac{\theta}{\rho^d}\right)} \qquad \text{Eq. 1.21}$$

where $\rho_\circ^d$ is the bulk density in the reference configuration at time $t_\circ$ which is independent of position, i.e., initially a uniform solid phase. The model does not directly include the effect of the swelling and shrinkage behavior of the soil on the unsaturated water flow.

Philip and Smiles (1969) assumed that, in a soil subjected to the water movement and one dimensional volume change, water potential, hydraulic conductivity and void ratio are unique functions of the volumetric water content during a particular wetting or drying process. Using this assumption, they developed an analysis in terms of the material coordinate slightly different from equation 1.13 in the form:

$$m = \int_{-\infty}^{Z} (1+e)^{-1} dZ \qquad \text{Eq. 1.22}$$

where Z is the positive downward space coordinate and is equal to zero at the soil surface. The mass balance equation is given as:

$$\frac{\partial}{\partial t}[(1+e)\theta] = \frac{\partial q}{\partial m} \qquad \text{Eq. 1.23}$$

Also, relative to the soil particles, Darcy's equation was used to express the flux of water, q, and for simplicity, the gravity term was ignored. Through these assumptions, they arrived at the following governing equation:

$$\frac{\partial}{\partial t}[(1+e)\theta] = \frac{\partial}{\partial m}\left[\frac{k}{1+e}\cdot\left(\frac{\partial \psi}{\partial m}\right)\right] \qquad \text{Eq. 1.24}$$

using the assumption that e is a function of θ, together with the use of Eq. 1.16 as a definition for diffusity function, D_m, they ended with the equation:

$$\left(1+e+\theta\frac{de}{d\theta}\right)\frac{\partial \theta}{\partial t} = \frac{\partial}{\partial m}\left(D_m \frac{\partial \theta}{\partial m}\right) \qquad \text{Eq. 1.25}$$

This expression for the flow through unsaturated, swelling soil is similar to that of Smiles and Rosenthal (1968) expressed by Eq. 1.17 and of Philip (1968) Eq. 1.20, except for the additional component on the left hand side of Eq. 1.25, which shows θ as the dependent

coefficient of the time derivative and replaces e with θ as the dependent variable.

Smiles (1974) reported that the statics and kinetics of water interaction with swelling soil particles are supported by little experimental information. Therefore, he decided to examine some aspects of the infiltration process into a saturated, swelling soil. He used the material coordinate m (expressed by Eq. 1.13), defined the moisture ratio ϑ as a dependent variable, and also considered an extra term in the total potential of the water, Ω_w, as follows:

$$\Phi = \psi + Z + \Omega_w \qquad \text{Eq. 1.26}$$

He explained that Ω_w arises because of the forces (i.e., the weight of the column plus any surface load) resisting the local one-dimensional increase in bulk volume following an increase in moisture ratio. The results were summarized by the following governing equation:

$$\frac{\partial \vartheta}{\partial t} = \frac{\partial}{\partial m}\left[D\frac{\partial \vartheta}{\partial m}\right] - \frac{\partial}{\partial m}[(1-\gamma)k] \qquad \text{Eq. 1.27}$$

where ϑ is the moisture ratio expressed by $\vartheta = \frac{volume\ of\ the\ water}{volume\ of\ the\ solid}$, γ is the wet specific gravity and D is denoted by the Eq. 1.16. The second term on the right hand side of Eq.1.27 states that in non-rigid soil, the term $\partial(\gamma \cdot k)/\partial m$ would reduce the effect of gravity in comparison with the rigid soil.

For the first time, Nofziger and Swarzendruber (1976) undertook the experimental verification of the theory of water infiltration into the unsaturated, swelling soil. Whereas

in the Smiles and Rosenthal (1968) and Smiles (1974) experiments, in which the soil parameters were measured destructively, they used the non-destructive gamma-ray attenuation method to obtain the results for water adsorption. Measurement of both water content, θ, and bulk density, ρ, were obtained with accuracy of one millimeter of soil column length. The samples was totally confined and was initially dry. They defined the material coordinate as:

$$m = \rho_s^{-1} \int_0^I \rho(u, t) du \qquad \text{Eq. 1.28}$$

where Z is the positive downward depth, $\rho(u, t)$ is the bulk density of the medium at position u and time t, and u is a dummy variable for integration.

They also considered the volumetric water ratio ϑ as the dependent variable. Finally they chose water saturation, or fractional saturation S:

$$S = \theta/\rho = \theta \cdot \rho_s/(\rho_s - \rho) \qquad \text{Eq. 1.29}$$

as the dependent variable and obtained a unique curve.

Sposito et. al.(1976) used the mass balance equations for the water and soil separately and a definition for Darcian flux (the same as Zaslavsky,1964) to derive the three dimensional flow equation as follows:

$$\left(\frac{\partial \theta_g}{\partial t}\right)_R = \frac{\rho_w}{\rho_b}(\nabla R \cdot \vec{\nabla}_R) \cdot (K_R \cdot \vec{\nabla}_R(\varphi_w)) \qquad \text{Eq. 1.30}$$

where θ_g is the gravitational water content, ∇R is the deformation second order tensor, $\vec{\nabla}_R$ is the lagrangian gradient vector, and φ_w is the water potential. This result is almost

the same as that of Raat and Klute(1969) and the swelling and shrinkage characteristics of the soil are not directly considered as important parameters. Nakava et al. (1986) defined the soil flux as:

$$q_s = K_s \frac{\partial \psi_s}{\partial Z} \qquad \text{Eq. 1.31}$$

where ψ_s was identified as a force responsible for the solid movement. Similar to the water diffusity, they introduced the material diffusity as:

$$D_s = K_s \cdot \frac{d\psi_s}{d\sigma} \qquad \text{Eq. 1.32}$$

where σ is the clay content.They established a formula for relative unsaturated hydraulic permeability of the soil which alone cannot explain the behavior of swelling soils under the unsaturated flow.

According to Young (1991), there is a need for the theory of soil water movement in general, and the infiltration theory in particular, to be extended to take into consideration complicating factors such as swelling and shrinkage of the soil. It should be mentioned that in the modeling of unsaturated flow through swelling soils, the parameters must be easily obtainable through experiment. Besides, the model should be based on a correct definition of the mechanism of unsaturated flow through swelling soils.

1.4.3. Summary

According to the literature review, most of the research has been done to develop models and techniques to investigate the unsaturated flow through non-swelling soils. There are not adequate studies to express clearly the mechanism of unsaturated flow

through swelling soils. Furthermore, experimental techniques are not sufficiently developed to measure the different parameters involved in the swelling phenomenon.

Consequently, it is obvious through the above discussions that there is a need, firstly, to develop a mathematical model to identify the mechanism of unsaturated flow through swelling soils, secondly, to improve or establish the techniques for measuring the flow parameters to be used in the model or for model verification. The present study attempts to achieve this goals.

CHAPTER

2
Theoretical Formulation

In the following chapter, based on some assumptions expressing the mechanism of water adsorption by soil particles due to unsaturated flow, a three dimensional mathematical expression will be developed. The model includes different soil hydraulic properties and swelling characteristics. Afterward, the model will be simplified to a one dimensional problem to be numerically solved and experimentally verified. Prior to the derivation of the model, some essentially important concepts are discussed.

2.1. Material Coordinate

The material coordinate must be used in the theoretical modeling of unsaturated flow through a deformable porous medium (e.g.Smiles et al. 1968, Philip 1970,Smiles 1974, Sposito et al. 1976, Giraldez et al 1985, Giraldez 1976,Raat and Klute 1969). In the Buckingham-Darcy flux equation, the flux of water is measured with respect to the solid part of the porous media. When the soil is rigid, the cartesian coordinate is used, because the soil particles (solid phase) do not move. Whereas, in the swelling soils, the soil particles move as the water flows through the pores. Therefore the Buckingham-Darcy equation

is no longer capable of estimating the water flux. Thus, some modifications are required and the coordinate system must be properly chosen so that the Buckingham-Darcy equation can be employed. Besides, it is more convenient to fix the boundary conditions with respect to the chosen coordinate. For these reasons, the moving coordinate, called the material coordinate, is used in the theoretical modeling of unsaturated flow through swelling soils. According to Raat and Klute(1968a) the general rate transformation operation can be expressed as:

$$\left(\frac{\partial \varphi}{\partial t}\right)_R = \frac{\partial \varphi}{\partial t} + \vec{q}_s \cdot \overrightarrow{\nabla \varphi} \qquad \text{Eq. 2.1}$$

where:

φ is an arbitrary scalar function.

$\left(\frac{\partial \varphi}{\partial t}\right)_R$ is the rate changes of scalar function φ with respect to the material coordinate i.e. the first material derivative with respect to the time.

$\frac{\partial \varphi}{\partial t}$ is the rate changes of scalar function φ with respect to the spatial coordinate (fixed with respect to the observer), i.e. the first cartesian derivative with respect to the time

$\vec{q}_s$ is the solid phase velocity vector with respect to the spatial coordinate.

In order to transfer the operator ∇ into the moving coordinate, we may use the following relationship:

$$\vec{\nabla} = (\widehat{\nabla R})\overrightarrow{\nabla}_R \qquad \text{Eq. 2.2}$$

where $\widehat{\nabla R}$ is a second order tensor called the gradient deformation matrix and can hardly be measured in the laboratory in three dimensions:

$$\widehat{\nabla R} = \frac{\partial \vec{R}_i}{\partial \vec{r}_j} = \begin{bmatrix} \frac{\partial R_x}{\partial r_x} & \frac{\partial R_x}{\partial r_y} & \frac{\partial R_x}{\partial r_z} \\ \frac{\partial R_y}{\partial r_x} & \frac{\partial R_y}{\partial r_y} & \frac{\partial R_y}{\partial r_z} \\ \frac{\partial R_z}{\partial r_x} & \frac{\partial R_z}{\partial r_y} & \frac{\partial R_z}{\partial r_z} \end{bmatrix} \qquad \text{Eq. 2.3}$$

ignoring the shear deformation:

$$\widehat{\nabla R} = \begin{bmatrix} \frac{\partial R_x}{\partial r_x} & 0 & 0 \\ 0 & \frac{\partial R_y}{\partial r_y} & 0 \\ 0 & 0 & \frac{\partial R_z}{\partial r_z} \end{bmatrix} \qquad \text{Eq. 2.4}$$

and if the swelling direction is allowed only to be in the vertical or horizontal direction:

horizontal swelling: $\nabla R_h = \begin{bmatrix} \frac{\partial R_x}{\partial r_x} & 0 & 0 \\ 0 & 1 & 0 \\ 0 & 0 & 1 \end{bmatrix}$ *vertical swelling:* $\nabla R_v = \begin{bmatrix} 1 & 0 & 0 \\ 0 & 1 & 0 \\ 0 & 0 & \frac{\partial R_z}{\partial r_z} \end{bmatrix}$

To better understand the physical aspect of this mathematical expression, consider a vertical column of swelling soil, free to swell in the upward direction. The arbitrary soil element with the volume of V_o between the position z_{o1} and z_{o2} at time t_o (Fig. 2.1a) would obtain the volume V_t , limited to the new position z_{t1} and z_{t2} after the time t, due to the increase the soil water content (Fig. 2.1b):

$$V_o = (z_{o2} - z_{o1}) \times A = dz_o \times A$$
$$V_t = (z_{t2} - z_{t1}) \times A = dz_t \times A$$

Dividing each side of the first equation by the corresponding side of the second and assuming mass conservation for the solid part results in:

$$\frac{dz_o}{dz_t} = \frac{V_o}{V_t} = \frac{1/V_t}{1/V_o} = \frac{m/V_t}{m/V_o} = \frac{\rho_{bt}}{\rho_{bt_o}}$$

or:

$$dz_t = \frac{\rho_{bt}}{\rho_{bt_o}} dz_o \qquad \text{Eq. 2.5}$$

where: ρ_{bt} is the bulk density at the time t and ρ_{bt_o} stands for the initial bulk density. The above equation may also be expressed as (Smiles and Rosental 1968):

$$dz_t = \frac{\rho_b}{\rho_s} dz_o \qquad \text{Eq. 2.6}$$

where ρ_b is the soil bulk density at depth z. Equation 2.6 is the one dimensional vertical transformation of the cartesian coordinate into the material coordinate.

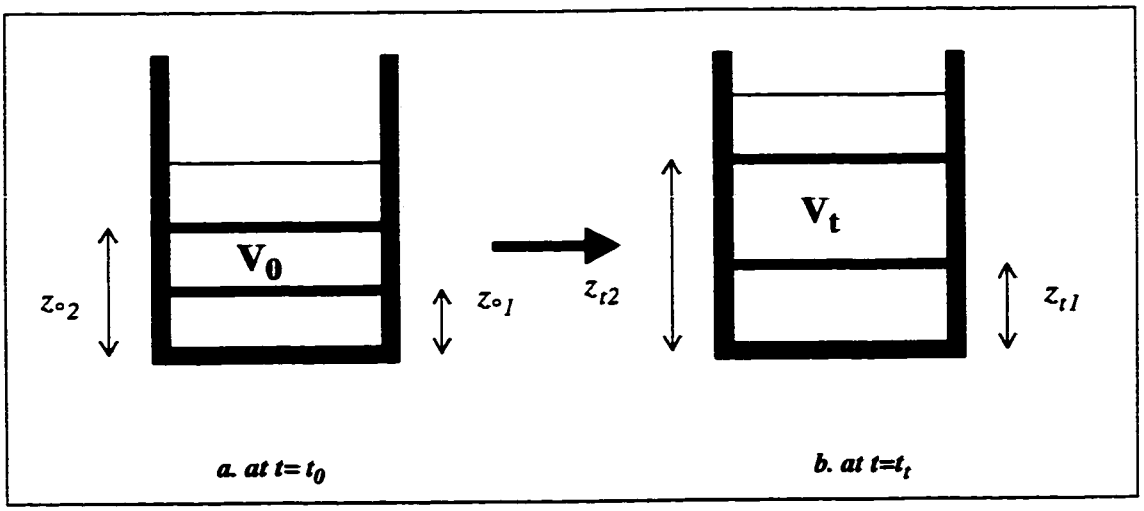

Fig. 2.1) The one dimensional volume change (in vertical direction)

2.2. Water adsorption

Water adsorption by soil particles in swelling soils is the major cause of soil expansion. According to Baver (1940) when water is added to the soil, part of the water fills the pores, and some part is attracted by the surface of the particles to cause the swelling phenomenon. It has been shown that water held in the Stern layer has different chemical properties than the water held in the soil pores and is considered immobile under ordinary forces. Therefore, the first molecules of water, added to the swelling soil, are adsorbed by the clay particles and become immobile. After satisfying the adsorption potential in the first layer of soil, the excess water will flow to the next soil layer and the adsorption process is repeated. These two complementary phenomena, water flow and soil expansion, are the result of repetition of water adsorption process. Based on this mechanism, it follows that any amount of water, added to the swelling soils, is divided into two parts; one part is adsorbed by the soil particles and the other part contributes to the flow process. Obviously the latter occurs very slowly at the very beginning of the saturation process and as the soil approaches saturated condition, the adsorption phenomenon progresses and more water contributes to the flow process. Therefore, the total soil moisture ratio may be divided into two parts:

$$\vartheta_w = \vartheta_a + \vartheta_d \qquad \text{Eq. 2.7}$$

where ϑ_w is soil moisture ratio, defined as the ratio of soil water volume to the volume of the soil particles and is related to the soil water content, θ_w by the following relationship:

$$\theta_w = \frac{\rho_b \cdot \vartheta_w}{\rho_s} \qquad \text{Eq. 2.8}$$

The quantity ϑ_a is the adsorbed water by the soil particle surface and ϑ_d is the mobile or Darcian water in the pores.

To determine the relation between the total amount of water and adsorbed water, it is assumed that all the initial water, added to a completely dry soil, contributes to the adsorption process. The rate of the water adsorption gradually decreases as the surface of the soil particles are saturated with the water. This is illustrated in Figure 2.2:

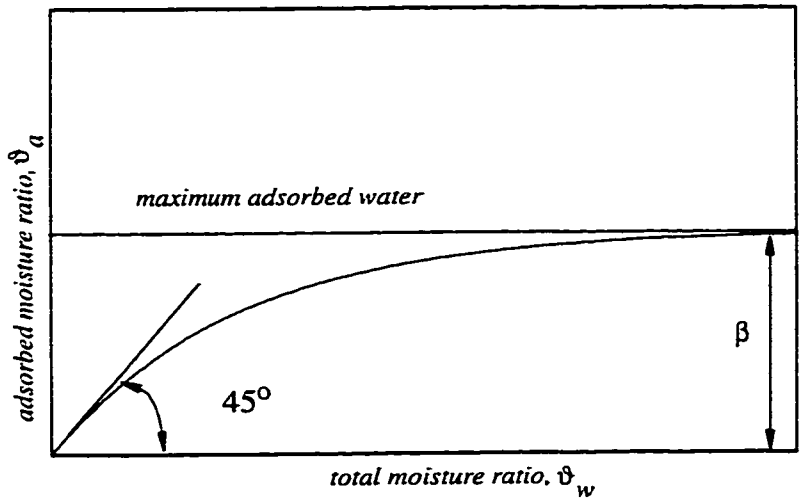

Fig. 2.2) Variation of adsorbed moisture versus total soil moisture

It follows that the slope of the curve at $\vartheta_a = \vartheta_w = 0$ is unity and when ϑ_w tends towards infinity the slope would be equal to zero. Thus the following equation may be used to describe these relationships:

$$\frac{d\vartheta_a}{d\vartheta_w} = 1 - \frac{1}{\beta} \cdot \vartheta_a \qquad \text{Eq. 2.9}$$

with the following condition:

$$at\ \vartheta_w = 0\,,\quad \vartheta_a = 0 \qquad \text{Eq. 2.10}$$

solving this ordinary differential equation leads to:

$$\vartheta_a = \beta\left(1 - exp\left(-\frac{1}{\beta}\vartheta_w\right)\right) \qquad \text{Eq. 2.11}$$

where β is regarded as the water adsorption coefficient and is the maximum water adsorbed by the clay particles with a dimension of L^3/L^3. The mobile water content, ϑ_b, may be calculated from Eq. 2.7:

$$\vartheta_d = \vartheta_w - \beta\left(1 - exp\left(-\frac{1}{\beta}\vartheta_w\right)\right) \qquad \text{Eq. 2.12}$$

2.3. Governing Equation

2.3.1. Assumptions

The assumptions undertaken in the theoretical approach can be summarized as;

a)- The hysteresis effect on the soil moisture retention curve is ignored.

b)- The isothermal condition is assumed.

c)- The shrinkage curve is a unique function for a certain overload, i.e., the adsorption and desorption (swelling and shrinkage) are almost the same.

d)- The soil is homogenous and isotropic

e)- Water and soil particles are incompressible liquid and solid respectively.

2.3.2. General Formulation

Considering soil as a mixture of continuous media, composed of three phases in the unsaturated condition (solid, liquid and vapor phase), three different laws of the continuum theory are applicable. According to this theory each phase may be regarded as a separate continuum medium. The first law is related to the kinematic part of the constituents. The second law involves the mass, energy or momentum balance equations, and the last law is the constitutive equations. By means of these three concepts a general three dimensional model will be derived. Eventually, the problem will be simplified to one (vertical) dimension.

There is some evidence that θ_w based equations for unsaturated water flow, particularly for deformable medium are either insufficient to express the soil conditions during water flow, or they have a very complex behavior in numerical analysis (Smiles and Rosenthal 1968, Raats 1965, Smiles 1974). Therefore, moisture ratio, ϑ, which is defined as the volume of water per unit volume of the solid particle, is used as a dependent variable. There are two major reasons to chose such a variable:

a)- The quantity ϑ is directly related to the gravimetric moisture content, ω, through: $\vartheta = \omega G_s$ where G_s is the specific gravity of soil solid, therefore, it can be precisely determined experimentally.

b)- Since θ_w is a function of both total soil volume and water volume whose changes might consequently neutralize each other, it may be less sensitive to the soil volume changes, particularly for saturated soil conditions.

The mass balance equation with respect to the fixed coordinate for the water phase may be

written as:

$$\frac{\partial \vartheta_w}{\partial t} = -\nabla \bullet \vec{q}_w - \frac{\partial \vartheta_a}{\partial t} \qquad \text{Eq. 2.13}$$

where ϑ_w is the total moisture ratio, $\vec{q}_w$ is the water flux vector of dimention (LT^{-1}) and ϑ_a is the adsorbed moisture ratio. All the parameters in Eq. 2.13 are considered with respect to the fixed coordinate and the term $\partial \vartheta_a / \partial t$ accounts for the adsorption phenomenon. Eq. 2.13 is insufficient to describe the movement of water in the expansive medium and it is more appropriate to look for a new expression in which the water flow can be referred to a reference frame moving together with the soil particles. Thus the water flow could be expressed independently of the solid phase velocity as pointed out by Zaslavsky (1964). Therefore, the relative flux equation could be employed as: (Zaslavsky 1964)

$$\vec{q}_w = \vec{q}_{wR} + \vec{q}_s \cdot \vartheta_w \qquad \text{Eq. 2.14}$$

in which $\vec{q}_{wR}$ is the water flux vector relative to the soil particle movement obeying the Darcian flux law, $\vec{q}_s$ is the soil particle flux vector and the term $\vec{q}_s \cdot \vartheta_w$ illustrates the mass flux of water due to the advection. Eq. 2.13 can be rewritten as:

$$\frac{\partial \vartheta_w}{\partial t} = -\nabla \bullet \vec{q}_w - \frac{d\vartheta_a}{d\vartheta_w} \frac{\partial \vartheta_w}{\partial t} \qquad \text{Eq. 2.15}$$

But from eq.2.11:

$$\frac{d\vartheta_a}{d\vartheta_w} = exp(-\beta \vartheta_w) \qquad \text{Eq. 2.16}$$

Using eq 2.16 and 2.15, and after some rearrangement of terms results:

$$-(1 + exp(-\beta\vartheta_w))\frac{\partial\vartheta_w}{\partial t} = \nabla\bullet\vec{q}_w \qquad \text{Eq. 2.17}$$

Applying the operator $\nabla\bullet$ on both side of the eq. 2.14 results:

$$\nabla\bullet\vec{q}_w = \nabla\bullet\overrightarrow{q_{wR}} + \nabla\bullet(\vec{q}_s \cdot \vartheta_w) \qquad \text{Eq. 2.18}$$

which upon substitution for $\nabla\bullet\vec{q}_w$ from eq.2.17 into eq. 2.18 yields:

$$-(1 + exp(-\beta\vartheta_w))\frac{\partial\vartheta_w}{\partial t} = \nabla\bullet\overrightarrow{q_{wR}} + \nabla\bullet(\vec{q}_s \cdot \vartheta_w) \qquad \text{Eq. 2.19}$$

In order to transfer the time derivative from a system coordinate at rest into a material moving coordinate, we use Eq. 2.1 with the scalar function ϑ_w, which results in:

$$\left(\frac{\partial\vartheta_w}{\partial t}\right)_R = \frac{\partial\vartheta_w}{\partial t} + \vec{q}_s \bullet \vec{\nabla}\vartheta_w \qquad \text{Eq. 2.20}$$

or:

$$\frac{\partial\vartheta_w}{\partial t} = \left(\frac{\partial\vartheta_w}{\partial t}\right)_R - \vec{q}_s \bullet \vec{\nabla}\vartheta_w \qquad \text{Eq. 2.21}$$

where the subscript R accounts for the material coordinate. Combining Eq.2.21 and 2.19 yields:

$$-(1 + exp(-\beta\vartheta_w))\left(\frac{\partial\vartheta_w}{\partial t}\right)_R = \nabla\bullet\overrightarrow{q_{wR}} + \nabla\bullet(\vec{q}_s \cdot \vartheta_w) - (1 + exp(-\beta\vartheta_w))\vec{q}_s \bullet \vec{\nabla}\vartheta_w \qquad \text{Eq. 2.22}$$

or:

$$-(1 + exp(-\beta\vartheta_w))\left(\frac{\partial\vartheta_w}{\partial t}\right)_R = \vec{\nabla} \bullet \overrightarrow{q_{wR}} + \vartheta_w\vec{\nabla} \bullet \vec{q}_s - exp(-\beta\vartheta_w)\vec{q}_s \bullet \vec{\nabla}\vartheta_w \qquad \text{Eq. 2.23}$$

2.3.2.1. Constitutive Equation for Wetting Fluid Phase

It is time to use the constitutive equations for water and soil particle flux. $\overrightarrow{q_{wR}}$ may be regarded as the flux of water that obeys Darcian flow law and similarly, $\vec{q_s}$ may be regarded as the soil particle flux which is proportional to the swelling pressure gradient. For Darcian flux we may write:

$$\overrightarrow{q_{wR}} = -K_w \overrightarrow{\nabla}_R H \qquad \text{Eq. 2.24}$$

where K_w is the unsaturated hydraulic permeability, which is a function of ϑ_b and void ratio, H stands for the total hydraulic head and $\overrightarrow{\nabla}_R$ represents the material gradient operator. For an unsaturated soil, the total hydraulic gradient, H, is the sum of the soil-water matrix and gravitational potential:

$$H = -\psi + Z_R \qquad \text{Eq. 2.25}$$

Here ψ is the soil water matrix potential (suction) and Z_R represents the gravitational potential, assumed positive downward. Therefore, Eq. 2.24 can be developed as follows:

$$\overrightarrow{q_{wR}} = -K_w \overrightarrow{\nabla}_R (-\psi + Z_R) \qquad \text{Eq. 2.26}$$

or:

$$\overrightarrow{q_{wR}} = -K_w (\overrightarrow{-\nabla}_R \psi + \vec{k}) \qquad \text{Eq. 2.27}$$

applying the operator $\vec{\nabla} \bullet$ on both sides of the Eq. 2.27 results in:

$$\vec{\nabla} \bullet \overrightarrow{q_{wR}} = -\vec{\nabla} \bullet K_w (\overrightarrow{-\nabla}_R \psi + \vec{k}) \qquad \text{Eq. 2.28}$$

By replacing the operator ∇ (gradient vector with respect to the fixed coordinate) with operator $\overrightarrow{\nabla_R}$, (gradient operator with respect to the material coordinate), Eq. 2.2, results in:

$$\vec{\nabla} \bullet \overrightarrow{q_{wR}} = -(\widehat{\nabla R})\overrightarrow{\nabla_R} \bullet K_w(-\overrightarrow{\nabla_R}\psi + \vec{k}) \qquad \text{Eq. 2.29}$$

Assuming:

$$\overrightarrow{\nabla_R}\psi = \frac{d\psi}{d\vartheta_d}\frac{d\vartheta_d}{d\vartheta_w}\overrightarrow{\nabla_R}\vartheta_w \qquad \text{Eq. 2.30}$$

then:

$$\vec{\nabla} \bullet \overrightarrow{q_{wR}} = -(\widehat{\nabla R})\left(\overrightarrow{-\nabla_R} \bullet \left(K_w\frac{d\psi}{d\vartheta_d}\frac{d\vartheta_d}{d\vartheta_w}\overrightarrow{\nabla_R}\vartheta_w\right) + \frac{dK_w}{dZ_R}\right) \qquad \text{Eq. 2.31}$$

where the term $\frac{d\vartheta_d}{d\vartheta_w}$ may be calculated using Eq. 2.12:

$$\frac{d\vartheta_d}{d\vartheta_w} = \frac{d}{d\vartheta_w}\left(\vartheta_w - \frac{1}{\beta}(1 - exp(-\beta\vartheta_w))\right) \qquad \text{Eq. 2.32}$$

or:

$$\frac{d\vartheta_d}{d\vartheta_w} = 1 - exp(-\beta\vartheta_w) \qquad \text{Eq. 2.33}$$

Substituting for $\frac{d\vartheta_d}{d\vartheta_w}$ from this equation into Eq.2.31 results in:

$$\vec{\nabla} \bullet \overrightarrow{q_{wR}} = -(\widehat{\nabla R})\left(-\overrightarrow{\nabla_R} \bullet \left((1 - exp(-\beta\vartheta_w))K_w\frac{d\psi}{d\theta_d}\overrightarrow{\nabla_R}\vartheta_w\right) + \frac{dK_w}{dZ_R}\right) \qquad \text{Eq. 2.34}$$

Defining the new soil-water diffusion coefficient as:

$$D_w = (1 - exp(-\beta\vartheta_w))K_w\frac{d\psi}{d\vartheta_d} \qquad \text{Eq. 2.35}$$

and substituting it in Eq. 2.34 results in:

$$\vec{\nabla} \bullet \overrightarrow{q_{wR}} = -(\widehat{\nabla R})\left(-\vec{\nabla}_R \bullet (D_w \vec{\nabla}_R \vartheta_w) + \frac{dK_w}{dZ_R}\right) \qquad \text{Eq. 2.36}$$

The water diffusity coefficient, obtained from Eq. 2.35, is less than that of the similar but non-swelling soil. This is true especially in the lower water content range as $exp(-\beta\vartheta_w)$ in Eq.2.35 assumes higher values. In other words, in the beginning of wetting phenomenon the Darcian velocity has less contribution in the flow process. That is because, in the early stage of wetting, the attachment of water to the soil particles is due more to other attractive forces rather than to matrix potential. Furthermore, β in Eq. 2.36 represents the soil capability to expand, i.e. the more active the soil (in terms of swelling behavior) the lower the value of β and consequently the lower the diffusity coefficient. It can be concluded that the soil with less expansion behavior has a diffusity coefficient closer to that of the ordinary Darcy-Buckingham for non-swelling soils.

2.3.2.2. Constitutive Equation for Solid Phase

Given that the flux of the soil particles is proportional to the pressure gradient, which develops between the soil particles and is due to the moisture variation, Nakano et al. (1986) assumed the following expression:

$$\vec{q}_s = -K_s \frac{d\psi_s}{dz} \qquad \text{Eq. 2.37}$$

where $\vec{q}_s$ is the soil particles flux, $(d\psi_s)/(dz)$ is defined as a potential responsible for the movement of soil particles and K_s is introduced on the analogy of the hydraulic conductiv-

ity. In a similar way, the three dimensional form of the above equation may be suggested for soil particles flux as:

$$\vec{q}_s = -K_s \vec{\nabla} \Omega \qquad \text{Eq. 2.38}$$

where K_s is introduced as the soil particle permeability (LT^{-1}), which is experimentally determined, and Ω is defined as the resisting and driving forces responsible for the swelling potential in terms of the water height:

$$\Omega = \frac{P_s + P_O + \int_0 \rho_t dz}{\rho_w g} \qquad \text{Eq. 2.39}$$

where P_s is the swelling pressure, P_O is the surface overload pressure, $\int_0^z \rho_b dz$ is the over burden pressure, ρ_t is the apparent wet density, ρ_w is the water density and g is the gravitational acceleration. Since Ω is a function of the soil water content and void ratio, we may write:

$$\vec{\nabla} \Omega = \frac{de}{d\vartheta_w} \frac{d\Omega}{de} \vec{\nabla} \vartheta_w \qquad \text{Eq. 2.40}$$

where $\frac{de}{d\vartheta_w}$ and $\frac{d\Omega}{de}$ are experimentally determined. Therefore, Eq 2.38 becomes:

$$\vec{q}_s = -K_s \frac{de}{d\vartheta_w} \frac{d\Omega}{de} \vec{\nabla} \vartheta_w \qquad \text{Eq. 2.41}$$

and by transferring the cartesian operator to the material operator Eq. 2.41 becomes:

$$\vec{q}_s = -\widehat{\nabla} R K_s \frac{de}{d\vartheta_w} \frac{d\Omega}{de} \vec{\nabla}_R \vartheta_w \qquad \text{Eq. 2.42}$$

Soil particle diffusity function is defined by the analogy of soil-water diffusity as follows:

$$D_s = \widehat{\nabla R} K_s \frac{de}{d\vartheta_w} \frac{d\Omega}{de} \qquad \text{Eq. 2.43}$$

Thus the constitutive equation for soil particle flux may be summarized as:

$$\vec{q}_s = -D_s \overrightarrow{\nabla}_R \vartheta_w \qquad \text{Eq. 2.44}$$

Applying the cartesian gradient operator on both side of Eq.2.44 leads to:

$$\vec{\nabla} \bullet \vec{q}_s = -\vec{\nabla} \bullet (D_s \overrightarrow{\nabla}_R \vartheta_w) \qquad \text{Eq. 2.45}$$

and altering the cartesian operator to become the material operator for the right hand side results in:

$$\vec{\nabla} \bullet \vec{q}_s = -(\widehat{\nabla R}) \overrightarrow{\nabla}_R \bullet (D_s \overrightarrow{\nabla}_R \vartheta_w) \qquad \text{Eq. 2.46}$$

2.3.2.3. Three Dimensional Flow Equation

Substituting for $\vec{\nabla} \bullet \overrightarrow{q_{wR}}$, $\vec{q}_s$ and $\vec{\nabla} \bullet \vec{q}_s$ in Eq. 2.23 using equations 2.36, 2.44 and 2.46 results in the equation:

$$-(1 + exp(-\beta\vartheta_w))\left(\frac{\partial \vartheta_w}{\partial t}\right)_R = -(\widehat{\nabla R})\left(\overrightarrow{-\nabla}_R \bullet (D_w \overrightarrow{\nabla}_R \vartheta_w) + \frac{dK_w}{dZ_R}\right) \qquad \text{Eq. 2.47}$$
$$-\vartheta_w \widehat{\nabla R} \overrightarrow{\nabla}_R \bullet (D_s \overrightarrow{\nabla}_R \vartheta_w) + exp(-\beta\vartheta_w) D_s \overrightarrow{\nabla}_R \vartheta_w \bullet \overrightarrow{\nabla}_R \vartheta_w$$

which after some rearrangement gives the final form of the three dimensional flow equation:

$$\frac{1}{\widehat{\nabla R}}(1 + exp(-\beta\vartheta_w))\left(\frac{\partial \vartheta_w}{\partial t}\right)_R = \overrightarrow{-\nabla}_R \bullet (D_w \overrightarrow{\nabla}_R \vartheta_w) + \frac{dK_w}{dZ_R} \qquad \text{Eq. 2.48}$$
$$+ \vartheta_w \overrightarrow{\nabla}_R \bullet (D_s \overrightarrow{\nabla}_R \vartheta_w) - D_s exp(-\beta\vartheta_w) \overrightarrow{\nabla}_R^2 \vartheta_w$$

Equation 2.48 is the complete three dimensional equation for unsaturated flow through the deformable porous media. Some important aspect of this equation are:

1) The time derivative coefficient on the left hand side contains extra terms in comparison with the conventional unsaturated flow equation for non-swelling soils. The term $exp(-\beta\vartheta_w)$, which varies from zero for a very large value of ϑ_w, to unity for a very small value of ϑ_w, is a function of β (water adsorption coefficient). Therefore, this term denotes how much water is adsorbed by the soil particles during the wetting process and acts as a time dependent source/sink term. The other time coefficient, $1/\widehat{\nabla R}$, represents the effect of soil body deformation on water retention in soil, which can vary from zero for a porous medium undergoing a very large amount of deformation, to unity for non-deformable media.

2) The first two components on the right hand side stand for Darcian flow in response to the matrix and gravitational potential. The diffusity function, D_w, is less than that of non-swelling soils particularly in lower water content; i.e., the higher the β in more active soil, the lower the D_w. Therefore, the diffusion of the water due to the gradient of the soil suction potential is much more limited as the soil becomes more active (particularly within the lower range of water content).

3) The third term stands for the advection of that part of the water which travels with the soil particles. The soil particles diffusity function, D_s, is a function of the slope of the shrinkage curve ($de/d\vartheta_w$, loading curve), swelling pressure-void ratio curve (dP_s/de) and soil particle permeability (K_S). All of these parameters were experimentally determined (chapter 3&4). This term also determines the degree of contribution of the soil activity (in terms of swelling behavior) to the water flow process; i.e., the more active the soil, the higher the Ds, and consequently the more important the role of this term.

4) The fourth term shows the contribution of the water adsorption phenomenon and soil particle movement to the flow process. The importance of this term

depends on the value of the adsorption limit coefficient, β ; i.e., the higher the value of β , the more important the term.

5) Equation 2.48 not only includes all the effects, prompted by the swelling phenomenon on the unsaturated flow process through swelling soils, but also can describe the water flow through an unsaturated non-swelling soil undergoing a deformation produced by pressures other than the swelling pressure (e.g. overload pressure). In other words, it can describe the soil water state in the consolidation of an unsaturated, non-swelling soil. In such a case the adsorption limit coefficient, β will be equal to zero and equation 2.48 changes into the following form:

$$\frac{I}{\widehat{\nabla R}}\left(\frac{\partial \vartheta_w}{\partial t}\right)_R = \overrightarrow{\nabla}_R \bullet (D_w \overrightarrow{\nabla}_R \vartheta_w) + \frac{dK_w}{dZ_R} + \vartheta_w \overrightarrow{\nabla}_R \bullet (D_s \overrightarrow{\nabla}_R \vartheta_w) \qquad \text{Eq. 2.49}$$

only the definition and determination of the soil particles diffusity need to be corrected. In other words, the terminologies of the three coefficients in the soil particle diffusity function, Eq.2.44, should be changed. The diffusity equation may be rewritten as:

$$D_s = \widehat{\nabla R} K_s \frac{d\Omega}{d\vartheta_w}$$

where $d\Omega/d\vartheta_w$ may be regarded as the slope of the pressure-moisture ratio, determined by applying a different overload to an unsaturated soil sample and measuring its final moisture ratio. K_S may be also determined using the same methodology described in chapter 3.

2.3.2.4. One Dimensional Flow Equation.

The three dimensional unsaturated flow equation, derived in the previous section, may be simplified to a one dimensional, vertical equation. The following reasons are the justification of this simplification:

a) In the field, most of the problems associated with unsaturated flow through

swelling soils are one dimensional problems i.e., the water movement as well as soil expansion occur in one dimension, particularly in the vertical direction.

b) The development of the techniques for measuring the flow parameters in three dimensions is either impossible or very difficult.

c. The model can be more accurately verified in one dimension through the experimental and numerical considerations.

Consequently, equation 2.48 is simplified as:

$$\frac{1}{\widehat{\nabla R}}(1+exp(-\beta\vartheta_w))\left(\frac{\partial\vartheta_w}{\partial t}\right)_{Z_R} = \frac{\partial}{\partial Z_R}\left(D_w\frac{\partial\vartheta_w}{\partial Z_R}\right)+\frac{\partial K_w}{\partial Z_R} + \vartheta_w\frac{\partial}{\partial Z_R}\left(D_s\frac{\partial\vartheta_w}{\partial Z_R}\right)-D_s exp(-\beta\vartheta_w)\left(\frac{\partial\vartheta_w}{\partial Z_R}\right)^2 \qquad \text{Eq. 2.50}$$

The deformation matrix, in one dimension, contains just one component as previously described. One may use equation 2.5 as the vertical, one dimensional transformation equation. Therefore the final form of equation 2.50 will be:

$$\frac{\rho_s}{\rho_b}(1+exp(-\beta\vartheta_w))\left(\frac{\partial\vartheta_w}{\partial t}\right)_{Z_R} = \frac{\partial}{\partial Z_R}\left(D_w\frac{\partial\vartheta_w}{\partial Z_R}\right)+\frac{\partial K_w}{\partial Z_R} + \vartheta_w\frac{\partial}{\partial Z_R}\left(D_s\frac{\partial\vartheta_w}{\partial Z_R}\right)-D_s exp(-\beta\vartheta_w)\left(\frac{\partial\vartheta_w}{\partial Z_R}\right)^2 \qquad \text{Eq. 2.51}$$

2.3.2.5. Initial and Boundary Conditions.

The initial and boundary conditions for equation 2.51, in the case of infiltration into a semi-infinite column, can be written as (Philip 1957):

$$\begin{aligned} \vartheta_w &= \vartheta_\circ \qquad t = 0 \qquad Z_R \geq 0 \\ \vartheta_w &= \vartheta_n \qquad t > 0 \qquad Z_R = 0 \end{aligned} \qquad \text{Eq. 2.52}$$

these conditions are valid for the soil sample free to swell in the upward direction. In different degrees of confinement, which were achieved in experimental work by applying an overload to the top of the samples, these conditions are valid only if the corresponding moisture ratio at $Z_R=0$ is known.

CHAPTER

3
Soil Hydraulic Properties

In the present and the following chapter, soil hydraulic and swelling parameters, involved in the mathematical model, were experimentally measured and modeled. In the present chapter, soil moisture retention and saturated and unsaturated hydraulic permeability, as the most important hydraulic properties of the soil, were investigated. In each measurement the sensitivity of soil samples to the initial soil parameters was also taken into account.

3.1. Saturated Hydraulic Permeability

The saturated hydraulic conductivity is highly dependent on the geometry of the soil porosity. In non-swelling soil, since the geometry of the soil pores doesn't change when the soil moisture content is changing, this property remains constant. Unlike the non-swelling soil, the size and shape of the soil pores in swelling soils, changes when the state of the water in the soil changes and accordingly, the saturated hydraulic conductivity is not constant. Therefore, one might consider the saturated hydraulic conductivity as a function of soil void ratio. Incorporation of this function into a mathematical formulation needs

experimental work and finally an empirical formula from the results.

3.1.1. Material and Methodology

Five soil samples, consisting of 50 percent bentonite and 50 percent sand were compacted with different initial water contents. Initial proprieties of the samples are illustrated in Table 3-1.

Table 3.1: Sample Initial Condition in Saturated Hydraulic Conductivity Test

Spec. No.	$\omega_{ini}^{1*}\%$	ρ_{ini}^{2*}	e^{3*}	height (*mm*)
1	15	2.20	0.41	9.3
2	33	2.16	0.70	9.3
3	55	1.91	1.23	9.3
4	81	1.62	2.09	9.6
5	119	1.53	3.00	9.5
6	185	1.25	5.24	14.85

1 initial water content 2* initial density (g/cm^3) 3* void ratio*

The apparatus used in this experiment is shown in Fig. 3.1(p.74). It consists of two compartments. The soil sample is compacted and located in the lower compartment. A mesh and a porous plate are centered on both the top and the bottom of the sample. To maintain the void ratio constant during the test, a perforated plexyglass plate was placed and fixed over the lower compartment. Distilled water was then added to the system inside the upper compartment. Air pressure was applied to the water surface through the upper cap. After completing the installation, the saturated condition is achieved after a few days by applying 30 kPa air pressure from the top.

By applying air pressure to the system, the hydraulic gradient between the top and bottom of the sample induced a saturated water flow through the sample and water began to run out from the bottom. At each applied pressure, after an arbitrary time interval within which the equilibrium was achieved, the amount of lost water was recorded. Finally, constant head formula is used for calculating the saturated hydraulic conductivity:

$$K_{sat} = \frac{Q \cdot L}{\Delta H \cdot A \cdot \Delta t} \qquad \text{Eq. 3.1}$$

where:

K_{sat} : *saturated hydraulic conductivity*
Q : *water leaving the system during time* Δt
Δt : *time interval between two measurements*
ΔH : *hydraulic gradient (pressure)*
A : *sample cross section area*
L : *sample length*

To verify the effect of the magnitude of applied pressure on the calculated hydraulic conductivity, the test was repeated for different amounts of applied pressure.

3.1.2. Results and Discussion

3.1.2.1. Experimental Results

Table3.2 shows the results of the test for five different values of applied pressure. In some cases, under low hydraulic gradient, no water outflow was observed. Therefore the saturated hydraulic conductivity was not calculated. On the other hand, a higher hydraulic gradient could disturb the sample making the measured water outflow unreliable; therefore in this instance also the saturated hydraulic conductivity could not be calculated.

Table 3.2: Calculated Saturated Hydraulic Conductivity for Different Applied Pressure

spe No	K_{sat} (m/s) in different Penumetric pressure (kPa)					Ave. K_{sat} cm/day
	140	210	275	415	550	
1	-	-	2.90e-11	3.20e-11	3.1e-11	3.10e-11
2	-	-	1.13e-10	1.18e-10	1.1e-10	1.14e-10
3	-	2.70e-10	2.50e-10	2.35e-10	2.4e-10	2.50e-10
4	6.70e-10	6.90e-10	6.60e-10	-	-	6.70e-10
5	1.55e-9	1.65e-9	-	-	-	1.62e-9
6	7.00e-9	-	-	-	-	7.00e-9

As a final result the hydraulic conductivity versus the void ratio is graphed in Fig.3.2 (p.75). From the figure, one may conclude that as the soil void ratio increases, the saturated hydraulic conductivity rises more rapidly. The existence of this relation is due to the fact that soil with the higher void ratio can hold a bigger amount of free water inside the pores, resulting in a higher conductivity coefficient. On the other hand, attractive forces exerted on the water molecules from the soil particle surface, decreases by the square of its distance from the particle surface. Consequently, the less distance between the particles, the higher dependency between the water inside the pores and soil particles, making the water more immobile.

3.1.2.2. Parametric Model

Since the numerical analyses of the unsaturated equation derived in the mathematical section needs a formulated model for every experimental relationship, a model was proposed for $K_{sat}(e)$. Ohtsubo et al.(1985) determined the permeability of low swelling

clay by fitting Terzaghi's theory of consolidation to the measured deformation versus the root time curve and proposed a general equation of:

$$log(K) = C + D \times e \qquad \text{Eq. 3.2}$$

where K is saturated hydraulic conductivity, e is void ratio and C and D are curve fitting parameters. Huerta et al.(1988) and Townsend and Mcway(1990) used a power relationship for describing the relation between saturated hydraulic conductivity and void ratio:

$$K = Ce^{D} \qquad \text{Eq. 3.3}$$

Messing and Jarvis(1990) employed a field method to determine the field saturated hydraulic conductivity and presented a power function model for their data as follows:

$$K_{fs} = Be^{n} \qquad \text{Eq. 3.4}$$

where K_{fs} is the field saturated hydraulic conductivity and B and n are the fitting parameters. The aforementioned models are not so accurate, especially for highly swelling clay as within the range of low void ratio they either underestimate or overestimate the saturated hydraulic conductivity in their prediction. Therefore in present research a more sophisticated three parameter model is proposed to be fitted over the experimental data. The model parameters are then determined using a statistical computer program (AXUM). The model is defined as:

$$ln(K_{sat}) = a + be^{c} \qquad \text{Eq. 3.5}$$

where a, b and c are the fitting parameter and e is soil void ratio. Table 3.3 summarizes the fitting parameters used in equation 3.2 through 3.5 for measured experimental data.

The results of different models are illustrated in Fig. 3.3 (p.75). As the figure shows, the proposed model fits better over the experimental results. Ohtsubo's model over-estimates the saturated hydraulic conductivity within the lower ranges of soil void ratio, while the power model underestimate it in the same range of soil void ratio. The magnitude of *ln(a)* in Eq. 3.5 may be assumed as the minimum saturated hydraulic conductivity for the sample if the maximum compaction is applied to the soil with optimum water content:

$$(K_{sat})_{min} = ln(a) \quad \textit{(in equation 3.5)} \qquad \text{Eq. 3.6}$$

Table 3.3: Fitting Parameters for Different Models

Eq. No.	Model Parameters				
	C	D	a	b	c
3.2	-9.69	0.29	-	-	-
3.3	9.3E-11	2.61	-	-	-
3.5	-	-	-29.02	6.53	.275

3.2. Soil Suction Measurement

In order to apply the moisture retention data to the theoretical model of unsaturated flow, the full range of soil suction measurement must be obtained in the laboratory. For the soils which are not subjected to volume change during the drying or wetting process, a usual extractor apparatus may be used. However, for swelling soil two additional important points should be taken into account. First of all, the apparatus must have the capability of keeping the soil volume constant from the starting time up to the point that the sample starts undergoing shrinkage phenomenon, i.e. the sample is not allowed to increase

it's bulk volume after it is compacted to a certain initial density in completely saturated condition. Secondly, since the change in the geometry of the pores depends upon the overload pressure, the latter should be taken into account as a third parameter (Groenenvelt et al. 1972). Thus, whereas in the non-swelling soil, in which the ψ-θ relationship (apart from hysteresis) is unique, in swelling soil this relationship depends also upon an extra parameter called load pressure or over burden pressure P (Stroosnijder et al. 1984). However, the volume change characteristic of the soil might be taken into account to fully characterize both the shrinkage and moisture retention of the soil. Consequently, two sets of bundle curves have been determined experimentally; the $\psi(\vartheta,P)$ bundle and $e(\vartheta,P)$ bundle. This section focuses on some investigation of the moisture retention characteristic curve for the swelling soil. First of all, the effect of initial moisture ratio and swelling constituent percentage of the soil mixture on the ψ-ϑ relationship will be investigated at zero loading and accompanying this, the adsorption limit moisture ratio for each curve will be approximated. Following that, the initial density effect, in the completely confined initial condition, will be considered and it will be compared with those under zero loading but with the same initial moisture ratio. In another part of this section the effect of the overload pressure, P, on the ψ-ϑ relationship will be sought. Doing this latter test, some extra readings will be taken to be used in the determination of unsaturated hydraulic conductivity. Eventually, Van Genuchten model will be modified to be fitted over obtained data and the relevant coefficients will be determined using RETC computer program.

3.2.1. Pressure Plate Apparatus

The pressure plate test apparatus works based on the fact that at any given pressure in the chamber, soil moisture starts flowing from around each soil particle down to the membrane, passing through it upon the hydraulic gradient induced between its top and bottom and out of the chamber. The flow is continued until the soil water potential (suction) gets the same value as the exerted air pressure. When this occurs, an equilibrium is reached and the flow of moisture ceases.

Details of this apparatus are shown in Fig. 3.4 (p.76). The apparatus mainly consists of three major parts: bottom plate, top plate and outer cylinder, the latter being separated from others by an O-ring placed in each side. The cellulose membrane used in the apparatus has the ability to cover the suction range from 0 to 100 bars which is high enough for the selected soil.

The test procedure was established as follows: first of all, a cut membrane disc which was thoroughly soaked in distilled water was laid on the screen drain plate over the bottom plate and centered. An "O" ring was then placed on the cellulose disc at the edge on which the outer cylinder was laid. The prepared samples were placed over the wet membrane inside the cylinder. It is desirable to keep the height of the samples small enough in order to keep equilibrium time reasonable. Then the second "O" ring was placed in the top groove of the outer cylinder and the top plate was centered over the system so that the top and bottom bolt slots lined up. The clamping bolts were then inserted and tightened down. After all connections were set up and controlled, the pressure regulator was opened slowly and adjusted to the extraction pressure desired. The outflow was led into a buret from

which the level of the water was recorded periodically and the approach to the equilibrium condition was thus followed. Samples were removed and weighed at the time of equilibrium. In all the tests, the volume of the sample in each pressure interval was measured using the same procedure (explained later where the soil shrinkage characteristic is discussed).

3.2.2. Equilibrium Time

The time required for the suction inside the soil to reach equilibrium with the soil moisture content depends on several parameters, such as soil type, temperature and the height of the sample. This equilibrium time varies from 2-12 days for the 50 percent bentonite mixture to 5 hours for the 10 percent bentonite mixture. The results show that the amount of outflow water, with the same air pressure increment applied to the sample, in the low range of soil suction is bigger than that obtained in the higher range; however, the equilibrium time is lower. These results lead us to the fact that the equilibrium time depends closely on the unsaturated hydraulic conductivity of the soil at the corresponding soil water suction. Details will be explained later where the unsaturated permeability is discussed.

3.2.3. Results

3.2.3.1. Effect of the Soil Initial Moisture Ratio (Type A)

In the first part of soil suction measurements, different samples were used to investigate the effects of the initial moisture ratio on the soil moisture retention characteris-

tic. Five samples with five different moisture ratios were prepared. All the samples contained 50% bentonite in the mixture. Table3.4 shows the initial conditions of the samples

Table 3.4: Soil Sample Specification in the First Test

No.	Ben.(%)	ω(%)	ϑ_{int} (V_w/V_s)	ρ_b * (g/cm^3)	ρ_t ** (g/cm^3)
KA1	50	300	8.30	.28	1.14
A2	50	197	4.98	.39	1.19
A3	50	105	2.84	.61	1.25
A4	50	61	1.64	.90	1.45
A5	50	50	1.33	1.01	1.52

** soil dry bulk density (oven dry mass over bulk volume at certain water content)*
*** soil ordinary density (total wet mass over bulk volume at certain water content)*

All the samples, except sample AK1 that was tested individually, were placed in the pressure cell at the same time. The moisture characteristic curves as a plot of matrix potential, ψ, versus soil moisture ratio, ϑ, are illustrated in Fig. 3.5 (p.77). It can be concluded from the Figure 3.5.a that the soil moisture ratio remains unchanged when the applied pressure tends towards 100 bars. Afterward, it seems that the mechanism by which the remaining water is held inside the pores is different from the usual matrix potential, i.e. the adsorption force, mostly due to the existence of ions double layer, is the major cause of water retention in high applied air pressure. As it discussed in chapter 2, this amount of water may be regarded as the water adsorption limit, β, which can be expressed in the form of moisture ratio, ϑ. Eventually, the water adsorption limit is estimated from a water characteristic curve, plotted in Figure3.5. The results are shown in Table3.5.

According to the Figure3.5, the water adsorption limit varies as the initial soil

condition changes. For a low initial moisture ratio this parameter is lower than that of the higher initial moisture ratio. This is because the adsorbed water by the soil particle is higher when the initial amount of water is high. Consequently even in a very high value of soil suction the particle may keep some more adsorbed water.

To investigate the effect of the initial water content on the moisture retention characteristic within the lower range of soil suction, data have been plotted in a logarithmic scale for the soil suction in Fig. 3.6 (p.78). As the curves show, for the higher initial moisture ratio, the curve has less negative slope than that of the lower moisture ratio. The main reason is that, soil with initially higher moisture ratio has higher porosity providing more free water to be squeezed by the same increment in soil suction. In other words, a higher void ratio for initially higher moisture ratio, introduces less capillary height and vice versa.

Table 3.5: Water adsorption limit in terms of moisture ratio for samples with different initial moisture ratio

	Specimen				
	A_1	A_2	A_3	A_4	A_5
β^*	0.53	0.47	0.41	0.36	0.33

β^* *is the water adsorption limit, expressed in terms of soil moisture ratio*

As it was discussed in chapter 2, the water inside the swelling soil pores has two individual characteristics: mobile or Darcian water and adsorbed water. Thus the moisture retention curves should be characterized considering the Darcian or mobile part of the soil water rather than the total water. Following this, one may use the Equation 2.12 in Chapter 2 to estimate the amount of the Darcian part of the soil water. The final moisture retention curves in which only the Darcian water has been contributed are illustrated in Fig. 3.6.a

and 3.6.b (p.78).

3.2.3.2. Effect of the Soil Swelling Constituent (Type B)

This investigation was done running the same test using five samples with five different percentages of the soil swelling component as shown in table3.6.

Table 3.6: Soil Samples Specifications in Swelling Component Effect Investigation

No.	liquid limit	Ben.(%)	ω(%)	ϑ_{int}	ρ_b (gr/ cm^3)	ρ_t (gr/ cm^3)
B1	300	50	302	8.3	.28	1.14
B2	215	40	193	6.28	.39	1.17
B3	110	30	145	3.94	.5	1.24
B4	66	20	97	2.55	.69	1.39
B5	51	10	57	1.74	.96	1.55

All the samples were molded at the initial water content close to their liquid limit to cover all the wetting range. Fig. 3.7 (p.79) shows the test results of these samples. From the results it can be followed that the adsorption limit, β, rapidly decreases as the swelling potential is reduced (from 50 percent bentonite to 10 percent in the mixture). This means that this parameter depends to a high degree on the swelling component of the soil. This also proves that the remaining water in expansive soils is not being held by the soil particle in the same way that water is held in non-swelling. The suction inside the pores of the soil depends on the curvature of the interface between wetting and non-wetting phases. Therefore if all the water in the pores was held by the surface tension force between the particles and water, applying reasonable air pressure in the test chamber should squeeze almost all the water out as happens in the soil with a very low percentage of swelling component, but

with smaller void ratio.

Table 3.7: Water adsorption limit in terms of moisture ratio for samples with different percentage of swelling component

	Specimen				
	B1	B2	B3	B4	B5
β*	0.53	0.36	0.24	0.13	0.03

** moisture ratio at the soil particle water adsorption limit*

As may be noted from Table 3.7 sample B1 with 50 percent bentonite has the maximum water adsorption limit and sample B5, consisting of 10 percent bentonite, the minimum value. The effect of the swelling constituent in the soil mixture within the low range of the soil suction was investigated using the logarithmic scale for the soil suction axis (Fig3.7.b p.79). From the figure it can be concluded that the slopes of all the curves in the low soil suction range are the same, i.e., in all samples, decrease in soil moisture ratio is accompanied with the same rate of increase in soil suction. This happens because the initial water content has been chosen close to the liquid limit for all the samples and consequently the amount of free water inside the pores for all the samples may be assumed to be the same. In other words, the slope of the logarithmic curve of moisture retention characteristic for different soil mixture is independent of the percentage of the soil swelling component if the initial moisture ratio is either chosen as the same or close to the liquid limit of that mixture.

Similar to previous conditions, the soil moisture retention curves may be replotted calculating the Darcian part of water through employing Equation 2.12. The results are plotted in Fig. 3.8 (p.80).

3.2.3.3. Effect of the Soil Initial Bulk Density (Initially Confined: Type C)

The effect of the initial bulk density was also examined by modifying the pressure plate apparatus. The sketch of the modified system has been shown in Fig. 3.9.a (p.81). Five remolded samples, with 50 % bentonite, were prepared and brought to the almost completely saturated point in saturated permeability test. The initial conditions of the samples are summarized in Table3.8.

Table 3.8: Soil Specifications in the Third Test (Investigating Bulk Density Effect)

No	liquid limit	Ben.(%)	ω(%)	ϑ_{int}	ρ_b (gr/ cm^3)	ρ_t (gr/ cm^3)
C1	320	50	47	1.30	1.51	2.22
C2	320	50	65	1.80	1.17	1.85
C3	320	50	99	2.74	.89	1.77
C4	320	50	136	3.77	.63	1.50
C5	320	50	217	6.01	.34	1.10

After that, they were placed inside the pressure cell and the top system by which the volume of the soil remains unchanged was set up. The plots of the soil water content versus soil suction and its corresponding logarithmic scale are illustrated in Fig. 3.10 (p.82). The water adsorption limits which are estimated from the curves are also summarized in Table 3.9.

Table 3.9: Water Adsorption Limit in Terms of Moisture Ratio for Samples with Different Initial Bulk Density under Completely Confined Condition

	Specimen				
	C1	C2	C3	C4	C5
β*	.32	.38	.4	.44	.49

** water content at the soil particle water adsorption limit*

One may note from the figure that the water adsorption limit for the soil sample with high initial bulk density may not be estimated from the shape of the graph as the vertical asymptotic line is somewhere out of the measured suction range. This is because the highest available applied pressure is not enough to squeeze all the Darcian water from the pores. In other words, the size of the pores gets smaller as the initial dry bulk density becomes higher. Consequently the suction potential of soil water increases and more air pressure is needed to move the water out. However, since the water adsorption limit for a certain amount of soil solid particles is almost constant and depends on the ions' concentration and initial available water, this limit, after applying enough air pressure, takes a value close to the one obtained for the samples through the first experimental results. In the lower ranges of soil suction, as Figure 3.10.b (p.82) shows, the capillary range for the low initial dry bulk density is very small, because of the larger size of the pores; that is, the slope of the curve, starting from the saturated point, is smaller than that of the highly compacted soil. The plot of the Darcian part of the moisture retention curves is shown in Fig.3.11 (p.83). These data will be employed in numerical analysis (Chapter 4).

3.2.3.4. Effect of the Soil Overload (Type D)

As discussed before, in the field the soil is more likely loaded; therefore the hydraulic properties which are employed in theoretical and numerical considerations should include such a condition. A new set up (Fig.3.9.b) was used to estimate both soil unsaturated hydraulic conductivity and moisture retention under two different overload conditions. The apparatus used in this test was originally the same as the apparatus used in test one and two. However, a simple overloading system was placed over the sample, that

is consisting of a heavy metal plate as an overload and a perforated plexiglass cap over the soil, the latter to enable the air pressure to penetrate into the soil sample. Also the outflow water was piped into a buret, to be used in estimating the unsaturated hydraulic conductivity, as will be discussed later. To achieve more resolution in measuring unsaturated hydraulic conductivity, samples' diameter were chosen two times bigger than those of the other tests and furthermore were placed inside the pressure cell individually. Initial soil conditions are shown in Table 3.10.

Table 3.10: Soil Specifications in the Fourth Test (Investigating Over-Load Effect)

No.	liquid limit	Ben. (%)	Over Load (kPa)	$\omega(\%)$	ϑ_{int}	ρ_b (gr/cm^3)	ρ_t (gr/cm^3)
D1	320	50	90	47	1.31	1.22	1.79
D2	320	50	50	74	2.15	0.91	1.57
D3	320	50	0	300	8.30	0.28	1.13

The results of this experiment are plotted in Fig. 3.12 (p.84) and Fig. 3.13 (p.85). It may be concluded from Fig. 3.12.a that as the amount of overload decreases, the curve tends to be more flat and covers a wider moisture ratio range. Since the maximum applied pressure was not enough to squeeze all the Darcian water out of the sample, as described in the previous experiment, the moisture ratio at the adsorption limit reached its value somewhere out of the experimental range. However, as this value depends on the initial moisture ratio and not the over load condition, the adsorption limit might be estimated from the unloading conditions corresponding to the same initial moisture ratio, i.e., the first experiment.The estimated adsorption limits for this test have been summarized in Table 3.1.

Table 3.11: Water Adsorption Limit in Terms of Moisture Ratio for Samples with Different Over-Load Pressure

	Specimen		
	D1	D2	D3
β*	0.31	0.38	0.53

**:moisture ratio at the soil particle water adsorption limit*

The effects of overload on the lower ranges of soil suction are shown in Fig. 3.12.b. In the low range of soil suction, the curve has less slope as the overload decreases, i.e., the capillary range is smaller for the same sample but with less overload. The reason for this is that the void ratio, and consequently the pore sizes are bigger for the sample with less overload. The moisture characteristic curves for the Darcian or mobile water are plotted in Fig. 3.13 using the Eq. 2.12. The overall shape of all the curves did not change. However, the range of moisture ratio has become shorter because the adsorption equation (Eq. 2.12) excludes the immobile water from total soil water.

3.2.4. Parametric Modeling

The moisture retention characteristic of the soil has to be modeled for further mathematical applications. In the present study, two different types of modeling have been employed. The five parameters model of Van Genuchten (1980) has been modified to be fitted over the data using a modified computer program named *RETC*. Later on, an alternative method called a *neural network model* will be employed to establish a new model to estimate the different hydraulic and swelling properties of the soil corresponding to the saturation state.

3.2.4.1. Van Genuchten model

The five parameters Van Genuchten model has the general form of:

$$\theta = \theta_r + \frac{\theta_s - \theta_r}{[1 + (\alpha \cdot \psi)^n]^m} \qquad \text{Eq. 3.7}$$

where θ is the volumetric water content, ψ is the soil suction (cm), θ_r: is the water content at retention point, θ_s is the water content at maximum saturation, and α, n, m are the fitting parameters.

An attempt has been made to modify this model to be fitted over the measured data. The volumetric water content and moisture ratio can both determine the soil saturation state and their relation is defined by:

$$\theta_w = (\vartheta \rho_b)/\rho_s \qquad \text{Eq. 3.8}$$

Therefore the soil water content, θ, can be replaced by moisture ratio, ϑ, using Eq.3.8. The equations 3.7 may now be rewritten as follows:

$$\vartheta = \frac{1}{\rho_b}\left(\rho_{br}\vartheta_r + \frac{\rho_{bs}\vartheta_s - \rho_{br}\vartheta_r}{[1 + (\alpha \cdot \psi)^n]^m}\right) \qquad \text{Eq. 3.9}$$

It should be mentioned that in non-deformable soil, since the dry bulk density(ρ_b) remains constant during saturation, one may use the simple form of this equation. The moisture ratio, determined through Eq.3.9 should have the Darcian water properties, since this equation directly contributes to the Darcy equation. In other words, in non-swelling soils, since the adsorbed water by soil particles is negligible, moisture ratio in Eq.3.9 stands for total soil water; whereas in swelling soil, as discussed before, part of the water may be adsorbed by soil particles by attractive forces other than soil suction potential.

However, the other part of the water, which is free to move due to the hydraulic gradient may be determined using Eq3.2. Since, the total residual water is the sum of the Darcian residual water and the maximum adsorbed water by soil particles, one should be aware that the RETC program estimates the Darcian residual water. Eq3.9 now takes the following form:

$$\vartheta_d = \frac{1}{\rho_b}\left(\rho_{br}\vartheta_{rd} + \frac{\rho_{bs}\vartheta_{sd} - \rho_{br}\vartheta_{rd}}{[1 + (\alpha \cdot \psi)^n]^m}\right) \qquad \text{Eq. 3.10}$$

where the additional subscript d stands for the Darcian part of water. The Darcian moisture ratio at saturated condition is assumed to be known either from the initial soil condition or, if the soil is not initially saturated, from $\vartheta - S$ relationship (S is saturation degree). The other four parameters in Eq. 3.3 can be statistically (least square method) estimated employing the RETC computer program, adapted from Van Genuchten. The RETC program was modified to estimate the corresponding moisture ratio from Eq.3.10. Modifications include the estimation of bulk density from the $\vartheta - \rho_b$ relationship which will be established in the later section where the shrinkage characteristic of the soil is discussed. The results of the computer program for all the 18 samples used in the four series of pressure plate tests, are summarized in Table3.12. It should be noted that for all the samples the suggested value for m is assumed to be (Van Genuchten 1980):

$$m = 1 - \frac{1}{n} \qquad \text{Eq. 3.11}$$

Table 3.12: Value for parameters in Eq.3.10, estimated from RETC computer program

	No.	ϑ_s	ϑ_r *	α	m	n	Res. Err.
Experiment Type A	A1	8.3	0	.0072	.335	1.504	.992
	A2	4.98	0	.00129	.392	1.646	.984
	A3	2.84	0	.00037	.49	1.96	.987
	A4	2.35	0	.0003	.44	1.787	.988
	A5	2.35	0	.0003	.399	1.663	.996
Experiment Type B	B1	8.3	0	.0072	.335	1.504	.992
	B2	6.28	0	.00697	.322	1.475	.993
	B3	3.94	0	.00882	.282	1.393	.974
	B4	2.55	0	.00339	.318	1.466	.962
	B5	1.74	0	.00112	.433	1.764	.977
Experiment Type C	C1	1.3	.19	.00021	.419	1.722	.996
	C2	1.8	0	.00027	.374	1.598	.996
	C3	2.74	0	.00049	.423	1.734	.997
	C4	3.77	0	.00084	.413	1.704	.997
	C5	6.01	0	.00202	.38	1.614	.994
Experiment Type D	D1	1.31	0	.00023	.245	1.325	.994
	D2	2.15	0	.00063	.307	1.442	.998
	D3	8.3	0	.0072	.335	1.504	.992

** value of moisture ratio at residual water which has been estimated by the program*

Figs. 3.14 (p.86) through 3.17 (p.87) illustrate the agreement between the experimental results and the modified Van Genuchten model for all four series of tests. It is concluded from the figures that except for the very high soil suction, there is a good agreement between the model and experimental results. This exception is due to the fact that in a very

high value of soil suction, soil water has the characteristic of adsorbed water, while the Van Genuchten model has been developed particularly for non-swelling soils.

In addition to the use of the empirical formula, a neural network technique will be described which is not only sufficiently accurate, but can also simultaneously include all the desired parameters that might affect the moisture retention characteristic.

3.3. Unsaturated Permeability

3.3.1. History

Solving unsaturated soil water flow problems with deterministic or stochastic models requires unsaturated hydraulic conductivity data. There are two existing methods to determine the relation between unsaturated hydraulic permeability and water content or suction in the soil.

3.3.1.1. Direct Methods

Using these methods, the unsaturated hydraulic conductivity is measured directly under steady-state or non-steady conditions. For instance, in the crust method (Bouma et al., 1983), the unsaturated hydraulic conductivity (K(u)) is determined through measuring, when the steady state is achieved, the flux density of water going into an unsaturated sample. Dirksen(1991) established the drip infiltration method in which the unsaturated hydraulic conductivity is found by infiltration. The flux density, q, supplied from a reservoir and dripped by needles over the sample, as well as the head gradient, $(\delta h)/(\delta z)$, are measured using a pulsating pump and tensiometers. Finally the unsaturated hydraulic con-

ductivity is calculated by Darcy's law:

$$q = -K(h)\left(\frac{dh}{dz} + 1\right) \qquad \text{Eq. 3.12}$$

Wildenschild (1997) followed the same method by using a two-stage procedure and employing a syringe pump. He recorded the rate of outflow during infiltration.

Wind(1968) proposed an evaporation method in which tensiometers are installed at regular depth intervals in saturated soil samples. Each sample is located on a balance with the surface exposed to the air. Evaporated water flux and head are recorded simultaneously and unsaturated hydraulic conductivity is determined using Eq.2.1. Mohrath (1997) analyzed the error of the evaporation method in determining the unsaturated hydraulic properties of soils. Tamari et al. (1993) modified the wind method assuming Van Genuchten's(1980) S-shape model for soil water retention to estimate the water content at different times and depths associated with measured water head. Also Wendroth et al.(1993) reevaluated the evaporation method. Hayashi (1997) used TRT method (Tensiometers Response Time) to estimate the unsaturated hydraulic conductivity in the field.

3.3.1.2. Indirect Methods.

In the past, indirect methods have relied on statistical pore size distribution models to predict the hydraulic conductivity from soil water retention data (Burdine, 1953; Mualem, 1976; Tomasella, 1997). Inverse methods (Zachmann et al., 1981) are also considered as an indirect method, since analytical formula are first assumed to describe the soil hydraulic properties. Assigning values to the parameters in these relations makes it possible to solve the water flow equation for the same initial and boundary conditions in

the experiment. The final hydraulic properties are calculated by using an iterative procedure. Gupta et al.(1974) used the one step outflow (OSO) experiment to determine the soil water diffusivity relationship. Pool et al. (1985) investigated the feasibility of using a parameter estimation approach to obtain $\theta(h)$ and $K(h)$ by recording the cumulative outflow using an initially saturated soil sample in a pressure desorption cell following a step change in gas pressure. More detail in experimental procedure has been illustrated by Parker et. al (1985). In the OSO method, the hydraulic properties are assumed to be described by Van Genuchten (1980) or Mualem models(1976).

$$S_e = (\theta - \theta_r)/(\theta_s - \theta_r) \qquad \text{Eq. 3.13}$$

$$h(S_e) = [(S_e^{-1/m} - 1)^{1/n}]/\alpha \qquad \text{Eq. 3.14}$$

$$K(S_e) = K_s S_s^{\lambda}[1 - (1 - S_e^{-1/m})^m]^2 \qquad \text{Eq. 3.15}$$

where S_e is the normalized volumetric water content, α, n and λ are empirical parameters, θ_r and θ_s are residual and saturated water content, K_s is the saturated hydraulic conductivity and $m=1-1/n$.The model parameters are optimized through a nonlinear least-squares optimization algorithm using a set of cumulative outflow measurements:

$$E(b) = \sum_{i=1}^{N} \{w_i[Q(t_i) - \hat{Q}(t_i, b)]\}^2 \qquad \text{Eq. 3.16}$$

where $Q(t_i)$ is the measured cumulative outflow, $\hat{Q}(t_i, b)$ is the numerical calculated outflow from the Richard equation (Eq.2.1) and the values of $h(\theta)$ and $K(\theta)$ (from Eqs. 2.2 to 2.4) through a set of trial vector parameters $\{\alpha, n, \theta_r\}$. Van Dam et. al (1992) reported

the problem of uniqueness in parameter optimization process and that the cumulative out-flow data alone contains insufficient information to estimate $K(\theta)$ curve accurately. He introduced the new objective function as follows:

$$O(\mathbf{b}) = \sum_{i=1}^{N_1} \{w_i[Q(t_i) - \hat{Q}(t_i, \mathbf{b})]\}^2 + \sum_{i=1}^{N_2} \{w_i v_i[\theta_0(h_i) - \theta_c(\mathbf{b}, h_i)]\}^2 \qquad \text{Eq. 3.17}$$

where v_i is an internal weighting factor determined by the program, and θ_0 is the measured water content. Other parameters are the same as in Eq.2.5. Also Hopmans et al.(1992) explained the influence of the initial water content of the sample on the results of OSO. He used X-ray tomography to measure the spatial and temporal changes in soil water distribution in OSO experiments. He concluded that better results may be obtained if the penumetric pressure is applied to a sample initially unsaturated.Stolte et al.(1994) compared the results of six direct and indirect methods used to determine unsaturated hydraulic conductivity.He concluded that it is difficult to compare the conductivity determined from different methods which is dependent on the chosen method and the sample situation.

Van Dam et al.(1990) introduced the multi-step out flow experiment, MOS, which is indeed a modification of OSO experiment. In this method, a series of increasing pressure steps are applied. The inverse methodology is coupled with the parametric models assumed for soil hydraulic properties to minimize an objective function, which is as the same used in OSO experiment (Eq. 3.14 and Eq. 3.15). Eching et al.(1994) employed two direct methods for measuring the hydraulic conductivity and compared the results with those of MSO experiment. He found an excellent agreement between these results. He also stated that the problem of uniqueness in the parameter values optimization process is reduced if the

cumulative outflow volume and the simultaneously measured soil water pressure head data are used in the objective function. Marion et al.(1994) evaluated some laboratory and field methods to determine the hydraulic properties of the unsaturated soil. He compared the instantaneous profile, miscellaneous and inverse modeling (MOS) methods. He concluded that the inverse method alone appears to be time effective, and in combination whit the instantaneous method, may be the only feasible technique to describe the $K-\theta$ relationship. Special attention was paid to the uniqueness of the solution by Van Dam et al.(1994). He compared the OSO and MSO approaches for estimating the soil hydraulic conductivity. He found that MSO experiment has theoretical and practical advantages over the OSO. However, he mentioned that these methodologies may fail for soil samples having shrinkage characteristics, since they may lose contact with the ceramic plate during the experiment, thereby affecting outflow.

Meerdink et al.(1996) determined unsaturated hydraulic conductivity by applying the laboratory and field methods. He also used the Van Genuchten-Mualem models(1976,1980), Brooks-Corey model (1966) and Fredlund et al. model(1994) as the three different parametric models to be fitted over his soil hydraulic data. He concluded that these models for the more active and compacted clay, specially those with very low water content, are very poor in predicting the unsaturated hydraulic conductivity. The reasons he advanced were, firstly, insufficient data is available in very low water content and, secondly, since the Van Genuchten-Mualem models (1976,1980) and the Fredlund et al. model(1994) are based on the statistical models of flow through a set of capillary tubes, they are unlikely to capture the complexities of water flow through such soils where flow occurs through interclod voids and intraclod pores. In addition, flow through these pores is

increasingly affected by mineral surface forces as the soil desaturates. Vereecken (1997) also examined the Multistep Outflow method to estimate the unsaturated properties of soils. He mentioned that the method is one of the most promising method among other indirect methods. Simunek (1997) employed the multiple tension disc infiltrometer data to estimate the unsaturated hydraulic properties of soils.

3.3.1.3. Parametric models

The use of numerical models for simulating the flow through unsaturated soil needs parametric functions of the soil hydraulic properties. There are two approaches to obtain these functions: *(i)* empirical equation and *(ii)* statistical models.

Leong (1997) reviewed the permeability functions for unsaturated soils. Among the empirical functions, models of Brooks and Croney(1964) and Smiles(1976) seem to be more reliable. Brooks and Crorey (1964) analyzed a large amount of data and ended up with an empirical conductivity function as follows:

$$K_r = \begin{cases} \left(\frac{\Psi_{ae}}{\Psi}\right)^{2+(5\lambda/2)} & (\Psi > \Psi_{ae}) \\ 1 & (\Psi \le \Psi_{ae}) \end{cases} \qquad \text{Eq. 3.18}$$

where Ψ_{ae} is the air-entry suction and λ is the pore size distribution index, which is defined as the negative slope of the effective degree of saturation, S_e, versus the matrix suction (U_a-U_w) curve (Fredlund et al. 1993). K_r is regarded as the relative permeability. Smiles (1976) conducted desaturation experiments on an initially saturated soil sample of red mud. Different initial water contents were chosen for the experiment. He found the following expression for the unsaturated hydraulic conductivity and matrix suction relation-

ship with respect to the material coordinate:

$$ln(K_m) = C + D\,ln(-\psi) \qquad \text{Eq. 3.19}$$

where K_m is the relative permeability. Mualem (1976) determined the relationship for both $\psi(\theta)$ and $K(\theta)$ based on some assumptions. First he assumed that the porous medium may be regarded as a set of the interconnected pores randomly distributed in the sample. The second assumption was that a simple laminar flow exists in the microscopic and macroscopic pores, and finally he considered the soil retention curve analogous to the pore radii distribution function. Also, in terms of the geometrical interpretation of the pores, Mualem considered the flow along a porous slab. Using these assumptions and a statistical procedure, he arrived at the following expression for the unsaturated relative hydraulic conductivity:

$$K_r = \Theta^{1/2}\left[\int_0^{\Theta} \frac{1}{h(x)}dx \Big/ \int_0^{1} \frac{1}{h(x)}dx\right]^2 \qquad \text{Eq. 3.20}$$

where h is the pressure head, given here by a function of dimensionless water content:

$$\Theta = \frac{\theta - \theta_r}{\theta_s - \theta_r} \qquad \text{Eq. 3.21}$$

In this equation subscripts r and s indicate saturated and residual values of soil water content. Van Genuchten (1980) solved Eq. 3.9 by assuming the following relation between the dimensionless water content, Θ, and the pressure head, h:

$$\Theta = \left[\frac{1}{1 + (\alpha h)^n}\right]^m \qquad \text{Eq. 3.22}$$

where α, n and m are the fitting parameters of the water retention data. Van Genuchten reached a particular form of an incomplete beta-function, and after integrating, he ended up

with the following formula for the relative unsaturated hydraulic conductivity:

$$K_r(\psi) = \frac{\{1-(\alpha\psi)^{n-1}[1+(\alpha\psi)^n]^{-m}\}^2}{[1+(\alpha\psi)^n]^{m/2}} \qquad \text{Eq. 3.23}$$

Fredlund et al (1994) used the statistical approach to derive the permeability function. First they defined a new relation for the soil-water characteristic curve as follows (Fredlund and Xing 1994):

$$\theta = C(\psi)\frac{\theta_s}{\{ln[e+(\psi/a)^n]\}^m} \qquad \text{Eq. 3.24}$$

where e is the natural number, a is the approximate air -entry value of the soil, n is the parameter that controls the slope at the inflection point in soil-water characteristic curve, m is the parameter related to the residual water content, and $C(\psi)$ is a correcting function defined as:

$$C(\psi) = 1 - \frac{ln\left(1+\frac{\psi}{C_r}\right)}{ln\left(1+\frac{10^6}{C_r}\right)} \qquad \text{Eq. 3.25}$$

and C_r is a constant related to the matrix suction at the residual water content. He combined Eq. 3.14 with the Childs and Collis-George's model for the permeability function and obtained the unsaturated permeability function in the form of:

$$K_r(\psi) = \frac{\int_{ln(\psi)}^{b} \frac{\theta(e^y)-\theta(\psi)}{e^y}\theta'(e^y)dy}{\int_{ln(\psi_a)}^{b} \frac{\theta(e^y)-\theta_s}{e^y}\theta'(e^y)dy} \qquad \text{Eq. 3.26}$$

where y is a dummy variable representing $\ln(\psi)$; $b=\ln(10^6)$ and ψ_a is the pressure at the air-entry point.

3.3.2. Proposed Method

Direct and indirect methods, briefly described in the previous section, have some difficulty to be employed for highly swelling clay. For instance, Stolte et al.(1994) compared six direct and indirect methods and excluded these kinds of soils from his study because of their inherent shrinkage and swelling. Moreover, Meerdink et al.(1996) reported that the statistical models have some difficulty to predict the hydraulic conductivity in very low range of water content. The reason he found was that in this range, the capillary concept, which is used in the primary assumption of statistical models, is increasingly affected by the mineral forces.

The soil with a high potential of swelling has respectively large deformation during the saturation or desaturation. Therefore, in the usual direct method, the subsequent problems, such as loss of contact between the sample and the container and also change of the pores' geometry due to shrinkage phenomena, make these methods very difficult to conduct. On the other hand, none of the empirical or statistical models consider the deformation phenomena which occurs during the saturation or desaturation of a swelling soil.

Upon the aforementioned evidence, a very simple procedure, similar to the one-step and multi-step outflow, is presented to estimate experimentally the unsaturated hydraulic conductivity in the soil with large shrinkage values. Furthermore, some parametric models are evaluated to be used in the numerical part for solving the flow equation.

The data and the cumulative outflow water and its corresponding time, obtained during the pressure plate experiment, are used to estimate the unsaturated hydraulic conductivity in the proposed method. The methodology used, in some aspects, is similar to the direct method employed by Eching et al.(1994). However, some appropriate assumptions should be made to achieve a practically simple but theoretically accurate approach. These assumptions are summarized as follows:

1) There is no flux at the top of the sample (i.e. $\partial h/\partial z = 1$ (Van Dam et al.1992).

2) There is a uniform water content over the column at time t, i.e. the rate of outflow depends on the rate at which this approximately uniform water content declines with the time (Passioura 1976).

3) The effect of gravity is neglected when the equilibrium in total soil-water head is achieved, i.e. If the sample height is chosen small enough (e.g. 1 to 2 cm) the variation in matrix pressure from the top to the bottom of the sample may be neglected in comparison to the matrix pressure head (Klute 1986).

The second and third assumptions are fairly accurate since the height of the sample is small enough ($L=1cm$), compare with the larger scale.

3.3.2.1. Theory

Of most significance to the proposed methodology is Zaslavsky's words that "Darcy's formula and the hydraulic conductivity K are meaningless unless q, the water flux, is actually measured relative to the soil particles. Otherwise, extremely different values of K can be found for the soil under the same flow conditions and gradients only

because the soil is translated at different velocities with respect to discharge-measuring pipes" (1964). According to this important statement, the following relation is assumed for the measured water flux as the outflow water:

$$q_t = q_r + q_{ws} \qquad \text{Eq. 3.27}$$

where q_t is the water flux measured at the outflow, q_r is the Darcian flux (i.e. flux relative to the soil particles) and q_{ws} is the flux of water moving with the velocity of soil particles. The Darcian flux and the flux related to the soil particle movement can be described as:

$$q_{ws} = \vartheta u_s \qquad \text{Eq. 3.28}$$

$$q_r = -K\left(\frac{dh}{dz} - 1\right) \qquad \text{Eq. 3.29}$$

where ϑ is moisture ratio, u_s is the soil particle velocity, h accounts for the soil water matrix potential and z is spatial coordinate, positive downward. Substituting Eqs. 3.28 and 3.29 in eq. 3.27 and multiplying both sides by $T.A$, in which T is the total equilibrium time and A is the cross section area of the sample, results in:

$$T \cdot A \cdot q = T \cdot A \cdot \left[-K\left(\frac{dh}{dz} - 1\right) + \vartheta u_s\right] \qquad \text{Eq. 3.30}$$

or

$$Q = T \cdot A \cdot \left[-K\left(\frac{\overline{\Delta h}}{\bar{L}} - 1\right) + \bar{\vartheta}\bar{u}_s\right] \qquad \text{Eq. 3.31}$$

where Q is the total outflow at total time T, $\overline{\Delta h}/\bar{L}$ is the mean hydraulic gradient over the sample, $\bar{L}$ is the average sample length, $\bar{\vartheta}$ is the average initial and final moisture ratio of

the sample, and $\overline{u_s}$ is the average soil particle velocity determined by:

$$\overline{u_s} = \frac{\Delta l}{T} \qquad \text{Eq. 3.32}$$

where Δl is the amount of shrinkage during time T. In order to calculate $\overline{\Delta h}$, the water pressure at the top and the bottom of the sample must be determined. The total head at the soil-cut membrane interface might be calculated from the following relation(Ahuja,1973):

$$H_i = H_b + \frac{d}{K_P}(\Delta Q / A \Delta t) \qquad \text{Eq. 3.33}$$

where H_i is the total soil water head at the soil-membrane interface, H_b is the constant total water head at the bottom of the membrane, K_P is saturated hydraulic conductivity of the membrane, d is the thickness of the membrane, and ΔQ is cumulated water outflow within the time interval Δt

Some necessary specifications of the membrane are summarized as follows:

1) Saturated hydraulic conductivity= 1×10^{-6} cm/sec

2) Thickness=.076 mm

3) Air entry value= over 1500 psi (100 Bars)

4) Average pore radius= 24A (1A=.0001 microns)

The matrix head at the bottom of the membrane, H_b, may be adjusted to zero by keeping the level of outflow water inside the burette, roughly level with the bottom of the membrane while opening to the atmosphere. Eq. 3.33 may be used to calculate the initial and final simultaneous water pressures at the soil-membrane interface by substitution of

the corresponding value $q = \Delta Q/\Delta t$ for the initial and final stages of each pressure step from the outflow-time curve, ignoring the gravity potential. The latter approximation has little effect on the calculated water pressure at the bottom of the sample. Eventually, the mean value of water pressure is calculated from:

$$\overline{h_i} = \frac{h_{i(ini)} + h_{i(fin)}}{2} \qquad \text{Eq. 3.34}$$

where $h_{i(ini)}$ and $h_{i(fin)}$ are the initial and final pressure heads at the bottom of the sample. The water pressure head at the top of the sample can be found from the following formula (Klute 1986):

$$h_{top} = h_a + h_m \qquad \text{Eq. 3.35}$$

where h_a is the applied gas pressure and h_m is the soil water matrix potential, which at the beginning of each pressure step, has the precedent final value from the previous step. Eventually, the air pressure increases the water matrix pressure gradually (i.e. make it more negative) and at the equilibrium, h_m gains its maximum value, $-h_a$. Therefore, the average value of water pressure at the top of the sample may be calculated as follows:

$$\bar{h}_{top} = h_a + \left(\frac{h_{mi} + h_{mf}}{2}\right) \qquad \text{Eq. 3.36}$$

considering $h_{mf} = -h_a$:

$$\bar{h}_{top} = \left(\frac{h_a + h_{mi}}{2}\right) \qquad \text{Eq. 3.37}$$

where h_{mi} and h_{mf} are the initial and final matrix potential of water. Finally, the average matrix pressure between the two ends of the sample will be:

$$\Delta h = \bar{h}_{top} - \overline{h_i} \qquad \text{Eq. 3.38}$$

considering equations 3.32 through 3.38, the unsaturated hydraulic conductivity may be calculated from equation 3.31:

$$K(\bar{\theta}) = \left(\frac{L}{\overline{\Delta h} - \bar{L}}\right)\left(\bar{\vartheta}\frac{\overline{\Delta L}}{T} - \frac{Q}{TA}\right) \qquad \text{Eq. 3.39}$$

one may find the total water outflow, Q, from the following relationship:

$$Q = AL(\vartheta_{ini} - \vartheta_{fin}) \qquad \text{Eq. 3.40}$$

where ϑ_{ini} and ϑ_{fin} are the initial and final moisture ratios in each pressure set.

3.3.2.2. Materials and Procedure

The sample specifications, used for the purpose of measuring unsaturated hydraulic permeability, are summarized in Table3.13.

Table 3.13: Samples Specification for Unsaturated Hydraulic Permeability Test

No.	Ben. (%)	Over load (kPa)	ω % (initial)	ϑ (initial)	ρ_b (initial)	Height (mm)
D_1	50 %	90	47	1.31	1.22	10
D_2	50 %	50	74	2.15	0.91	10
D_3	50 %	0	300	8.30	0.28	10

Three different overload conditions were applied to the soil in order to determine the full relationship of unsaturated hydraulic conductivity with soil moisture ratio and overload condition. The samples are located over the cut membrane in the pressure plate test apparatus as described in Section 3.2. An overload pressure was applied on the top of

the soil inside the pressure cell. Then an initial relatively small air pressure, not the actual value, was applied over the samples and the outflow and the corresponding time were recorded. This step was carried out to remove the non-uniform outflow reported by Passioura(1977) which occurs at the early stage of the outflow, because of air-gap inside the water-permeable membrane pores. After reaching the initial equilibrium, the pressure was adjusted to the actual value. After the final equilibrium was observed, the samples were weighed to find their moisture ratio, and also a hight measurement was carried out to find the vertical shrinkage of the samples during the drainage. The shrinkage in other directions, other than the vertical, may be neglected since it is a very small fraction of the sample section area. This assumption will be much more reliable if the sample diameter is chosen much bigger than the height.

After preparing all the necessary data, the mean unsaturated hydraulic conductivity corresponding to the mean soil moisture ratio can be calculated from Eq. 3.39. The results for three selected soil samples have been illustrated in Fig. 3.18 (p.87). It can be concluded from the figure that an increase in the magnitude of overload pressure produces a decrease in soil unsaturated hydraulic conductivity. It is thought that the decrease in soil void ratio and the expansion restriction of the sample, due to overload pressure, can be the major causes of reduction in the value of the unsaturated hydraulic conductivity.

The effect of the overload pressure on the unsaturated hydraulic conductivity-soil suction relationship is more clear when a three dimensional diagram is provided (Fig. 3.19 p.88). The two horizontal axes of this graph show the soil suction and overload pressure, and the vertical direction presents the unsaturated hydraulic conductivity. From the Figure, one may predict the value of unsaturated hydraulic conductivity, corresponding to a certain

value of soil suction and overload pressure.

3.3.3. Parametric Model

In order to apply the unsaturated hydraulic conductivity-moisture ratio relationship to the unsaturated water flow model, and to verify the results of the selected experimental method, a statistical parametric model (Van Genuchten-Mualem models) is selected. The model is modified to the following form:

$$K_r(S_e) = S_e^{1/2}[1-(1-S_e^{1/m})^m]^2 \qquad \text{Eq. 3.41}$$

where:

$$S_e = \frac{\vartheta_d - \vartheta_{dr}}{\vartheta_{ds} - \vartheta_{dr}} \qquad \text{Eq. 3.42}$$

or in terms of the soil suction:

$$K_r(\psi) = \frac{\{1-(\alpha\psi)^{n-1}[1+(\alpha\psi)^n]^{-m}\}^2}{[1+(\alpha\psi)^n]^{m/2}} \qquad \text{Eq. 3.43}$$

where ϑ_d is the Darcian moisture ratio, ϑ_{dr} is the Darcian residual moisture ratio, ϑ_{ds} is the Darcian moisture ratio at the saturated soil condition, and m and n are the model parameters. The unsaturated hydraulic conductivity may be determined by multiplying the relative hydraulic conductivity, K_r, and saturated hydraulic conductivity described in section 3.1. The result is:

$$K(S_e) = K_r(S_e) \cdot K_{sat} \qquad \text{Eq. 3.44}$$

where

$$K_{sat}(e) = exp(a + be^{c}) \qquad \text{Eq. 3.45}$$

in which e is the soil void ratio and a, b and c are the fitting parameters determined in section 3.1 as:

$$a=-29.02 \ , \ b=6.53 \ , \ c=.275$$

Eqs. 3.44 and 3.45 describe the unsaturated hydraulic permeability in terms of the soil moisture ratio and the soil void ratio, corresponding to the specific overload conditions. By use of a statistical computer program, AXUM, the model defined by Eq.3.43 was fitted over the experimental results, and the parameters were found through a nonlinear regression and summarized in Table3.14. Fig. 3.20 (p.89) shows the comparison between the model and the experimental results. It might be followed from the figure that there is a reasonable agreement between the two results. One may find the model parameters of unsaturated hydraulic permeability slightly different from those summarized in Table 3.12 for the moisture retention model. This difference exists because the moisture retention model was developed regardless of the change in soil pores'geometry during drainage, and can only agree with the experimental results for non-deformable porous media; however, it may still be applicable to the deformable porous media as well if the changes in pores' geometry are somehow taken into account.This was considered in two procedures: when $K_{sat}(e)$ was multiplied by $K_r(\theta)$ to calculate the unsaturated hydraulic permeability, $K(\theta)$, and in the experimental procedures (Eq. 3.27).

In the numerical analysis of the developed unsaturated flow model, a general neu-

ral network model is proposed to estimate the unsaturated hydraulic conductivity in which the soil suction, moisture ratio, the overload pressure and the volume change's effects are taken into account.

Table 3.14: Different Model Parameters Estimated by Statistical Computer Program (AXUM)

	No.	ϑ_s	ϑ_r^*	α	m	n	Res. Err.
Experiment Type D	D1	1.31	0	1.3e-4	0.3119	1.458	0.994
	D2	2.15	0	7.1e-5	0.234	1.315	0.998
	D3	8.30	0	4.1e-5	0.3345	1.495	0.992

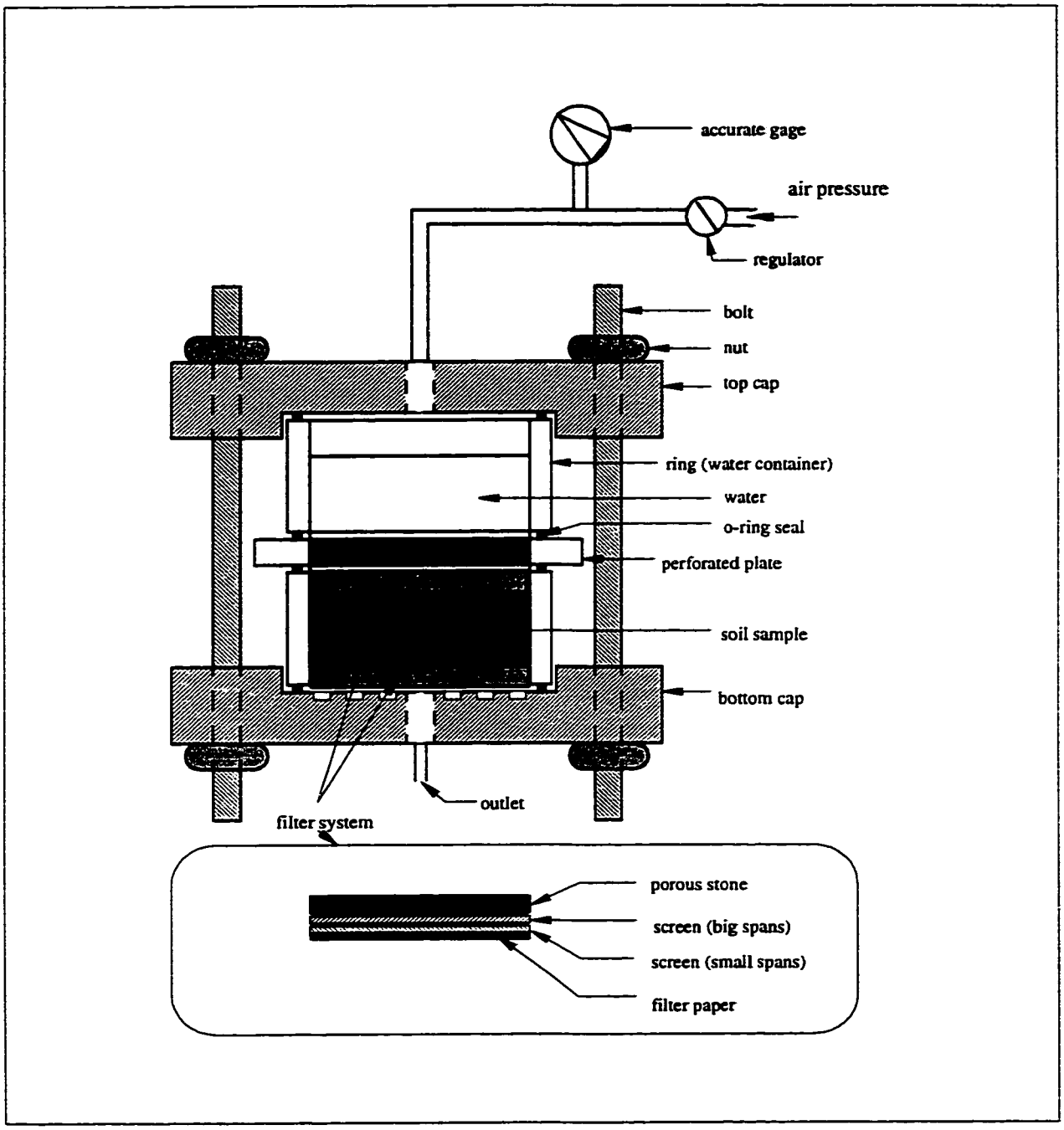

Fig. 3.1) Apparatus for measuring the swelling soil saturated water content

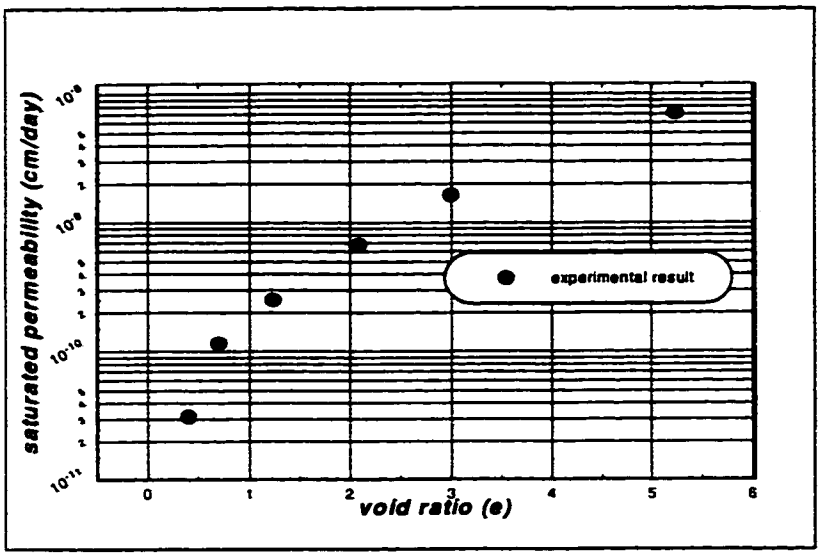

Fig. 3.2) Saturated hydraulic conductivity v.s. void ratio: Experimental result

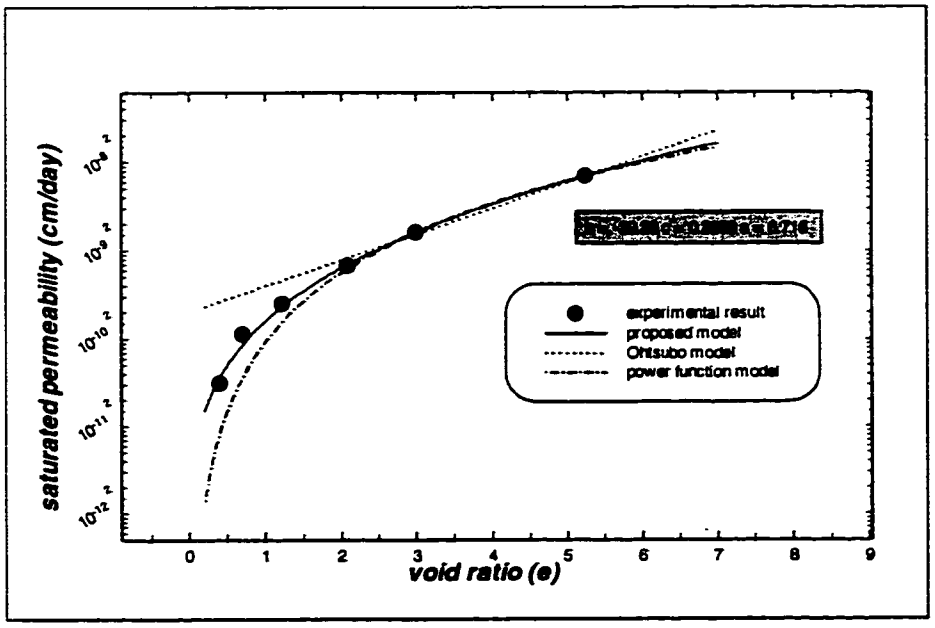

Fig. 3.3) Comparison between Ohtsubo(1985), power function and proposed model

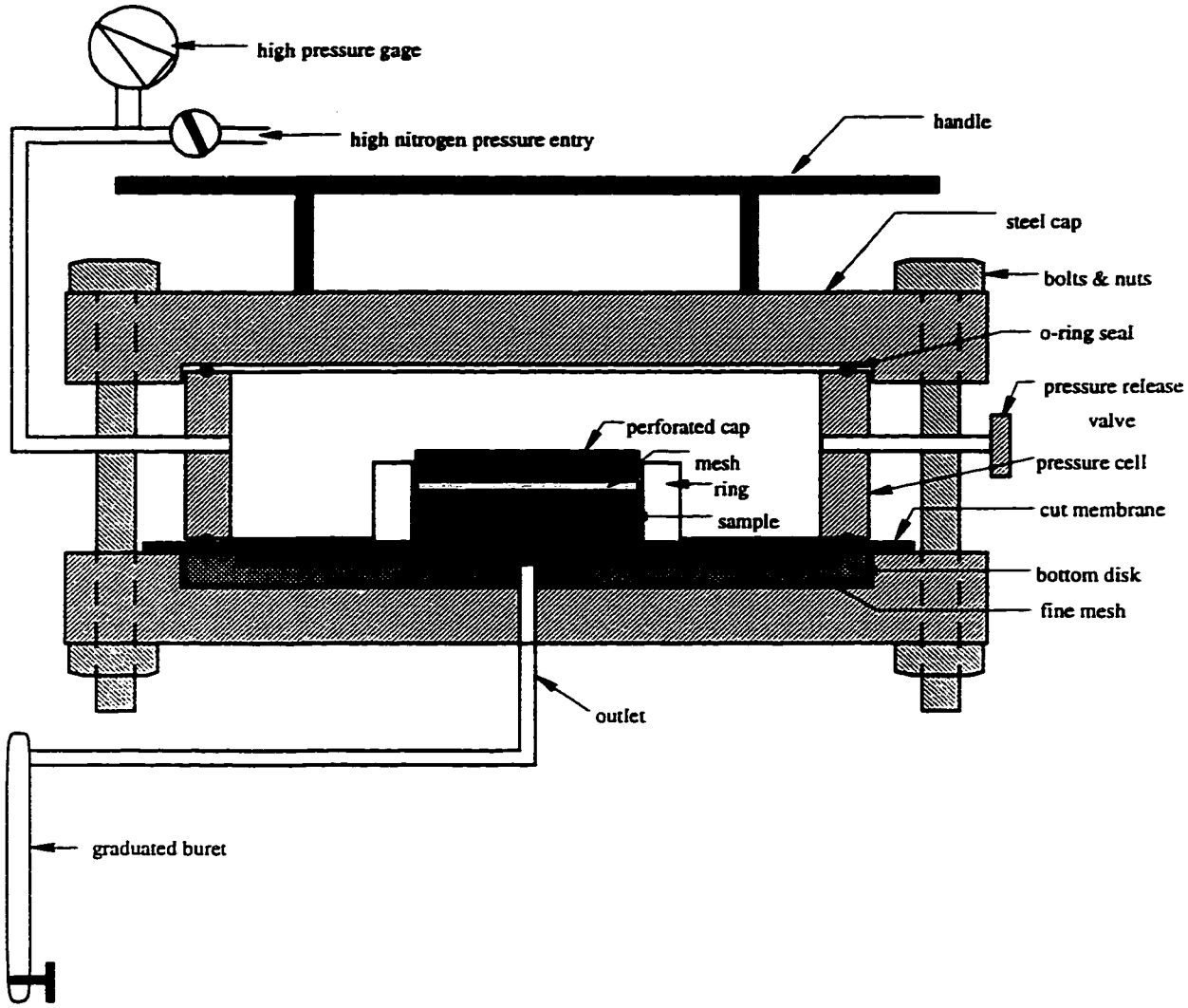

Fig. 3.4) Detail of the pressure plate apparatus

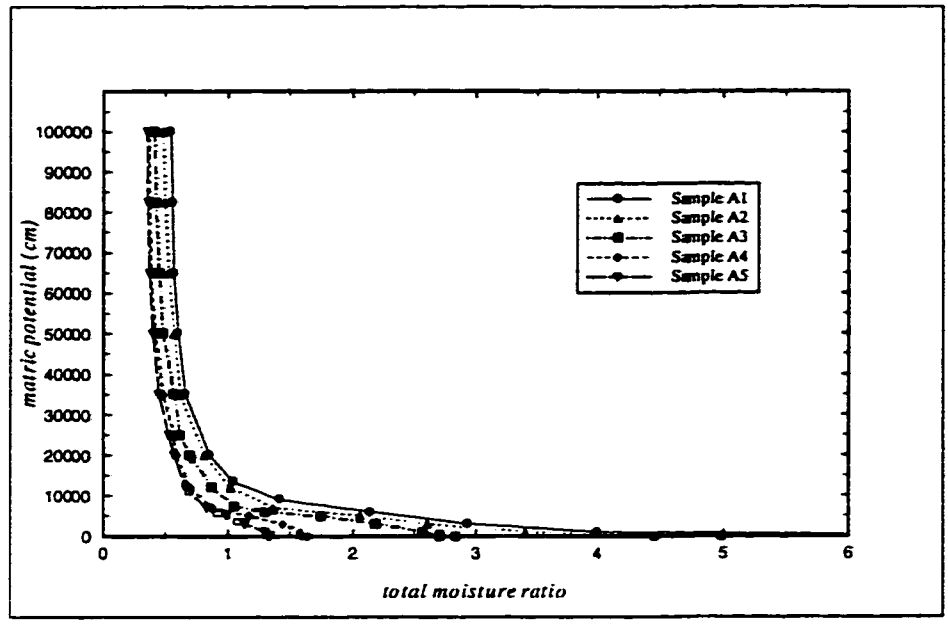

(a)

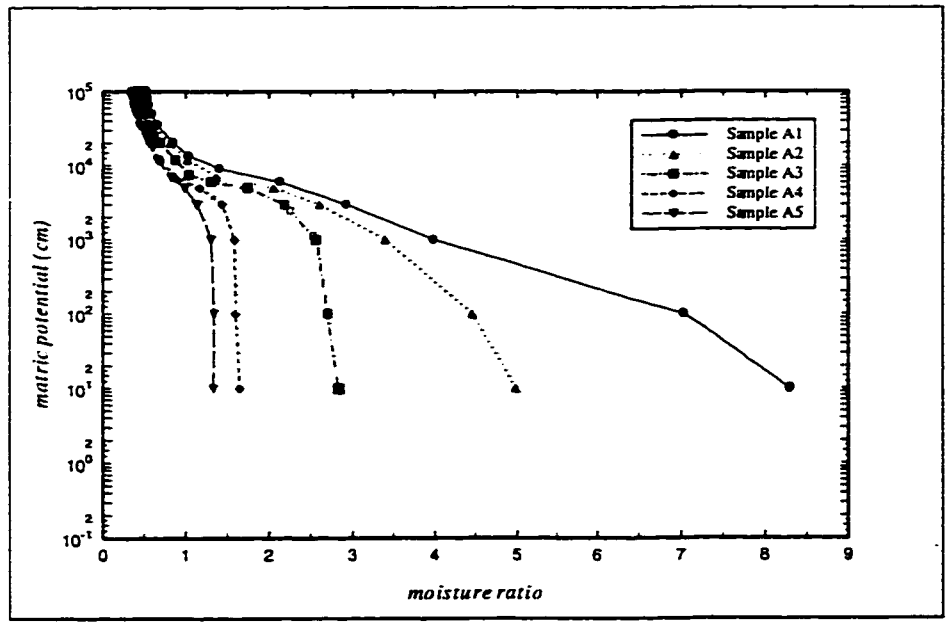

(b)

Fig. 3.5) Soil suction versus moisture ratio for different initial moisture ratio a) normal scale b)logarithmic scale

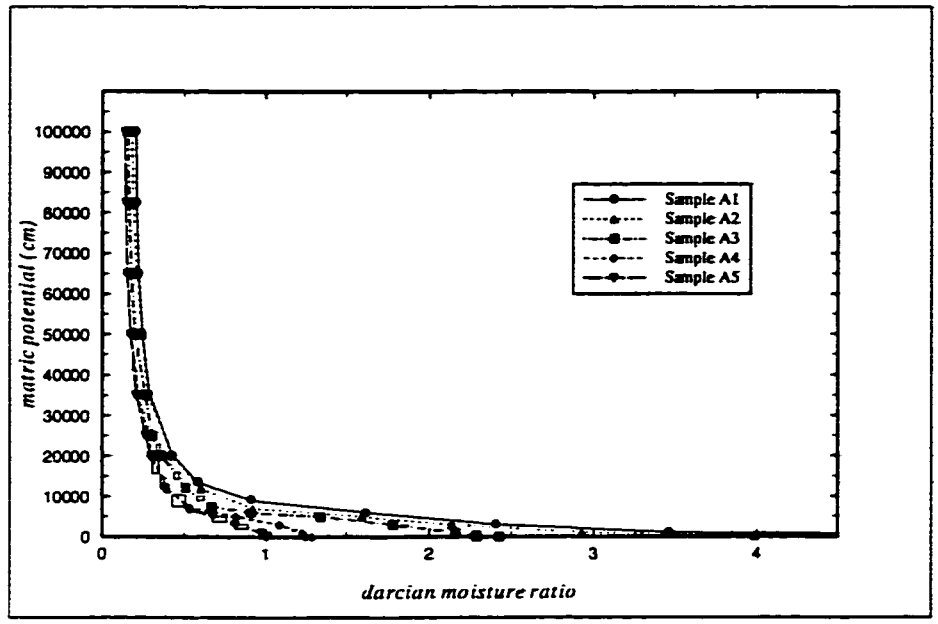

(a)

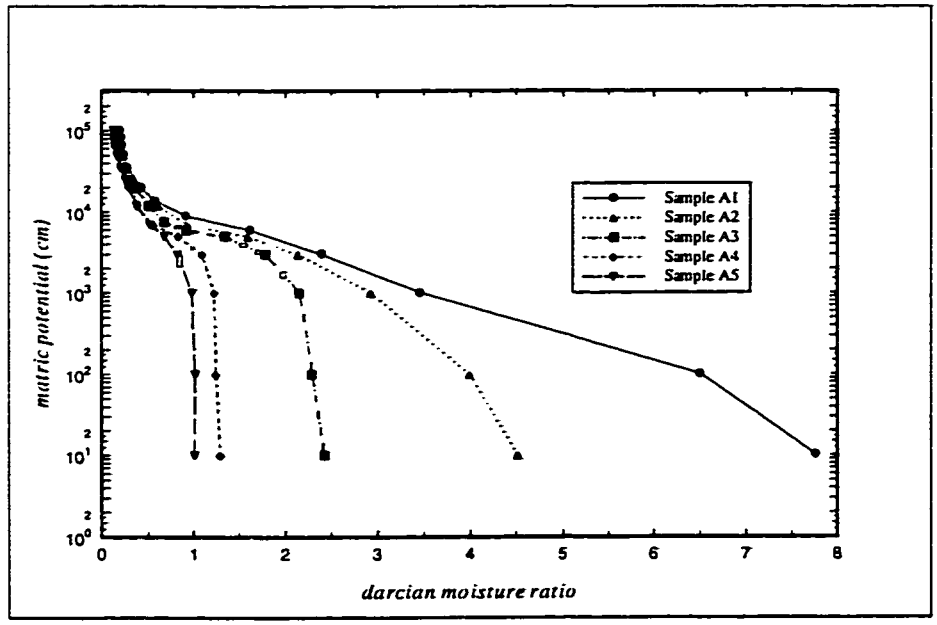

(b)

Fig. 3.6) Soil suction versus darcian moisture ratio for different initial moisture ratio a) normal scale b)logarithmic scale

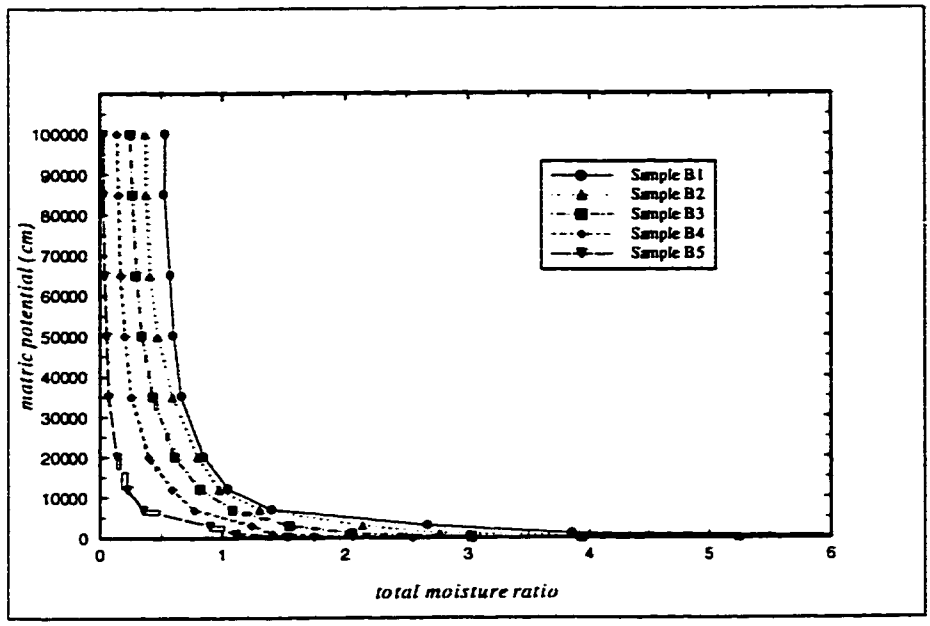

(a)

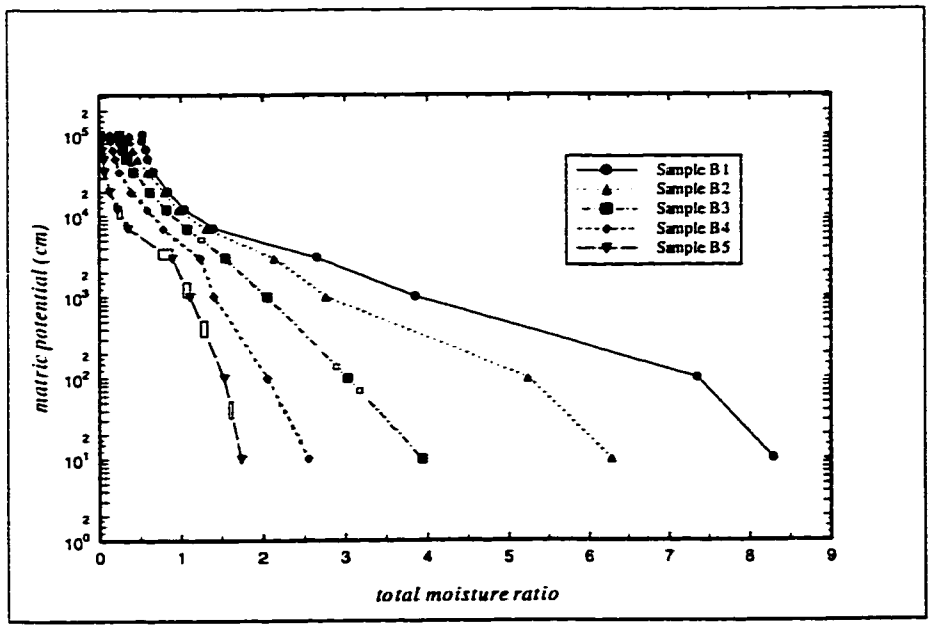

(b)

Fig. 3.7) Soil suction versus moisture ratio for samples with different percentage of swelling componant a) normal scale b)logarithmic scale

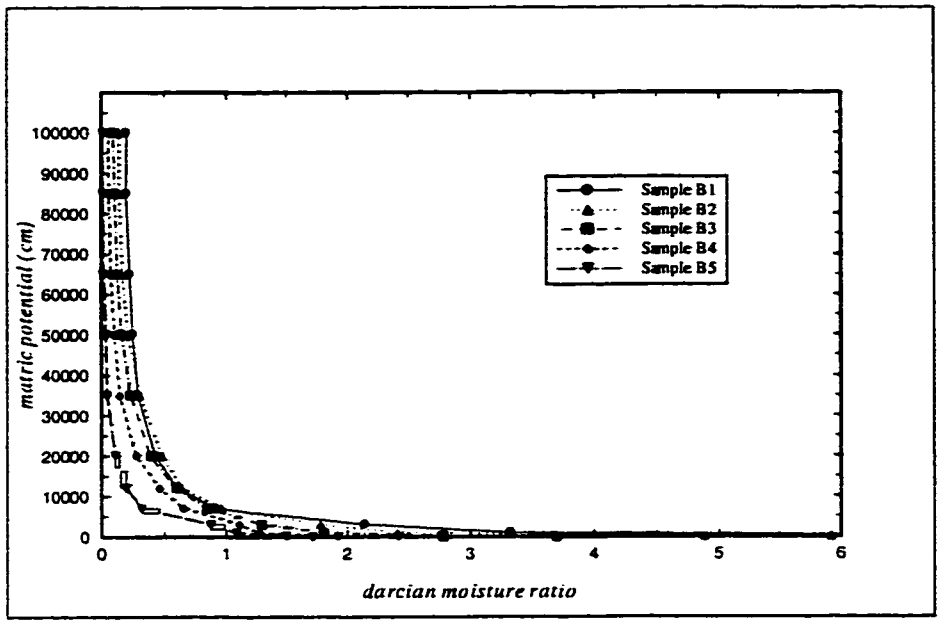

(a)

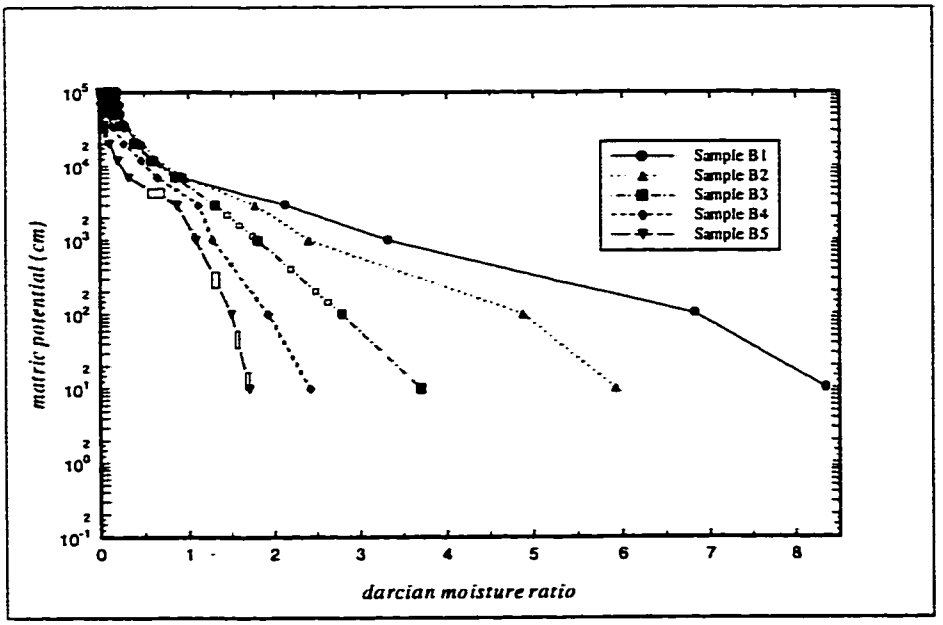

(b)

Fig. 3.8) Soil suction versus darcian moisture ratio for samples with different percentage of swelling componant a) normal scale b)logarithmic scale

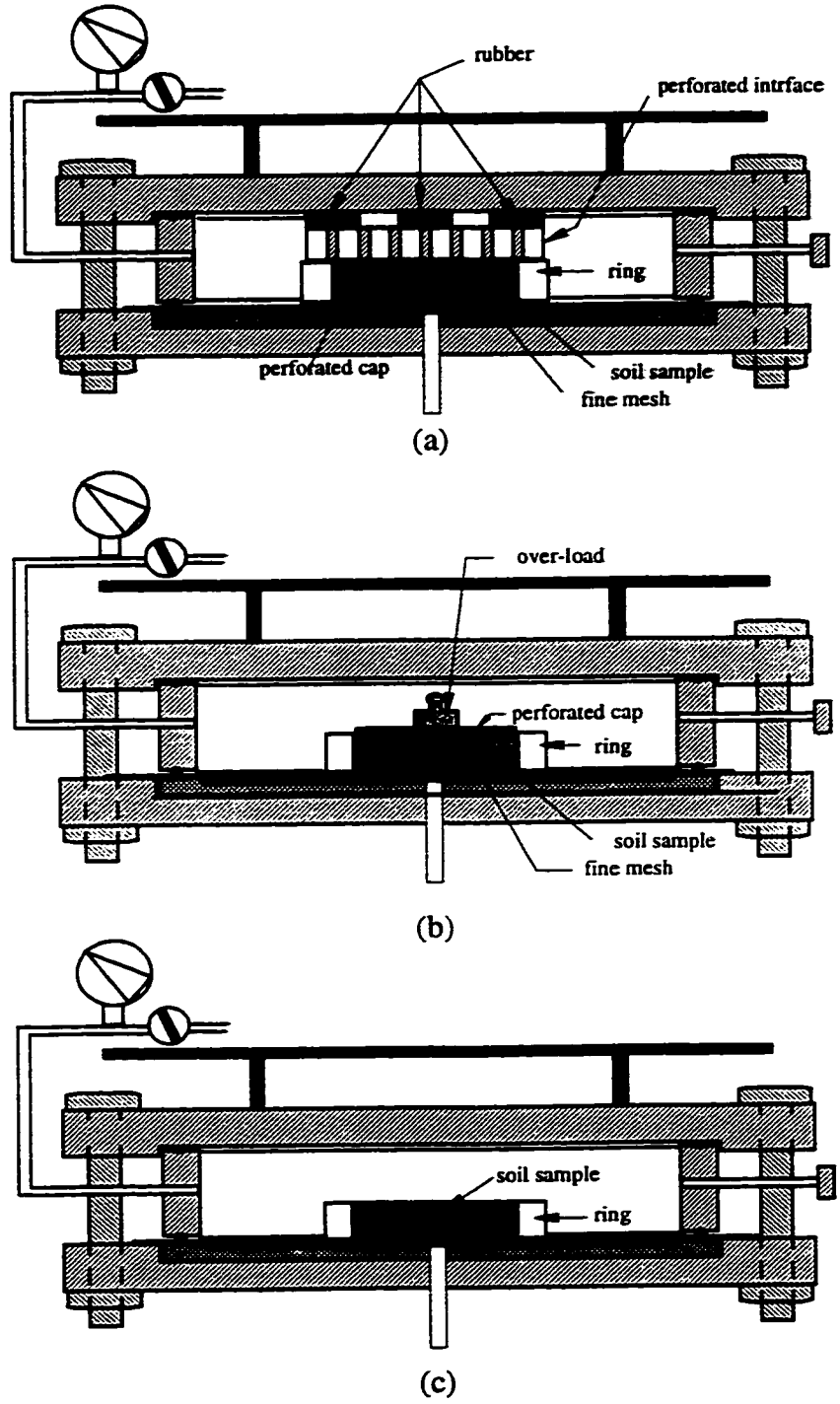

Fig. 3.9) Different set up of P.P.T. apparatus a)constant bulk density b)over-load effect c)simple condition

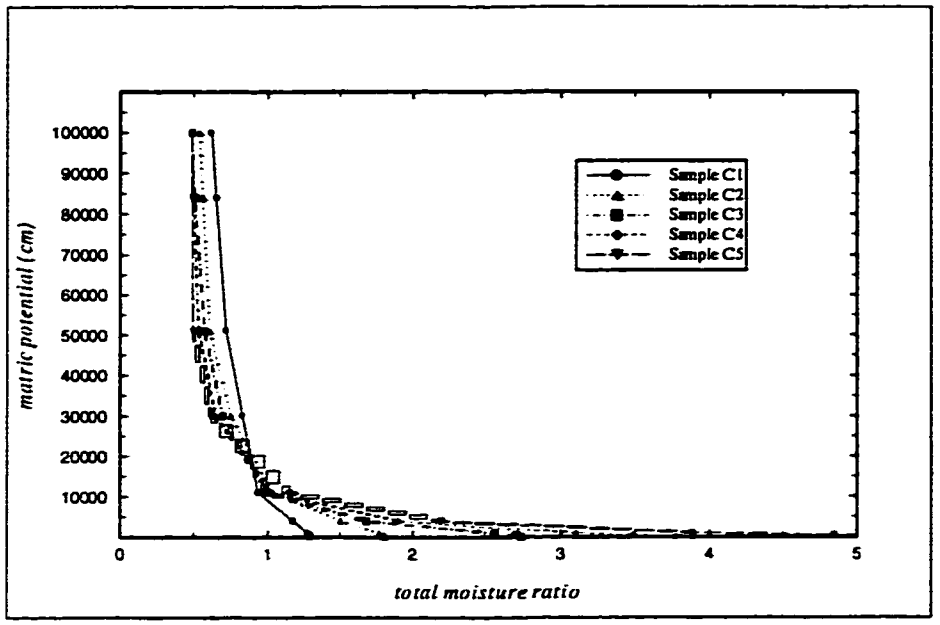

(a)

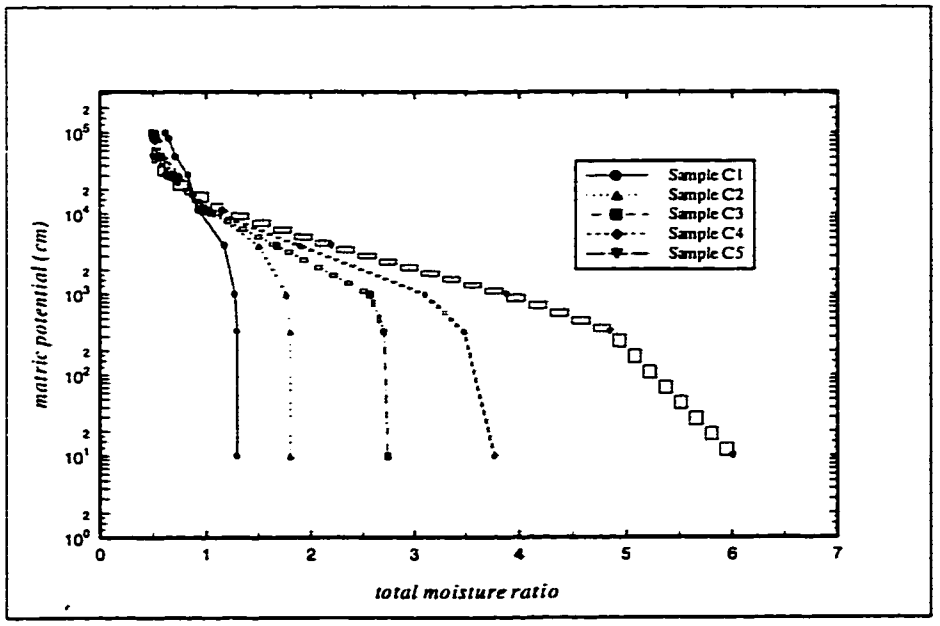

(b)

Fig. 3.10) Soil suction versus moisture ratio for samples with different initial bulk density under completly confined condition a) normal scale b) logarithmic scale

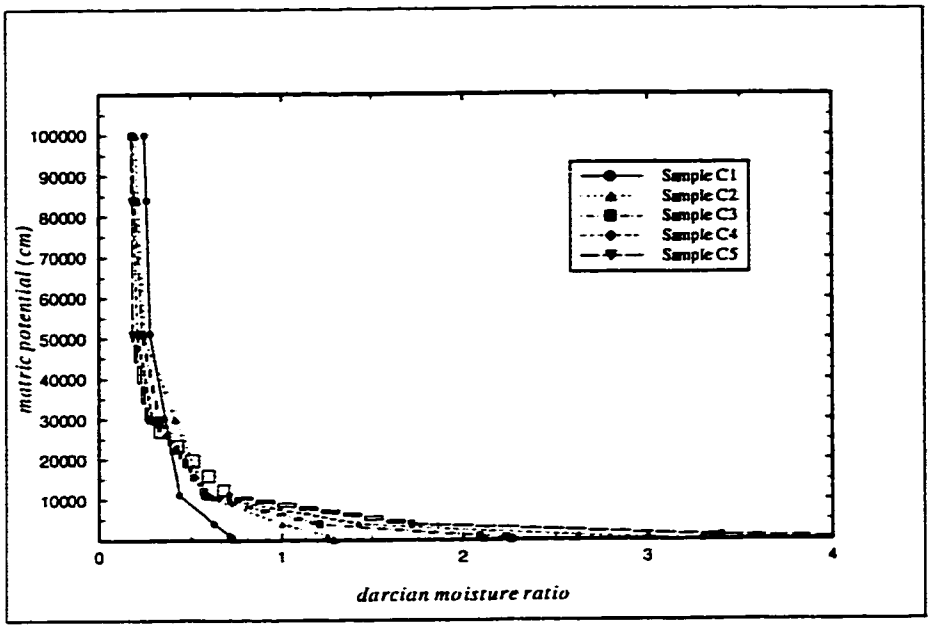

(a)

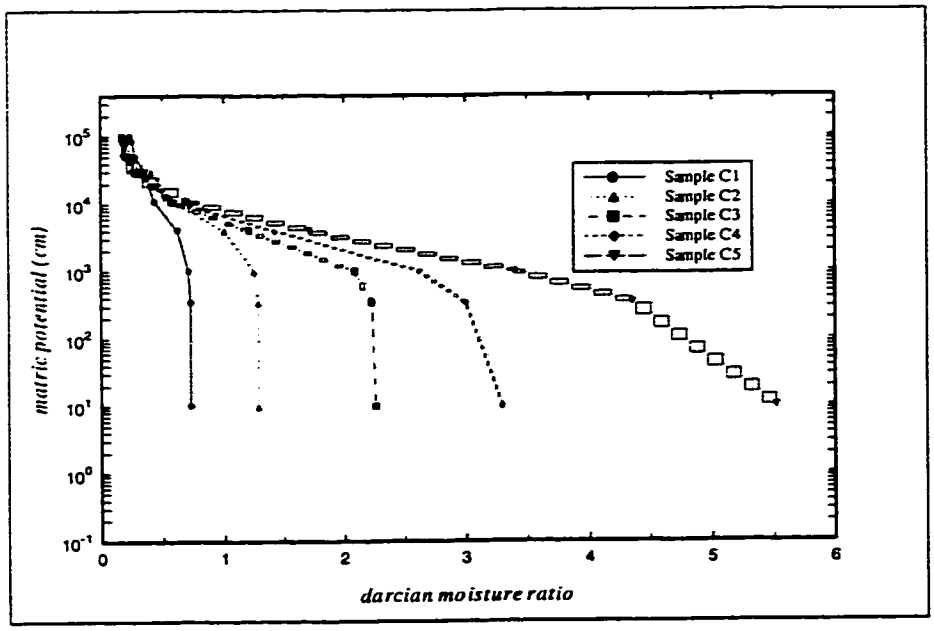

(b)

Fig. 3.11) Soil suction versus darcian moisture ratio for samples with different initial bulk density under completly confined condition a) normal scale b)logarithmic scale

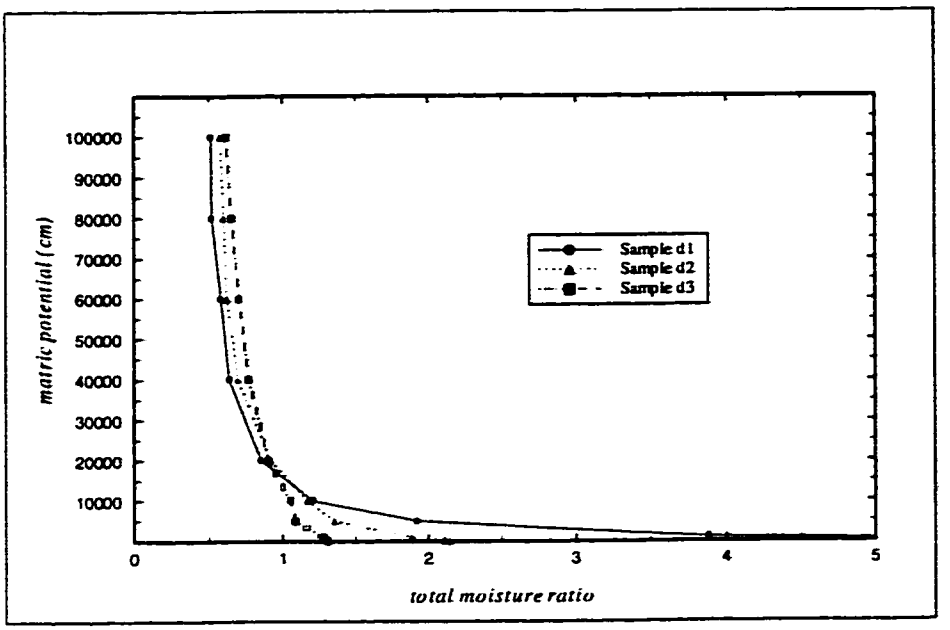

(a)

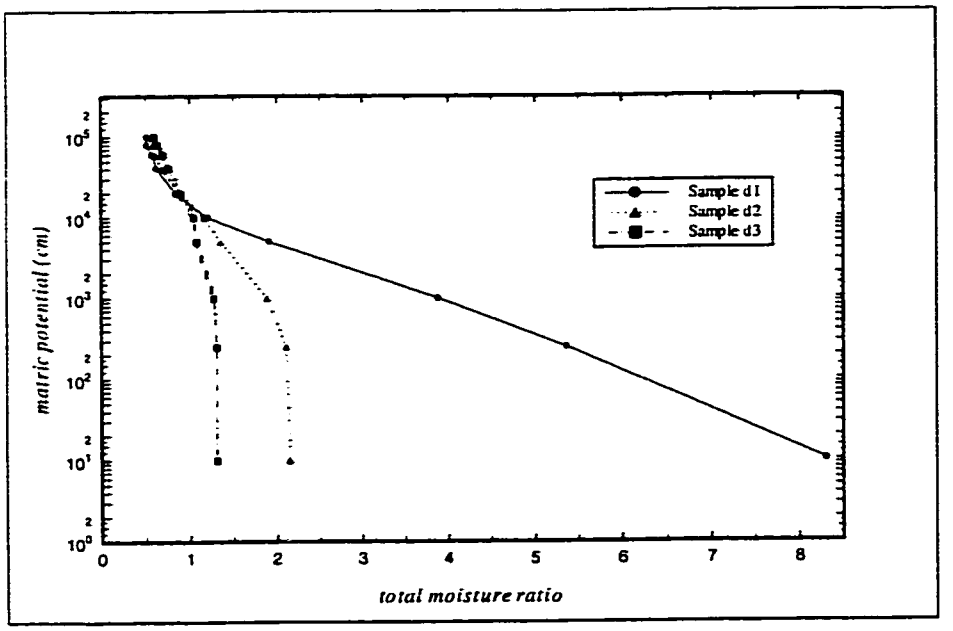

(b)

Fig. 3.12) Soil suction versus moisture ratio for samples with different magnitut of over-load a) normal scale b)logarithmic scale

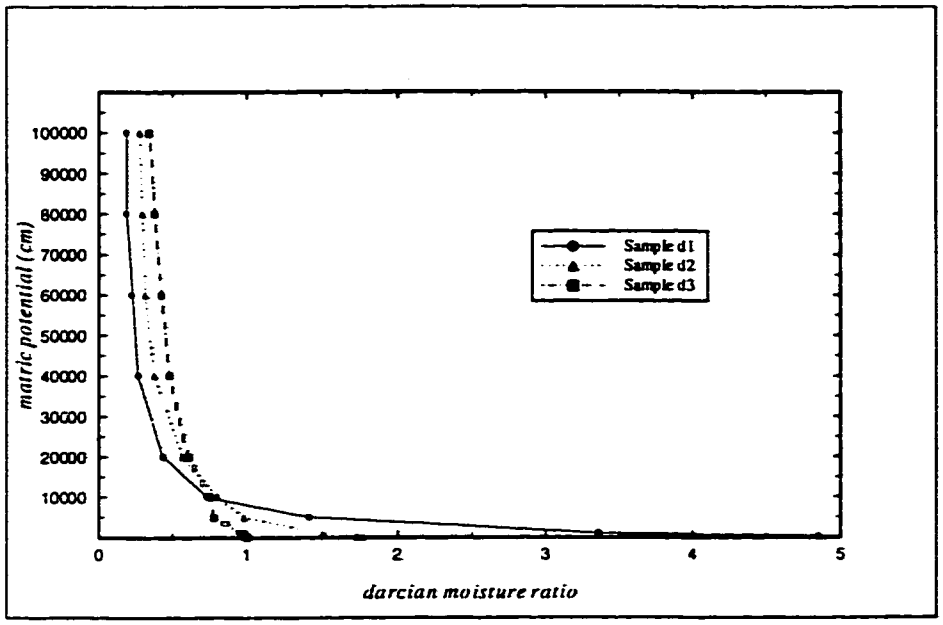

(a)

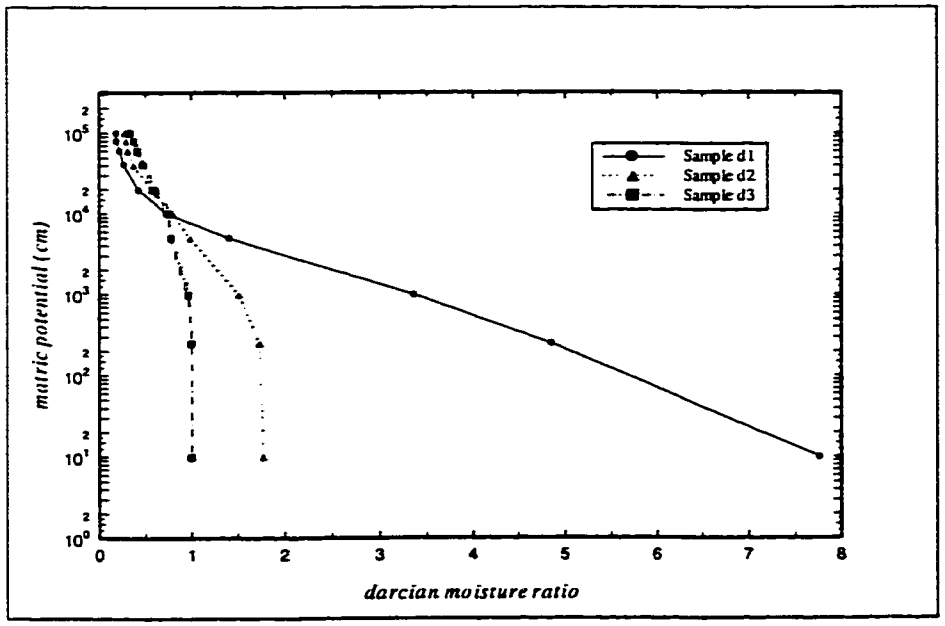

(b)

Fig. 3.13) Soil suction versus darcian moisture ratio for samples with different magnitut of over-load a) normal scale b)logarithmic scale

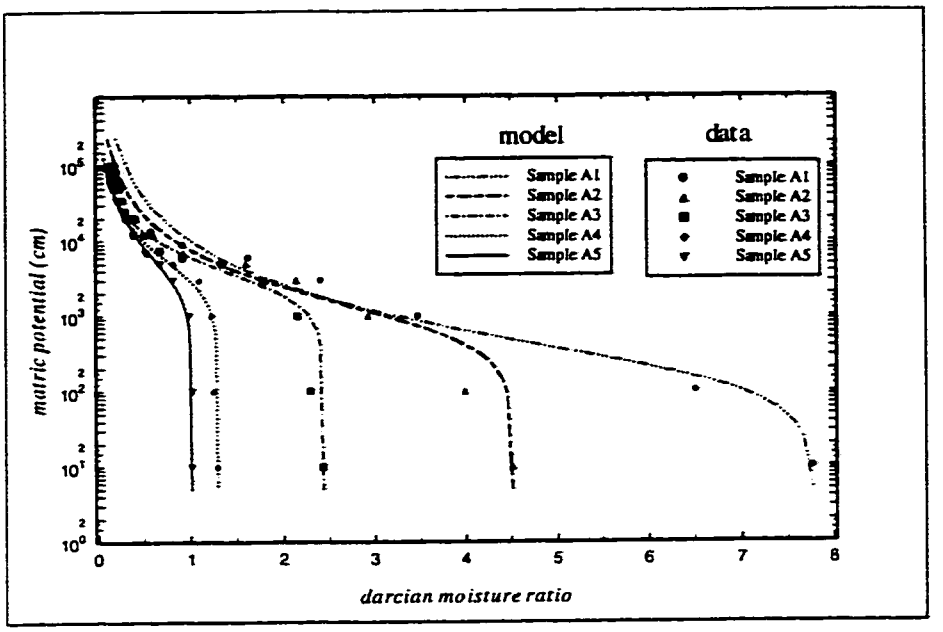

Fig. 3.14) Comparison between modified Van Genuchten model and experimental data for the first test of soil moisture retention charactristic

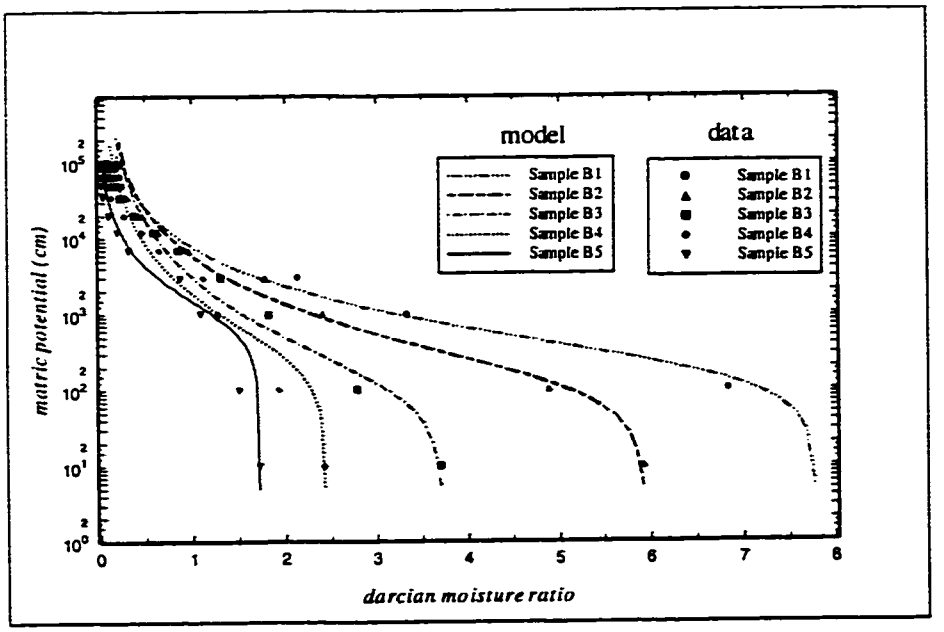

Fig. 3.15) Comparison between modified Van Genuchten model and experimental data for the second test of soil moisture retention charactristic

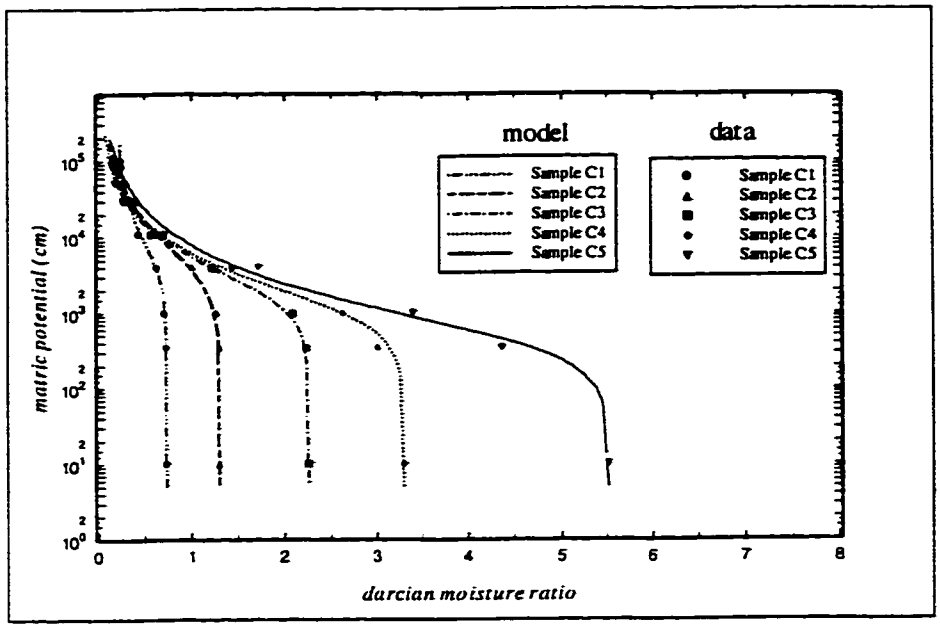

Fig. 3.16) Comparison between modified Van Genuchten model and experimental data for the third test of soil moisture retention charactristic

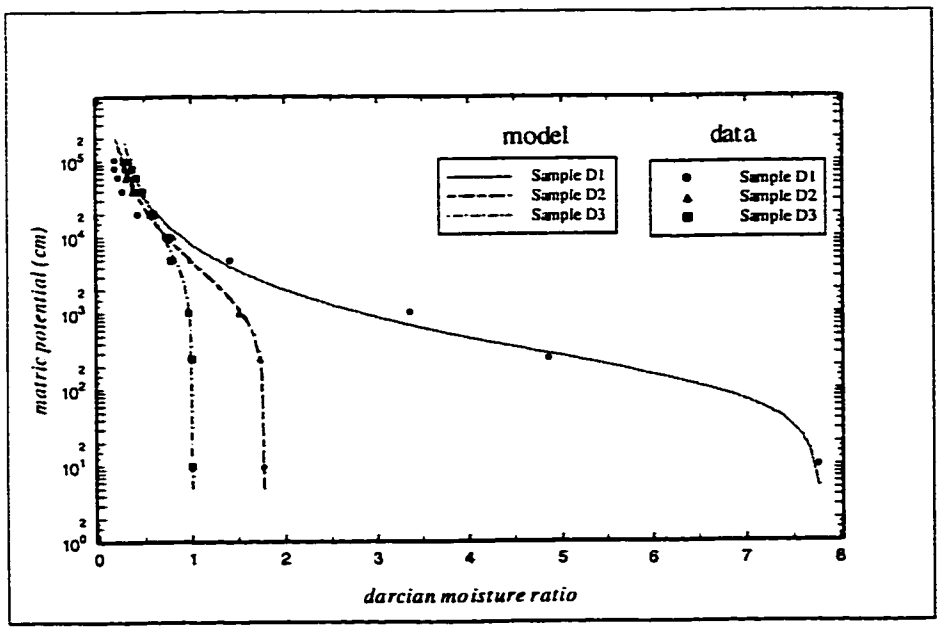

Fig. 3.17) Comparison between modified Van Genuchten model and experimental data for the fourth test of soil moisture retention charactristic

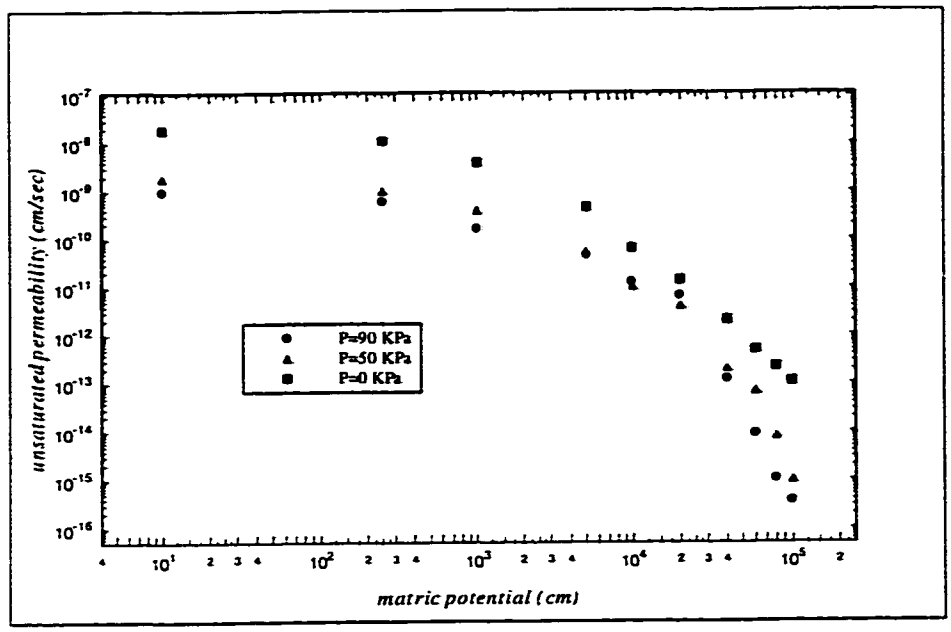

Fig. 3.18) Unsaturated hydraulic permeability and suction relationship, estimated from Eq. 3.39 using pressure plate test data

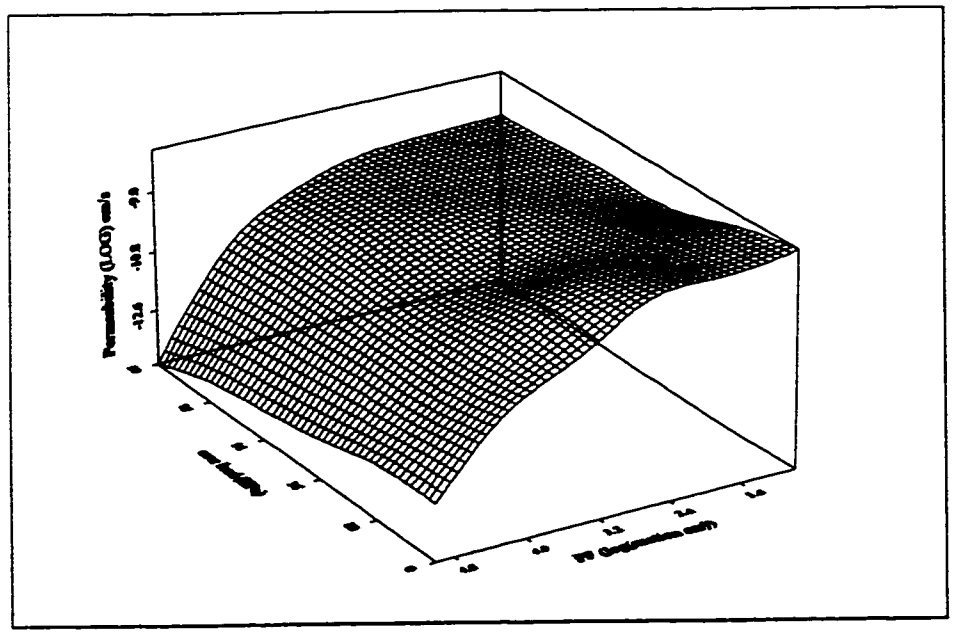

Fig. 3.19) 3D presentation of the relation between unsaturated hydraulic conductivity, suction and overload condition of the soil sample

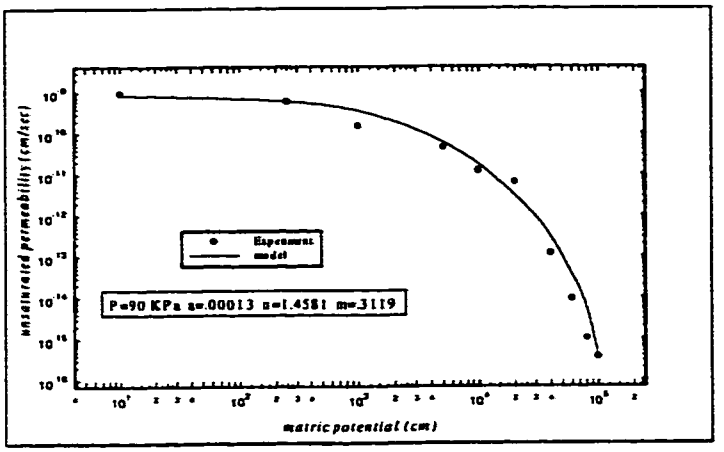

(a)

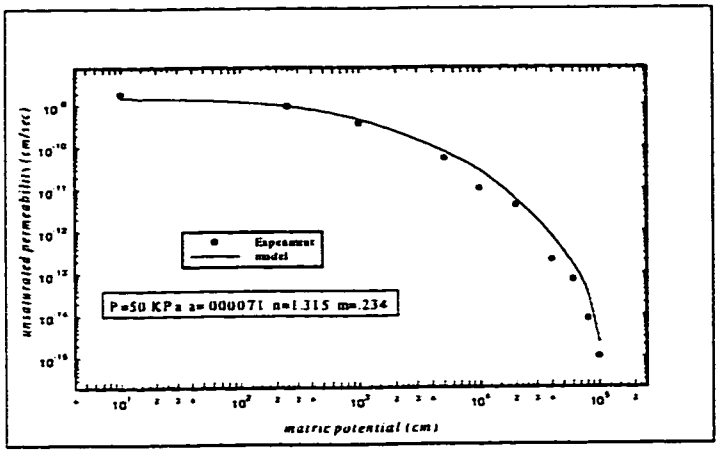

(b)

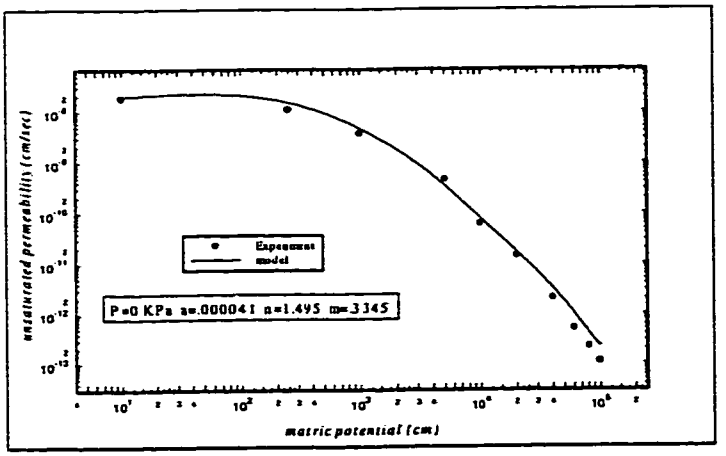

(c)

Fig. 3.20) Comparison between the unsaturated hydraulic conductivity obtained from model and experimental result a) sample D1 b) sample D2 c)sample D3

CHAPTER

4
Soil Swelling and Shrinkage Properties

In the previous chapter, soil hydraulic parameters were discussed. In the present chapter, as a complementary subject, swelling and shrinkage properties of the soil are discussed and measured. The sensitivity of the results to the initial soil parameters are also investigated. Furthermore, some empirical models are established to formulate the experimental results.

4.1. Swelling and Shrinkage Characteristic

It is necessary to characterize the soil volume changes due to the variation of the soil moisture content if a theoretical and numerical modeling of the flow through the swelling soils is to be performed. These phenomena may be specified in terms of many different variables: specific volume of the soil, v (the sample bulk volume per unit mass of oven dry soil) against gravimetric water content, θ_g (the mass of water per unit mass of the oven dried soil) (Giraldez et al. 1983 and McGarry and Malafant, 1987), volume reduction percentage (rather than gravimetric water content (Reeve and Hall, 1987)), and more convenient void ratio e (volume of void per unit volume of solids), vs. the moisture ratio, ϑ

(volume of water per unit volume of solids) (Groenevelt and Bolt, 1972, Philip 1969, Talsma 1977). A typical shrinkage characteristic curve has four distinct shrinkage ranges: structural, normal, residual and zero shrinkage range (Bronswijk,1991). When the soil is completely saturated, the structural range occurs. In this range without any accompanying equal soil volume change, the large pores which are already filled with water, may be emptied. That is because some air enters into the large pores. In the normal range, the slope of the curve is unity which means the reduction in the volume of the soil is almost equal to the water lost. Thus the volume of the air remains constant.

The residual shrinkage occurs where the water content is less than the air entry point but the change in soil bulk volume is less than the water lost. At this point a very important change takes place in the soil and the clay micelles (combined mineral layer) begin to align themselves in parallel order, forming a more oriented structure. With further loss of water, the soil matrix does not adjust itself and the pores, emptied of water, are filled by air. This range is called zero shrinkage range.

In the swelling soils, there are four parameters which describe the shrinkage and water retention characteristic: moisture ratio (ϑ), water potential (ψ), overload (P) and void ratio (e). The first and second parameters describe the amount and state of soil air-water, while the third and fourth determine the overload and the soil volume change. The relationship between these parameters are well described by Groenevelt et al. (1972) and Stroosnijder et al. (1984). Two sets of experiments, with completely different procedure, were conducted, based on the fact that the shrinkage characteristic involved in unsaturated flow modeling should include the overload condition as well. In the first part, the effect of

the initial soil moisture ratio and the swelling component of the soil on the shrinkage characteristic of an unloaded sample was examined and in the second part the shrinkage characteristic was evaluated under certain overload pressures.

4.1.1. Part 1: Unloaded Soil Sample

The unloaded shrinkage curves for different soil initial condition were obtaind by drying initialy saturated samples and measuring their weights and volume changs frequently. In the following Section the detail of the test is presented.

4.1.1.1. Sample Preparation and Apparatus

The sample characteristics used in the two runs of the shrinkage experiments were shown in Table 4.1. In the first run, the effect of the initial water content and in the second, the effect of the swelling constituent of the soil mixture were investigated.

Table 4.1: Samples Specification Used in Unloaded Shrinkage Experiment

	No.	Ben.(%)	ω(%)	θ_{int}	ρ_b (gr/cm^3)
Ex. no. 1	A1	50	103	0.71	0.69
	A2	50	146	0.78	0.53
	A3	50	208	0.84	0.4
	A4	50	320	0.89	0.28
Ex. no. 2	B1	50	320	0.89	0.28
	B2	40	230	0.86	0.37
	B3	30	178	0.83	0.46
	B4	20	125	0.76	0.6
	B5	10	67	0.63	0.92

There are several methods for measuring the shrinkage characteristic of the unloaded soil sample. However, all the methods are based on the determination of the soil bulk density by measuring the weight and volume of the specimen while being dried. For instance, McIntyre and Stirk(1954), Bronswijk (1988) and Tariq and Durnford (1993) employed different methods in measuring the volume of the specimen; however, they followed the same general procedure.

In the present study the method employed by Tariq and Durnford (1993), with some modifications, has been used. Unlike the previous methods, this method does not require the use of toxic chemicals for coating the specimen. The soil volume was determined by weighing the excess water sucked by a small vacuum from the liquid container in which the specimen is submerged. Two main different parts of the apparatus have been shown in Fig. 4.1 (p.111). The first part, called the drying part, consisted of: 1-stand hanger and its clips, 2-small pump system for blowing the dry air inside the balloon, 3-rubber cap and its pipes for air entry and exit. The specimen, after the preparation, was placed very gently inside a dry balloon and a rubber cap provided the isolation. Prior to this, the weight and volume of the balloon set were measured using the volume measurement system and a balance with .01g accuracy. The second part of the apparatus, called the volume measurement system, consisted of a cylindrical container with several overflow holes located close to the top at the same level, a small vacuum (-3 psi), and the excess water collector. The second part, which can measure a bigger volume of the specimen with an accuracy as high as $\pm.05$ cm^3, was the modified part of Tariq's apparatus.

4.1.1.2. Methodology

The sample, after it was prepared and weighed, was placed inside the plastic balloon and the initial volume was measured. Then it was hung up from the rubber cap by a clamp fixed to the stand hanger. The air entry and exit pipe were then connected to the rubber cap and dry air was blown into the balloon with the proper pressure so that all the sides of specimen were almost dried uniformly. Depending on the drying rate, during the experiment the weight and volume of the system (specimen plus balloon and rubber cap) were recorded. The mechanism used for measuring the volume of the sample was designed for the sample with the maximum diameter of 7 cm. The cylindrical container with one open side and several holes on the wall at the same level, was used for water storage. These holes acted as spillway when the water reached the level of the holes. A small vacuum was connected to both the holes sucking the excess water and the balloon removing the inside air.

Having obtained the soil initial moisture ratio and the volume of the samples at chosen times, the void ratio and the moisture ratio were calculated. In the soil shrinkage experiment, as mentioned before, two different investigations were carried out the results of which are discussed below.

4.1.1.3. Effect of Initial Water Content Results

Four samples, with the initial conditions summarized in Table 3.15, were selected. The results were plotted as the void ratio versus the moisture ratio in Fig. 4.2 (p.112). As expected, the load line, with the declination of 45^{o}, for all the samples is the

same. The difference between the lowest and the highest air entry point is not considerable.That means the porosity at which the air begins to enter the pores, is slightly influenced by the initial water content of the samples having the same percentage of swelling material.

The entire shrinkage range for five samples has been shown in Fig 4.2b. No distinct structural range is observed in the curves. However, apart from the normal range which increases as the initial water content of the sample increases, there is no significant difference between the curves in the residual and zero shrinkage ranges. Table 4.2 presents some shrinkage parameters obtained from Fig. 4.2 (p.112).

Table 4.2: Shrinkage Parameters of the Samples with Different Initial Water Content

sample	*Air entry point*		*Zero limit*	
	ϑ_a	e_a	ϑ_z	e_z
A1	1.87	1.95	.06	1.18
A2	1.89	1.97	.06	.93
A3	1.91	1.99	.06	.85
A4	2.12	2.20	.06	.72

Furthermore, for all the samples the moisture ratio at which the zero shrinkage zone begins is the same and is located on the line ϑ_z=.06. The most important difference between the curves is in terms of the void ratio value at the zero shrinkage limit. The highest void ratio value, when the sample is almost dry, belongs to the sample with the highest initial water content; with diminishing initial water content, this value also decreases. This may be explained by the fact that the samples with a higher initial water content pro-

vide a higher degree of random structure for the soil particles.

4.1.1.4. Effect of the Soil Swelling Constituent Percentage

In the second part of the shrinkage experiment, five samples with different percentages of the swelling component and the specifications summarized in Table 4.3, were chosen. The initial moisture content of the samples were selected close to their liquid limits to cover all the possible moisture content ranges. The test procedure was exactly the same as the previous test. The results are illustrated in Fig. 4.3 (p.113). Air entry points and zero shrinkage limits, obtained from Fig. 4.3, were also illustrated in Table3.17.

Table 4.3: The Shrinkage Parameters of the Selected Samples

sample	*Air entry point*		*Zero limit*	
	ϑ_a	e_a	ϑ_z	e_z
B1	2.12	2.20	.06	1.18
B2	2.05	2.1	.1	1.07
B3	1.81	1.84	.14	.96
B4	1.48	1.49	.18	.86
B5	1.02	1.02	.23	.72

One may understand from Fig. 4.3 that the normal shrinkage range decreases as the percentage of the swelling constituent decreases and is zero for non-swelling soils. As expected, the table shows a rapid reduction in the air entry point as the percentage of the swelling constituent in the soil decreases. The reason is that a soil with higher swelling activity has a respectively higher initial void ratio when the water content is close to the

liquid limit and consequently, the soil particles at the air entry point, have more random orientation. Another conclusion is that the value of the moisture ratio for the starting point of the zero shrinkage limit is bigger for soil with a respectively lower percentage of swelling constituent. The zero shrinkage range might be distinguished from other ranges by drawing line a-a described by the following mathematical expression:

$$e_z = 1.34 - 2.68\vartheta_z \qquad \text{Eq. 4.1}$$

The above equation relates the soil void ratio to the corresponding moisture ratio at the shrinkage limit. Using this equation, one may find the corresponding void ratio to the moisture ratio of soil having a specified swelling activity.

4.1.2. Part 2: Overloaded Soil Sample

The overloaded shrinkage curves for different soil initial condition were obtaind by drying initialy saturated samples and measuring their weights and volume changs frequently. In the following Section the detail of the test is presented.

4.1.2.1. Sample Preparation and Apparatus

Three samples, with the different overload pressures and the initial conditions as presented in Table 4.4, were chosen for the next set of experiments to find the relationship between the overload pressure and the shrinkage characteristics. The results for unloaded samples were adapted from the first experiment.

Table 4.4: Samples Specification Used in Loaded Shrinkage Test

	No.	Ben. (%)	over load (kPa)	ϑ	θ_{int}	ρ_b (gr/cm^3)
Set C	C1	50	90	1.31		1.22
	C2	50	50	2.15		.91
	C3	50	0	8.3	.89	.28

The design of the apparatus was adapted from Stroosnijder et al.(1984) and illustrated in Fig. 4.1c. The overloaded samples of 5 cm diameter, after being completely saturated, were dried in an oven at 40°-50° C during 10 days. Periodically, the volume changes were determined using a micrometer gage installed on the top and simultaneously, the lost water was recorded by weighing the samples.

4.1.2.2. Results

The results are illustrated in Fig. 4.4 (p.114). For the unloaded sample, on which the previous method was applied, the shrinkage curve is quite acceptable. However, for two other overloaded samples, for which the new experimental method was employed, results are not as expected. The main cause of such undesired curves is the creation of cracks in the soil due to the fact the sample was prevented from laterally shrinking by applied overload pressure. Fig. 4.5 (p.115) shows the results, after accounting for the estimated volume of the cracks by measuring their depth and width. The different shrinkage parameters, concluded from the curves, are summarized in Table 4.5. The normal shrinkage range and the air entry points decrease as the overload pressure increases. The main reason may be that the lower initial void ratio corresponds to the higher overload pressure.

Also, an increase in the overload pressure produces an increase in the zero shrinkage limit, i.e., the higher the overload pressure, the wider the zero shrinkage range. Eventually, a three dimensional image of the relationship among the overload pressure, moisture ratio and void ratio, is plotted in Fig 4.6 (p.115). According to this figure, as the overload pressure decreases, more deviation of $\vartheta - e$ curves from the load surface is observed; i.e., the less the overload pressure, the bigger the residual range. Obviously higher porosity of the less overloaded sample can be stated as the main reason.

Table 4.5: Shrinkage Parameters of Samples with Different Amount of Overload Pressure

sample	*Air entry point*		*Zero limit*	
	ϑ_a	e_a	ϑ_z	e_z
C1	1.09	1.08	.47	.68
C2	1.24	1.2	.36	.8
C3	2.12	2.2	.06	1.18

4.2. Inter-Particle Pressure

The produced pressure gradient in a soil column, due either to the variation of the soil water content or to the overload pressure, is responsible for the soil particles flux. As discussed in the theoretical chapter, the mathematical expression of this statement can be written as follows:

$$\vec{q_s} = -K_s \vec{\nabla} \Omega \qquad \text{Eq. 4.2}$$

where K_s referred to the coefficient of the particles permeability and Ω is interparticle

pressure whose gradient is responsible for the soil particle flux. Interparticle pressure, indeed, is a combination of some other pressures:

$$\Omega = \frac{P_s + P_O + \int_0 \rho_t dz}{\rho_w g} \qquad \text{Eq. 4.3}$$

where P_s is the swelling pressure, P_O is the surface overload pressure, $\int_0 \rho_t dz$ is the soil weight pressure, ρ_t is the apparent wet soil bulk density, ρ_w is the water density and g is the gravitational acceleration. While the estimation of the surface overload pressure and that of the soil weight can be easily performed, the estimation of the swelling pressure is rather difficult. However, the variation of this pressure, due to the increase in soil water content, should be determined as a function of water content or, indeed, as a function of soil void ratio. This may be done using several experimental procedures described in the literature. In the following paragraph, some of these methodologies and their benefits are discussed, together with a newly proposed method employed in the experimental work to characterize the dependency of swelling pressure on the soil void ratio.

4.2.1. History

Swelling pressure, as a favorite index of soil activity, has two possible definitions (Khaddaj et al. 1992):

a) Swelling pressure is the pressure that is necessary to be exerted on the soil sample to keep its volume unchanged. The method may also be called the "direct" or "constant volume" method.

b) In contrast with the first method, swelling pressure may also be defined as being the pressure necessary to bring the sample back to its initial volume.This is called the "different pressure" or "pre-swell" method.

There are some experimental methods that although in details are slightly different depending on the soil field condition, belong either to the first or the second category (Agarwal et al. 1989). For instance, the following is a very brief description of some test procedures for which more details may be found in Khaddaj et al. (1992):

"Different pressure" method. This method determines the relationship between the overload pressure and the soil void ratio from which the swelling pressure of the soil sample may be estimated. This can be done using a conventional consolidation apparatus. Several specimens are prepared and each is loaded at different vertical stresses and then allowed to swell as water is added. After stabilization, the soil void ratio of each sample is recorded and the results are reported as a graph of soil void ratio versus the overload pressure. The value of the swelling pressure corresponding to the initial void ratio is estimated by intersecting the line $e=e_o$ with the curve.

"Pre-swell" method. This method provides the same information as the first method, using the inverse procedure; i.e., the sample is allowed to swell with addition of water under almost no over-load pressure in the same apparatus and, after stabilization is reloaded step by step to cancel the whole deformation. Eventually, the graph of the overload pressure versus the soil void ratio is plotted and the swelling pressure, if needed, is estimated in the same way as applied to the first method.

"Direct" or "constant volume" method with increasing overload pressure. The procedure employed in this method is principally different from the two other methods, since the sample volume is forced to remain unchangeable during the test. An consolidation apparatus should be modified to be able to increase the overload pressure to keep the sample vol-

ume constant, while being wetted. The only result of this test is the value of the final overload pressure at the maximum saturation which is taken as the swelling pressure. A properly designed apparatus is described by Agarwal et al. 1989.

"Direct" or "constant volume" method with no overload pressure. In this method a direct measurement of the swelling pressure is performed with the use of a proving ring. The final pressure, created by the wetting, is assigned as the swelling pressure.

Comparison of methods. The swelling property of a soil is not unique and there is some evidence that the swelling and swelling pressure, determined by different experimental procedures, have a strong stress-path dependency (Brackley, 1975; Alonso et al. 1992). However, according to the literature, the direct method in which the overload pressure increases gradually, can be respectively more reliable in estimating the swelling pressure, since only one sample is used and furthermore, the soil condition is more likely the same as in-situ. The last method (direct method with no overload pressure) can also be reliable if either some corrections are applied to the estimated swelling pressure to take care of the errors due to the deformation of the proving ring (Salas et al. 1957), or a pressure sensor without any significant deformation is used (Khaddaj et al, 1992).

4.2.2. Proposed Experimental Method

The swelling properties of soil are influenced by such factors as density, water content, soil structure, electrolyte concentration and confinement condition. However, the dependency of the swelling pressure on the soil moisture or void ratio is the interest of the present study, since the other parameters were kept constant in all the tests. Furthermore, the evidence shows that swelling pressure is a function of only the total void ratio (Brack-

ley et al. 1973). In other words, since the effects of the other parameters appear as a change in the soil void ratio, the determined swelling pressure as a function of the soil void ratio can include the dependency of swelling pressure on the other variables as well. This is because the soil void ratio is one of the four soil parameters (overload pressure, void ratio, suction and moisture ratio) through which the state of the soil is unambiguously defined. Thus, an attempt was made to determine the relationship between the swelling pressure and the soil void ratio by modifying the direct method with no overload pressure. To this end, a relatively rigid load cell, (to avoid the errors caused by the load cell deformations), was used to record the final swelling pressure due to the saturation. In order to compare the obtained results with at least one other method, the "different pressure method" was also examined.

4.2.2.1. Apparatus and Test Procedure

Fig. 4.7a (p.116) illustrates the apparatus designed for the purpose of the experimental work of this part of the study. It consists of three major parts: 1-a fixed frame by which the produced pressure is taken, 2-a pressure measurement system consisting of one load cell, interface piston and accessories for adjusting the distance between soil surface and piston face to obtain the desired void ratio, 3- a sample cell and its accessories. Unpredictable axial deformation of the system was controlled by employing a micrometer gage installed above the apparatus. The prepared sample, with the specification shown in Table 4.6, was placed in the cell between the top and the lower porous stones and the face of the perforated piston was adjusted over the sample so that the desired final void ratio was achieved. Then the sample was allowed to swell upon accessing the water and after stabili-

zation, the final swelling pressure, associated with the adjusted void ratio was recorded. In the next step the face of the interface piston was gently pulled up and leveled so that the new void ratio was achieved. The procedure was repeated until enough data were obtained. The elastic deformation of the apparatus was within an acceptable range and additionally, an exclusive micrometer gage reading was performed to control any unpredictable deformation (caused by set up configuration). If there was any, corrections to the soil void ratio would be applied.

Table 4.6: Sample Specification Used in Swelling Pressure Test

No.	Ben.(%)	ω(%)	ϑ	e
A1	50	3.5	0.1	0.7

4.2.3. Different Pressure Method

In order to verify the results of the above method, an alternative procedure was employed. Thus, the above apparatus was modified to be capable of measuring the amount of the swelling by means of a micrometer installed above the sample, as illustrated in Fig 4.7b. The overload pressure was exerted to the sample by hanging equal weights on both sides of the load arm. Six samples were prepared with the initial conditions as summarized in Table 4.7 and placed in six different cells. Each sample was subjected to a certain overload pressure (Table 4.7). Afterwards, the samples were wetted and allowed to swell and after stabilization, final void ratios associated with the applied overload pressure were recorded.

Fig. 4.8 (p.117) shows the evolution of swelling with time for six samples used in

the adapted method. The maximum swelling values at stabilization were used to calculate the soil void ratio, corresponding to the applied overload pressure. As a final result of the first and second experiments, the soil void ratio was plotted versus the overload pressure in Fig. 4.9 (p.117). Results show that, apart from a small range in lower soil void ratio values, the proposed model agrees well with the "different pressure" method. However, the proposed model is more reliable, since only one specimen was used in the test and as well, it enjoys the benefit of the "constant volume" method in measuring the swelling pressure. The results of the proposed experimental method were used in the numerical analysis of unsaturated flow modeling

Table 4.7: Sample Specification Used in "Different Pressure Method"

No.	Overload (kPa)	Ben.(%)	ω(%)	ϑ	H_o (mm)
B1	19	50	3.5	0.1	8.2
B2	46	50	3.5	0.1	8.2
B3	69	50	3.5	0.1	8.2
B4	93	50	3.5	0.1	8.2
B5	139	50	3.5	0.1	8.2
B6	186	50	3.5	0.1	8.2

4.3. Coefficient of Soil Particle Conductivity, K_s

The coefficient of soil particle permeability was introduced in the theoretical formulation of water flow through unsaturated, swelling soils (chapter 2). Yong et al.(1969)

introduced this coefficient as the counterpart to the hydraulic permeability coefficient, to develop a mathematical expression for unsaturated flow through swelling soils. They did not mention its physical aspect and a possible experimental procedure to measure this coefficient. With the lack of a proper definition and experimental method, one cannot correspond any value to this coefficient in the numerical analysis of the developed theoretical model. In this part, an attempt will be made to establish a simple definition and an experimental procedure to quantify this parameter.

As discussed in the theoretical model development, soil particle flux may be assumed to be a function of the total inter particle pressure gradient (Eqs.4.2 and 4.3). In the Eq. 4.2 K_s may be regarded as the particle flux, if a unit inter particle pressure is applied over the unit length of the sample within a certain span of time. This definition is very similar to that of hydraulic permeability. Since the inter particle pressure, Ω, according to the Eq. 4.3, has the dimension of length, the K_s dimension will be the same as that of q_s, i.e., LT^{-1}. It is obvious that K_s in a non-swelling soil is equal to zero, since the soil is not subject to any volume changes while saturating.

4.3.1. Methodology and Measurement

The same philosophy behind the methods for measuring the soil saturated or unsaturated hydraulic permeability may be used to determine the soil particle permeability. According to Eq. 4.2, if a unit gradient of inter particle pressure is applied to a column of soil sample having a certain soil moisture ratio, the flux of the particles per unit of time, is taken as the soil particle permeability associated with the soil moisture ratio. Since the soil particles flux acquires different values when the soil moisture ratio changes, it may be con-

cluded that the particle permeability is a function of soil moisture ratio.

Two different procedures are proposed in order to find the $K_s(\vartheta)$ relationship: overload pressure addition and overload pressure reduction. In the first method, a sample, with the moisture ratio ϑ and the initial height of H_1, is prepared and overloaded by a pressure of magnitude P_0 is applied. Due to the applied overload pressure, the height of the sample decreases over a certain time to reach an equilibrium between the applied overload and the inter particle pressure. After reaching equilibrium, the height of the sample reduces to $H_2<H_1$. The amount of soil particles, displaced over time T, might be determined through the following equation:

$$Q_s = A \cdot (H_1 - H_2) \qquad \text{Eq. 4.4}$$

where A stands for soil section area. On the other hand the total amount of the displaced soil particles can be expressed as:

$$Q_s = A \cdot T \cdot q_s \qquad \text{Eq. 4.5}$$

in the latter equation, T accounts for the total equilibrium time and q_s is the soil particle flux that can be determined by Eq. 4.2. The combination of Eqs. 4.2, 4.4 and 4.5 results in:

$$K_s = \frac{(H_1 - H_2)}{T} \cdot \frac{\Delta Z}{\Delta \Omega} \qquad \text{Eq. 4.6}$$

where $\Delta\Omega$ is the net interparticle pressure which at the beginning is equal to the total applied over load pressure and at equilibrium, zero. Therefore, the average, $\Delta\Omega = P_o/2$, should be substituted in Eq 4.6. The pressure is applied on the sample with the average height of $(H_1 + H_2)/2$. Thus $\Delta Z = (H_1 + H_2)/2$. Substituting for $\Delta\Omega$ and ΔZ in Eq. 4.6 results in:

$$K_s = \frac{(H_1^2 - H_2^2)}{T \cdot P_o} \qquad \text{Eq. 4.7}$$

In the overload pressure reduction method, after sample preparation, a proper overload pressure is applied to the soil from the top and the sample is left until equilibrium is achieved. Then the applied overload pressure is removed and the soil swelling with respect to the time is recorded. The maximum height and time at equilibrium are measured. In contrast to the first method, the final height is bigger than the initial height of the sample. Therefore, Eq 4.7 may be rewritten in the following form:

$$K_s = \frac{(H_2^2 - H_1^2)}{T \cdot P_o} \qquad \text{Eq. 4.8}$$

The only disadvantage of the second method is the larger time consumption. However, in the first method water may leave the sample due to rapid consolidation and consequently, some portion of the decreased height might be due to the consolidation phenomena and not to swelling. Such a phenomenon is unlikely to happen in the second method, since the sample is not subject to any consolidation process. In the present study, the second method was employed and Eq. 4.8 was used to estimate the soil particle permeability corresponding to the associated soil moisture ratio, ϑ. By preparing different samples with different moisture contents and following the same procedure, the $K_s(\vartheta)$ was obtained. It should be mentioned that the sample was isolated from the lab environment to keep its moisture ratio unchanged during the test.

4.3.2. Apparatus

Fig. 4.10 (p.118) shows the designed apparatus used for measuring the soil particle permeability coefficient. Samples, initially wetted up to the desired moisture ratio, were placed inside the cell and overloaded. They were isolated using a multi-layer plastic seal. After the first equilibrium condition was achieved, overload pressure was removed and thereafter the increasing height was recorded using a micrometer gage, fixed at the top of the sample. At the final equilibrium, samples were dried in the oven to determine the moisture ratio. The magnitude of the overload pressure was properly chosen to achieve a measurable soil particle flux. In this regard, the range of the overload pressure is chosen from 80 kPa, at the minimum to 20 kPa at the maximum water content.

4.3.3. Sample Preparation and Results

The sample specifications are summarized in Table 4.8 and the experimental results are illustrated in Fig. 4.11 (p.118) as a plot of soil particle permeability versus soil moisture ratio. The results show very reasonable values of K_s, which are considerably higher than the amount of unsaturated hydraulic permeability. This result means that water flow in swelling soil can be extremely influenced by the motion of soil particles. The general shape of $K_s(\vartheta)$ curve is similar to the one representing the saturated hydraulic conductivity and void ratio relationship. For further mathematical usage, an empirical formula from the experimental results was established by means of the statistical program, AXUM. Investigation showed that the curve which best fits the empirical data, has an exponential form as follows:

$$K_s = a(e^{\vartheta})^b \qquad \text{Eq. 4.9}$$

where ϑ is the soil moisture ratio and a and b are the fitting parameters, which were determined as:

$$a=1.03e\text{-}9 \qquad b=.6645 \qquad \text{Eq. 4.10}$$

in which the value of "a" may be regarded as the minimum value of K_s for an almost dry soil sample.

Table 4.8: Sample Specification and Final Result in Soil Particle Permeability Test.

No.	overload (kPa)	Ben.(%)	ω(%)	ϑ	K_s (gr/cm^3)
A1	86.2	50	22	0.61	1.3e-9
A2	86.2	50	34	0.94	2.4e-9
A3	75.4	50	52	1.45	3.2e-9
A4	64.6	50	68	1.89	4.6e-9
A5	53.9	50	104	2.89	7.4e-9
A6	43.1	50	147	4.07	1.3e-8
A7	32.3	50	196	5.44	2.3e-8
A8	21.5	50	305	8.46	6.4e-8

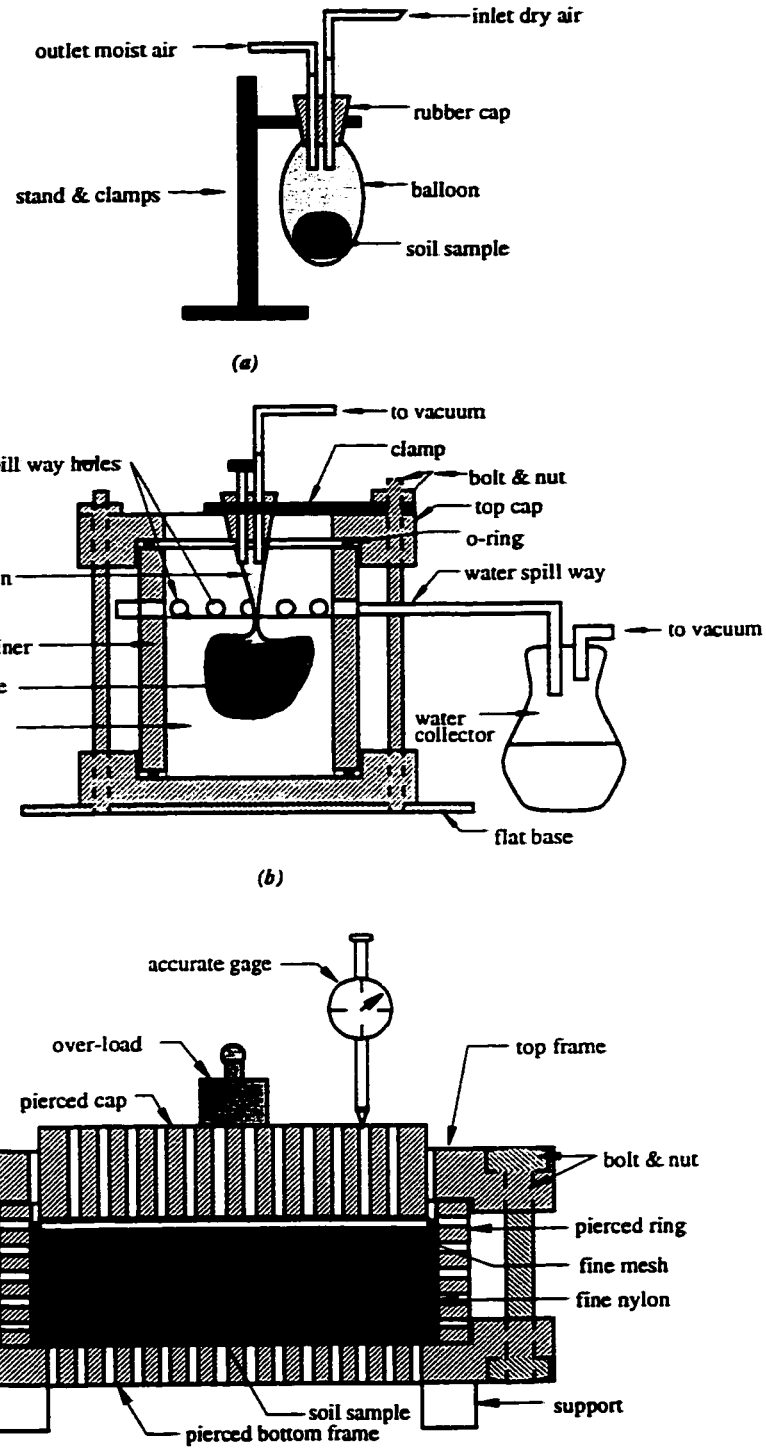

Fig. 4.1) Apparatus for measuring volume change of soil sample during drying condition a) drying system in unloaded sample condition b) sample volume measurement system for unloaded condition c) drying system and volume measurement in overloaded condition

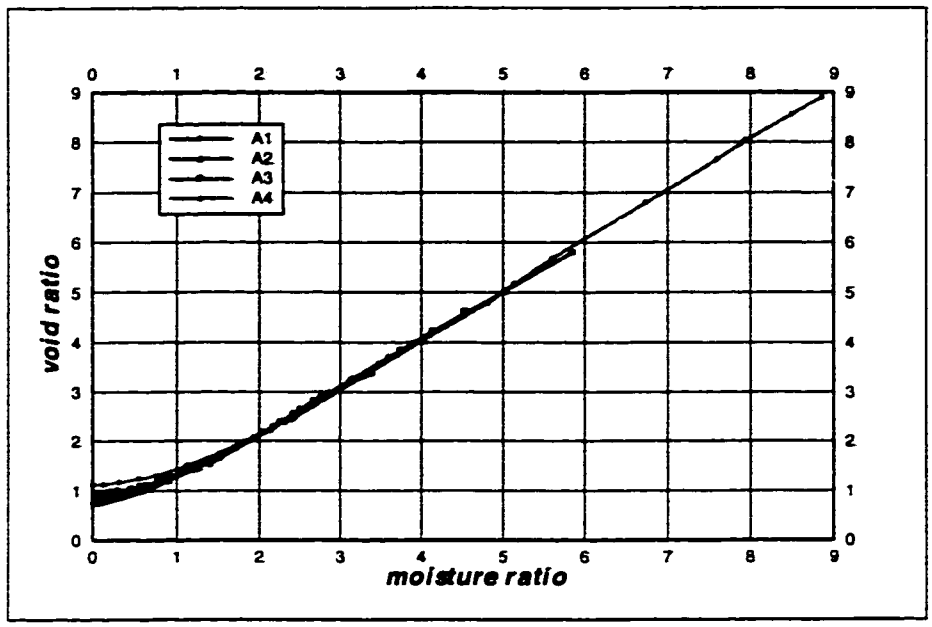

(a)

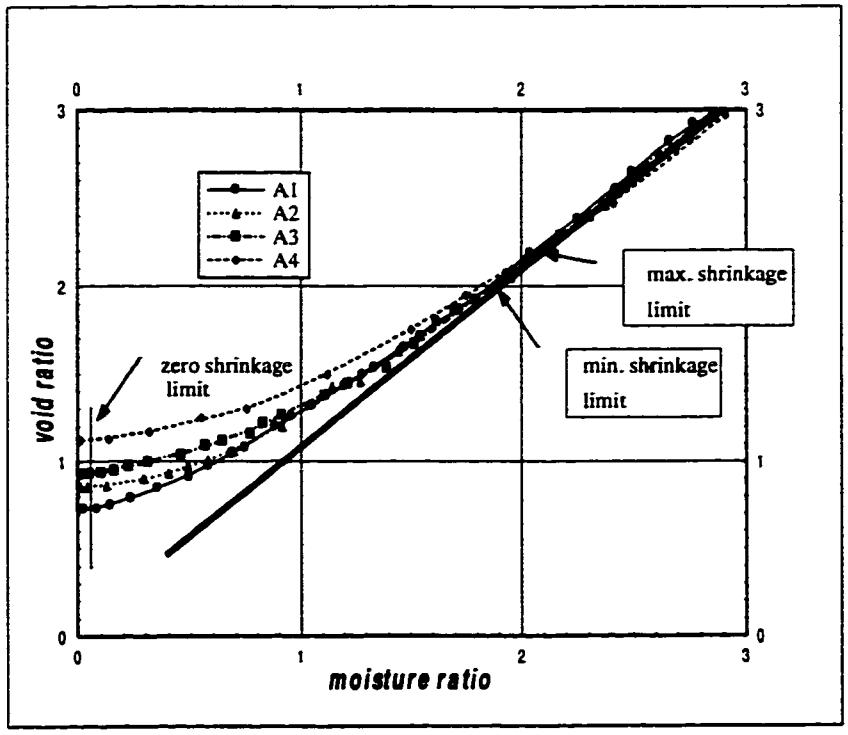

(b)

Fig. 4.2) Volume change characteristic for samples with different initial water content a) complete data b) zero and residual limit only

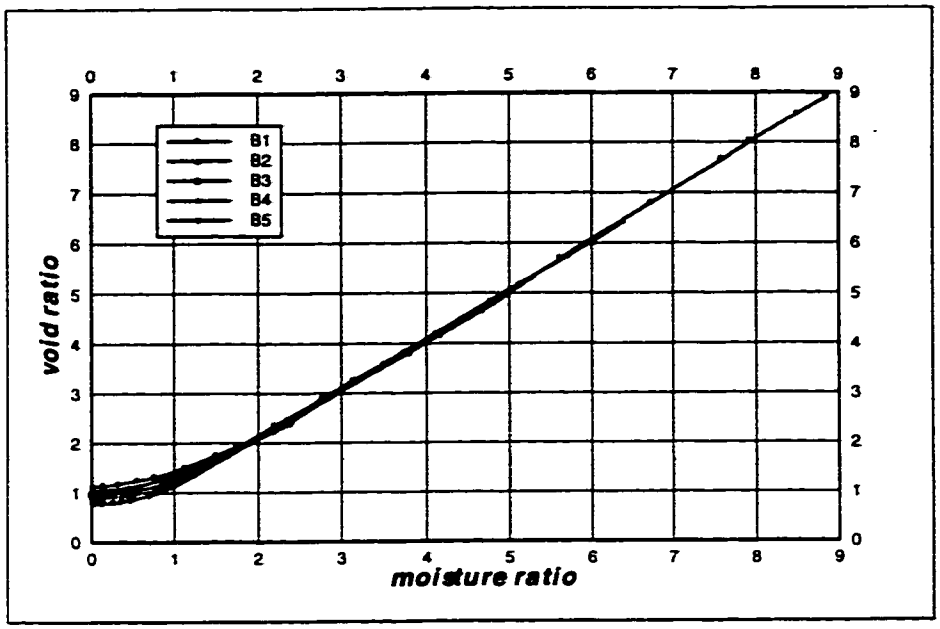

(a)

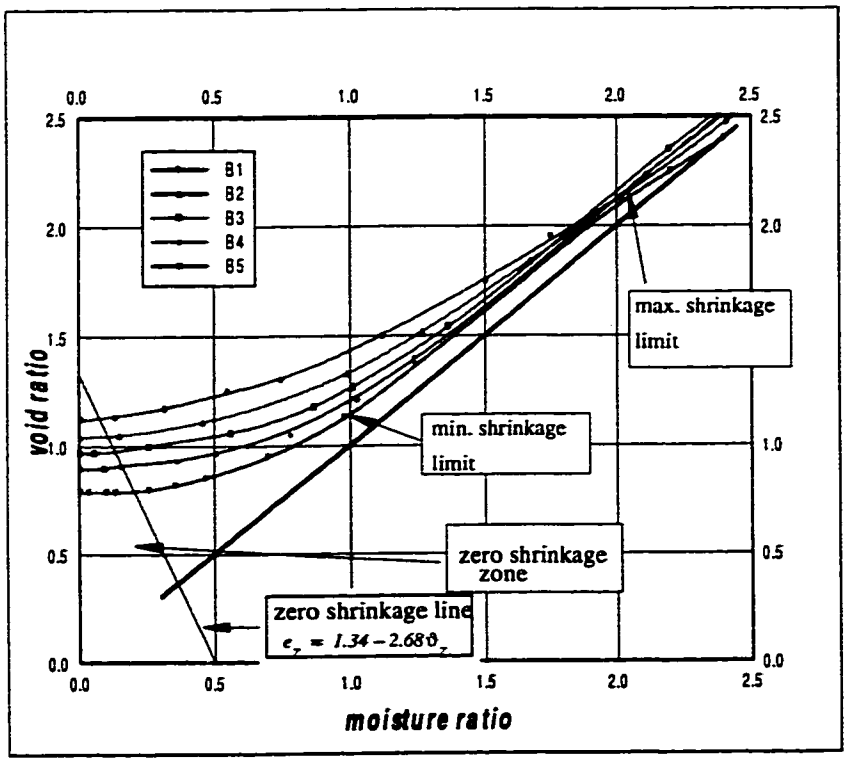

(b)

Fig. 4.3) Volume change characteristic for samples with different swelling constituent percentage a) complete data b) zero and residual limit only

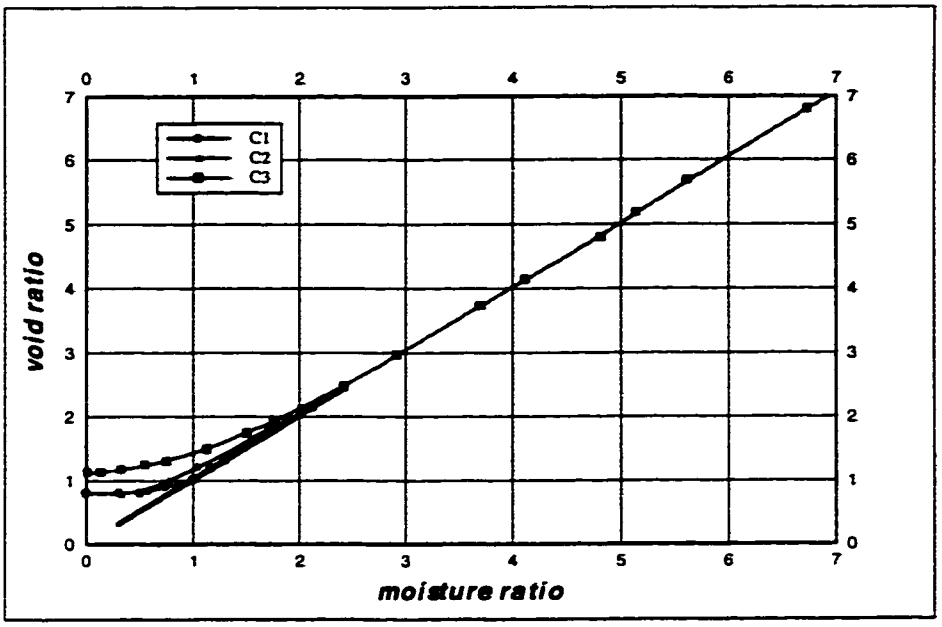

(a)

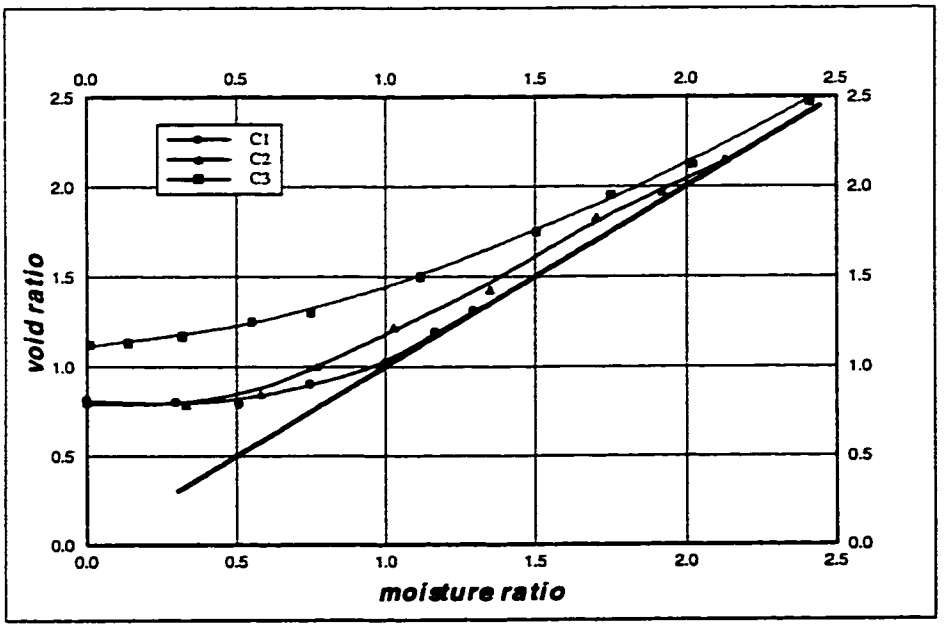

(b)

Fig. 4.4) Overload effect on the shrinkage characteristic (unmodified data) a) entire range b) residual and zero shrinkage range only

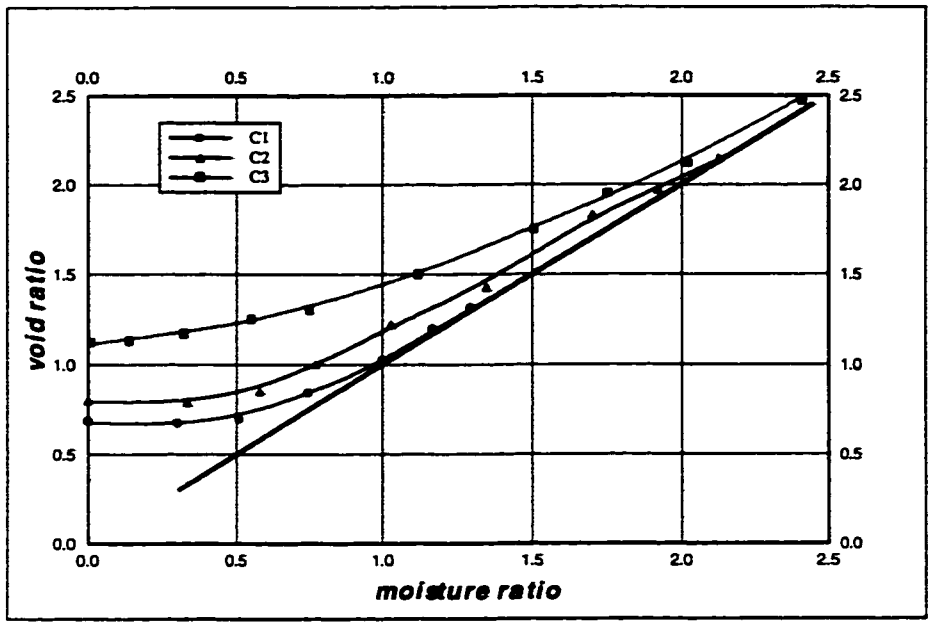

Fig. 4.5) Overload effect on the shrinkage characteristic after volume correction a) entire range b) residual and zero shrinkage range only

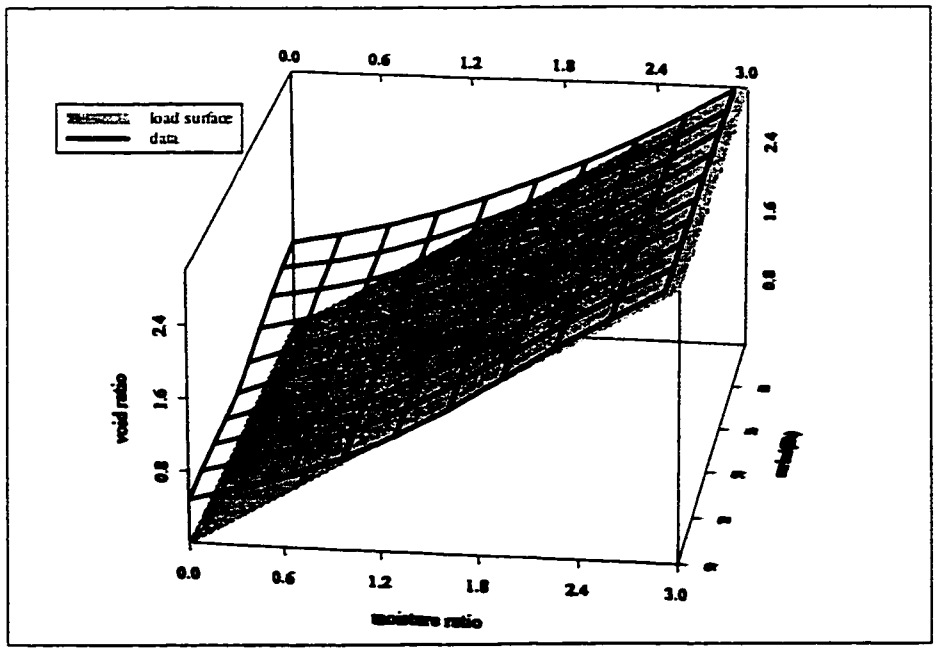

Fig. 4.6) 3D presentation of the $\vartheta - e - p$ relationship

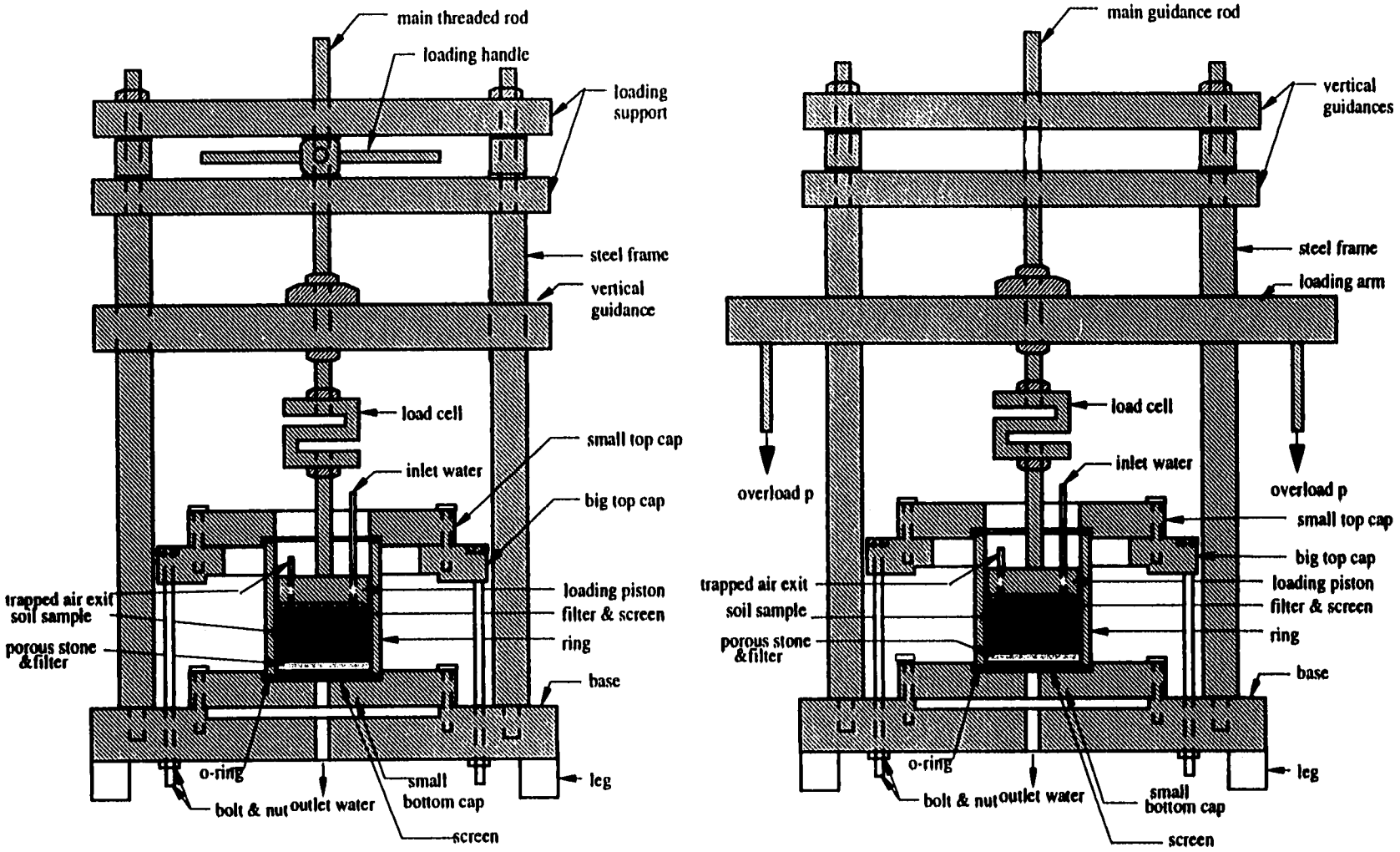

Fig. 4.7) Swelling pressure test apparatus a) modified direct method without overload pressure b) different pressure method

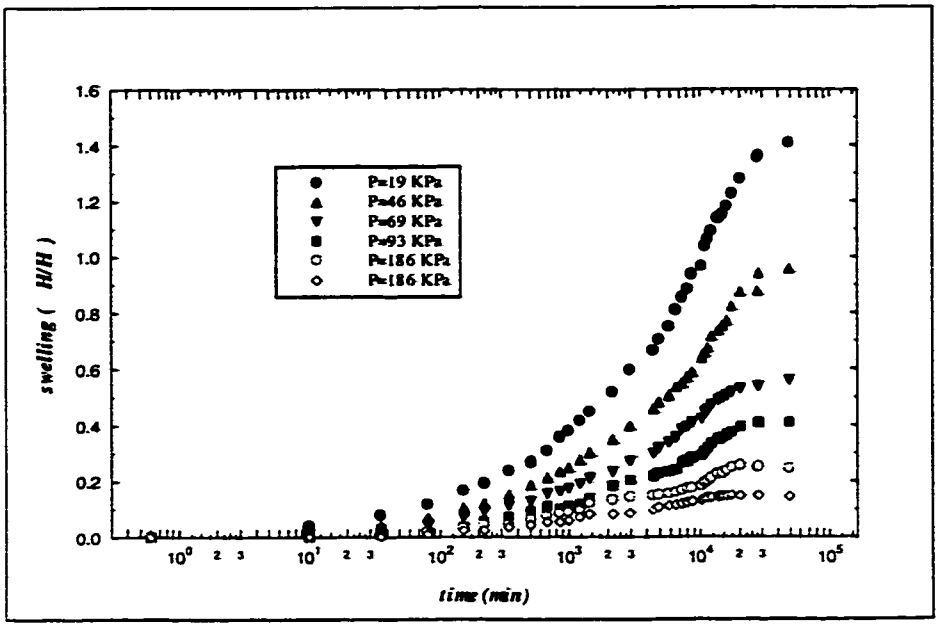

Fig. 4.8) Result of "different pressure" method experiment as plot of swelling v.s. time for six sample with different overload pressure

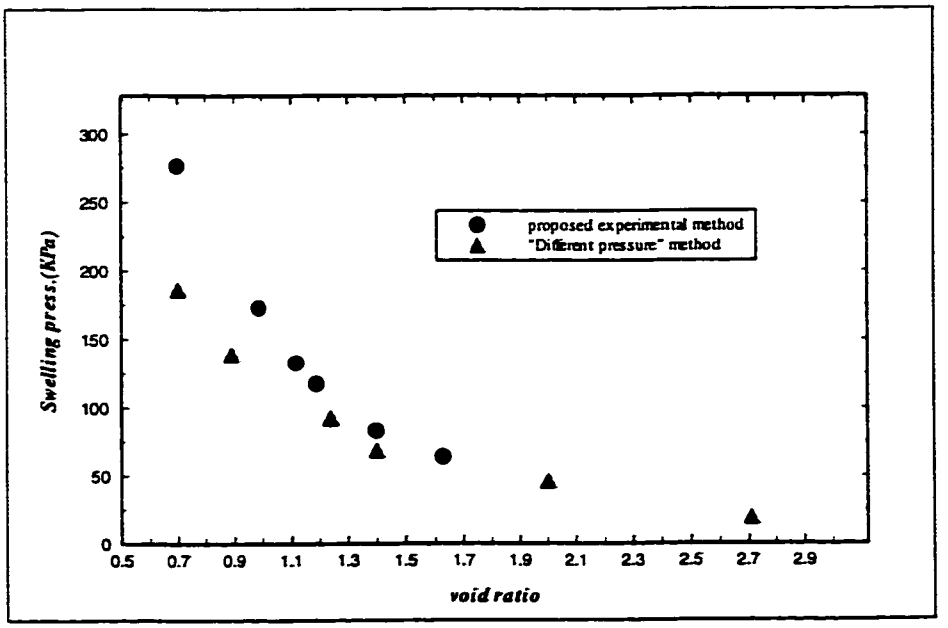

Fig. 4.9) Comparison between the results of two different experimental methods for characterizing the swelling pressure

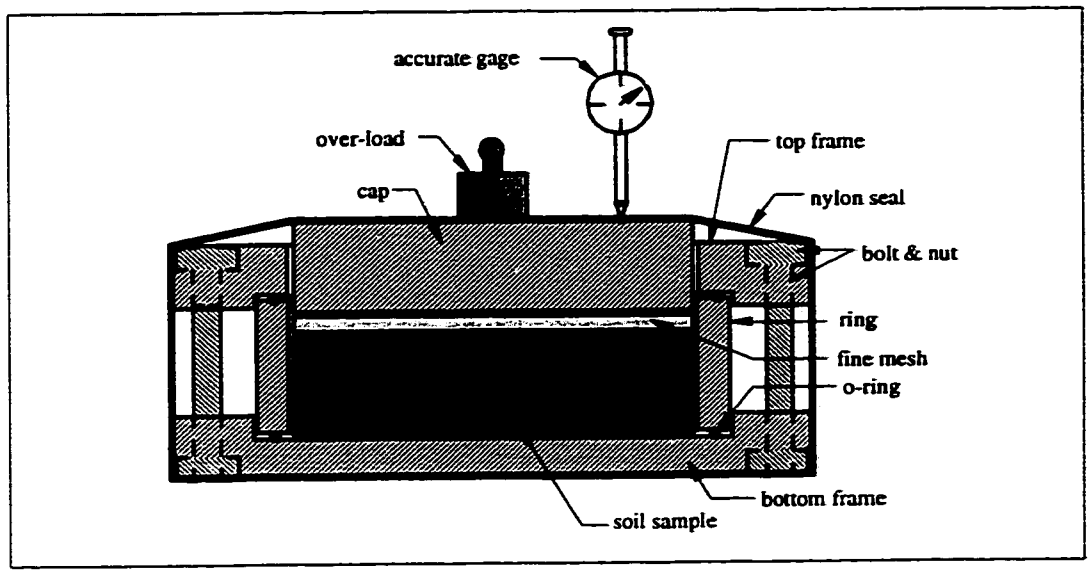

Fig. 4.10) Apparatus for measuring the soil particle permeability coefficient

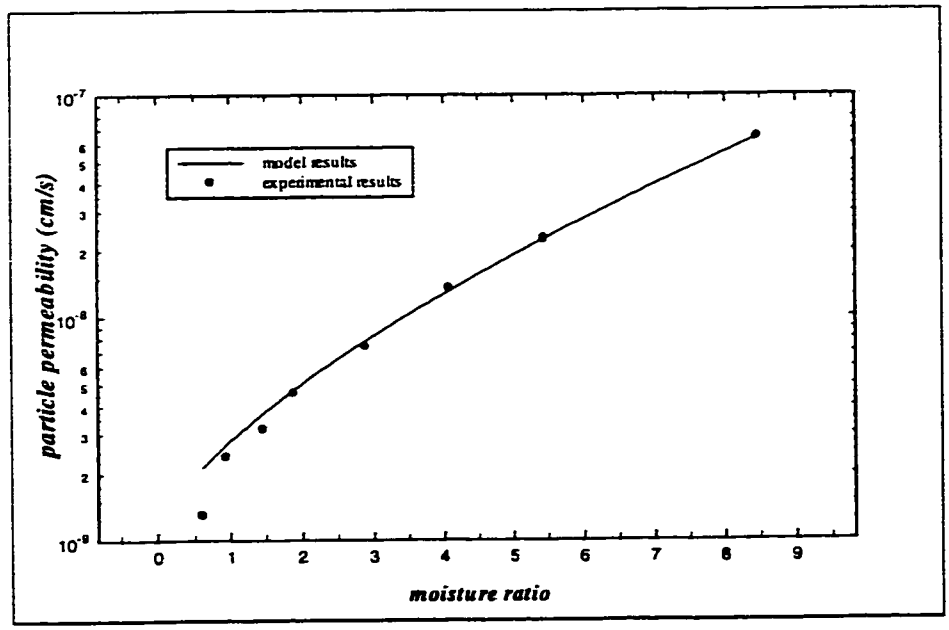

Fig. 4.11) Experimental and model results of soil particle permeability coefficient as a function of soil moisture ratio

CHAPTER

5
Numerical Analysis and Model Verification

In chapter 2, a generalized three dimensional equation was derived on the basis of a water adsorption mechanism during the water flow through unsaturated, expansive soils. Subsequently it was simplified into the one dimensional equation (Eq. 2.51), with a dependent variable, ϑ, and non-linear coefficients, characterized and measured in chapter 3.

In the present chapter, in order to investigate the validity of the mathematical model, a numerical method is introduced. Furthermore, a series of unsaturated flow column tests are conducted to verify the numerical results. In the first part of this chapter, a neural network model is established to accomplish the proper estimation of hydraulics and swelling parameters of the soil sample. Afterward, Eq.2.51, the governing equation of flow, is solved employing an implicit finite difference method with the help of a developed computer program in C++ language.

In the second part of this chapter, the results from the numerical evaluation of governing equation are verified against certain tests for which an apparatus was designed and set up to perform a series of column tests. The tests were conducted in three different conditions upon applied overload pressure: completely confined, semi-confined and free to

swell.

5.1. Part I: Numerical Analysis

This section deals with the numerical techniques developed to achieve a proper solution to Eq.2.51 derived as follows:

$$\frac{\rho_s}{\rho_b}(1+exp(-\beta\vartheta_w))\left(\frac{\partial\vartheta_w}{\partial t}\right)_{Z_R} = \frac{\partial}{\partial Z_R}\left(D_w\frac{\partial\vartheta_w}{\partial Z_R}\right)+\frac{\partial K_w}{\partial Z_R} + \vartheta_w\frac{\partial}{\partial Z_R}\left(D_s\frac{\partial\vartheta_w}{\partial Z_R}\right)-D_s exp(-\beta\vartheta_w)\left(\frac{\partial\vartheta_w}{\partial Z_R}\right)^2$$

considering:

$$T_1 = \frac{\rho_s}{\rho_b}(1+exp(-\beta\vartheta_w)) \qquad T_2 = D_s exp(-\beta\vartheta_w)$$
$$D_1 = D_w \qquad D_2 = D_s \qquad \text{Eq. 5.1}$$

or:

$$T_1\left(\frac{\partial\vartheta_w}{\partial t}\right)_{Z_R} = \frac{\partial}{\partial Z_R}\left(D_1\frac{\partial\vartheta_w}{\partial Z_R}\right)+\frac{\partial K_w}{\partial Z_R}+\vartheta_w\frac{\partial}{\partial Z_R}\left(D_2\frac{\partial\vartheta_w}{\partial Z_R}\right)-T_2\left(\frac{\partial\vartheta_w}{\partial Z_R}\right)^2 \qquad \text{Eq. 5.2}$$

which is subject to the initial and boundary condition as follows:

$$\vartheta_w = \vartheta_\circ \quad t = 0 \quad Z_R \geq 0$$
$$\vartheta_w = \vartheta_n \quad t > 0 \quad Z_R = 0 \qquad \text{Eq. 5.3}$$
$$\vartheta_w = \vartheta_l \quad t > 0 \quad Z_R = L$$

and T1, T2, D1 and D2 are functions of ϑ_w. They should be evaluated from the experimental data in each iteration procedure in the finite difference program having the necessary soil parameters. Next section discusses the evaluation of these coefficients.

5.1.1. Neural Network Model

Objectives for adopting the neural network technique to model the different experimental functions incorporating into the mathematical model, can be embodied in the following statements (Freeman and Skapura, 1992; Zurada, 1992):

a) The model can include as many input parameters as possible such as soil initial conditions (such as water content, bulk density, void ratio,...), swelling and shrinkage parameters and overload pressure.

b) There is an excellent agreement between the results of the trained model and those of the original function presented by experimental data.

c) The results of the model may be mathematically presented as a continuous and differentiable function for further use in the numerical solution.

d) The model is extremely flexible and is not restricted for the particular shape or condition of experimental function, i.e., it can be trained for any unusual or irregular dependency of the target on the input vector.

However, it should be mentioned that, like any other model, the neural network model has some disadvantages of which the most important are:

a) The model can better approximate a function within the training range and the extrapolation beyond the training range is considered to be rather difficult task unless some extra treatments are provided.

b) The accuracy of the evaluated output on the presentation of a set of input highly depends on the number of training sets in the learning process.

c) The generalization problem may be treated by presenting random input data and minimizing the number of neurons in each layer.

Despite the above difficulties, acceptable results may be achieved if the following considerations are correctly encountered:

a) Letting the model experience the possible range of data that is predicted to be used according to numerical needs.

b) Training the model using a set of random input data. In other words, if the experimental function consists of different sequential classes of data, these data should be randomly picked from the different classes and presented to the model.

c) Presenting a repetitive and random set of input data rather than unique presenta-

tion so that the training result will be much more reliable.

5.1.1.1. Terminologies

The neural network has been trained to perform complex functions in various fields of application. The field of the neural network has a history of some five decades but has found solid application only in the past ten years, and the field is still developing rapidly.

A neuron is an essential part of a neural network model that transmits input x through a connection that multiplies its value by weight w to form the following product (Fig. 5.1):

$$y = F(w \cdot x) \qquad \text{Eq. 5.4}$$

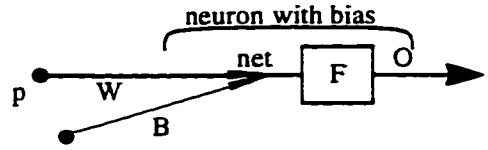

Fig. 5.1) A simple neuron with one input and one output

Function F, called activation function, generally calculates the output of a neuron by acting on the weighted input (the sum of the previous layer's output that has been multiplied by the weights). There are two major categories of activation functions: Continuous and Descriptive. The latter category mostly applies to logic, pattern recognition and classification. "Hard limit function," which limits the output of the neuron to either 0 or 1, is one of this type. The continuous functions have some analytical applications that generally can be either linear or non-linear. "Linear transfer function," which has an output equal to the input multiplied by a constant plus the bias, is usually used in the output layer since the

output can be covered from minus to plus infinity. A non-linear function is called unipolar or "Sigmoid function" if it squashes the input (which may have any value between plus and minus infinity) into the range between 0 and 1, and is called bipolar or "Tansig function" if it squashes the input into the range between -1 and 1. In practice, instead of a single neuron, one or multi layered neurons are employed. Generally the network can have a set of inputs/targets rather than a single pair (Fig. 5.2).

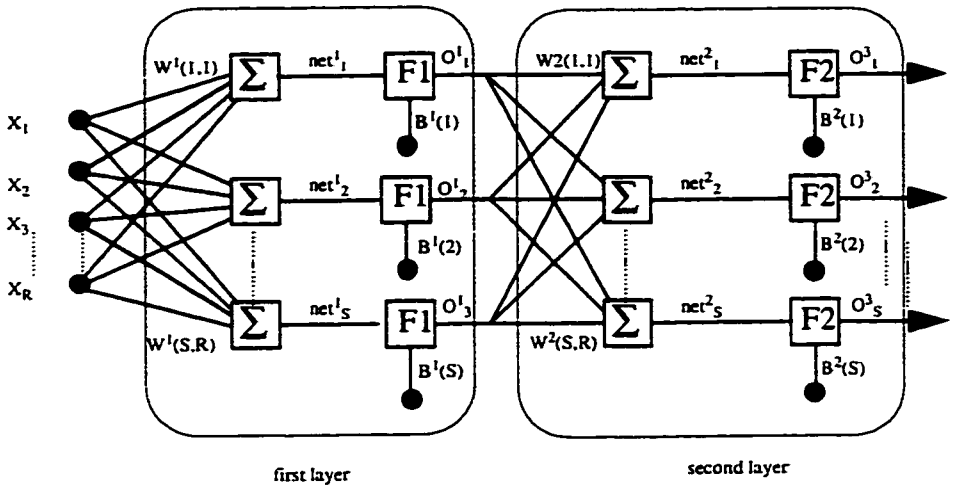

Fig. 5.2) Multi layered neurons with multi-input (R= # input and S= # neurons)

Hereafter, the different "notations" and script conventions, used to present the model, are adapted from Yazdizadeh et al. (1997). In such a complex model, the mathematical algorithm of each neuron's output takes the following form:

$$net_i^j = \sum_{k=1}^{n} W_{ik}^j \cdot X_k^j \qquad \text{Eq. 5.5}$$

$$Y_i^j = F_i^j(net_i^j) \qquad \text{Eq. 5.6}$$

where superscript j is the number of layers, subscript i stands for number of neurons in layer j and the second subscript, k, accounts for the number of neurons in the layer

j-1. X for the input layer is the input vector and for the other layers is the output of the previous layer.

For the purpose of this study, that is, to approximate the measured experimental functions, a learning method called back propagation network (BPN) was employed. In this method, input vectors and corresponding output vectors are used to train a network until it can approximate a function. The BPN learning rules are used to adjust weights and biases of networks, minimizing the sum of the squared errors of the network. A trained BPN tends to give reasonable answers when inexperienced inputs are presented. More intensive information about this method in particular and neural networks in general may be found in Freeman and Skapura (1992) and Zurada (1992). Also a typical "notations" and script conventions can be found in Yazdizadeh et al.(1997).

Table 5.1: Descriptions of Sub-Neural Networks Employed in the Main Model

name of the network	*inputs*	*output*
Net^a	$\vartheta, P, \vartheta_{ini}, B\%$	e
Net^b	$\vartheta, P, \vartheta_{ini}, B\%, e$	Ψ
Net^c	$\vartheta, P, \vartheta_{ini}, B\%, \Psi$	$K(\vartheta)$
Net^d	e	K_{sat}
Net^e	e	K_s
Net^f	e	P_s

The main frame of the neural network model, developed for the purpose of this study, was supported by several sub-networks, each of which is individually responsible for approximating one of the experimental functions. The assignments and corresponding experimental functions of all the sub-networks have been summarized in Table 5.1. The relations between the networks are illustrated in Fig. 5.3.

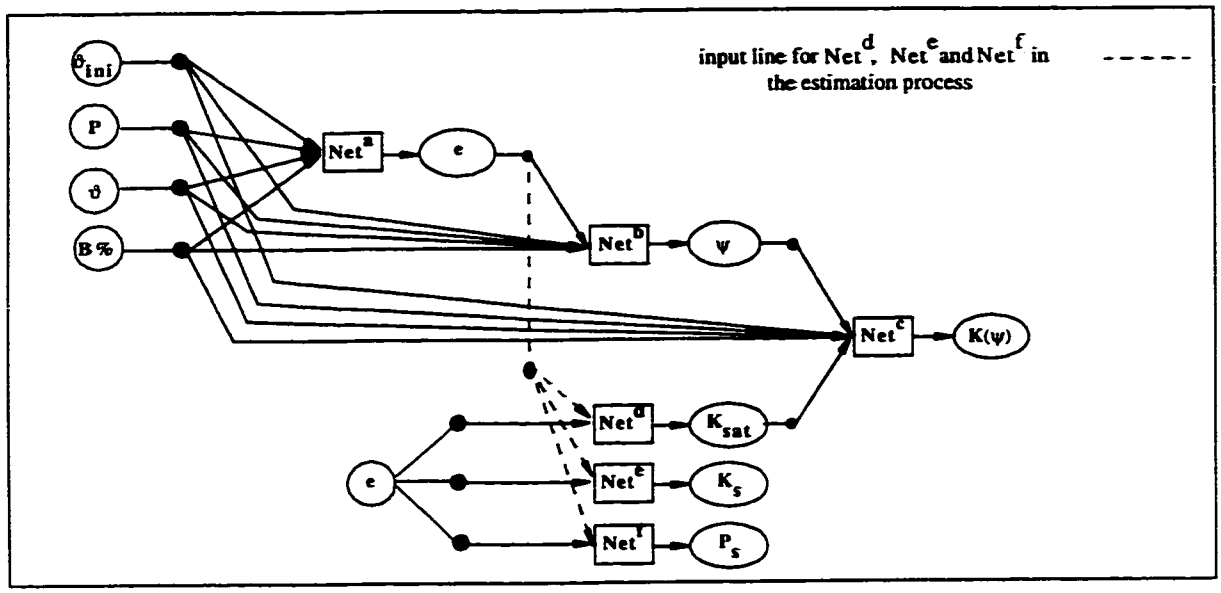

Fig. 5.3) Training and estimation sequence of the proposed neural network model

Before presenting the particular details of the network's analysis, it is helpful to illustrate the inter-relationship between the sub-networks. In training and estimation processes, an additional input, ***e***, which was in turn the output of network Net^a, was introduced to network Net^b, to evaluate the soil suction more accurately. On the other hand, the saturated hydraulic permeability, as an extra input, was presented to network Net^c to better estimate the unsaturated permeability. Networks Net^e and Net^f were trained parallel

to each other and independent of the others. However, in the estimation process, the output of network Net^{a} was considered as the only input of these networks.

In the following, the formal mathematical description of the BPN method, used for each individual sub-network, is presented.

5.1.1.2. Model Description

Each individual BPN includes four layers; the input layer, two hidden layers of the neurons and the output layer. The specifications of each layer has been summarized in Table 5.2

Table 5.2: Neural Network Model Specifications

layer	*S*	*F*
input	-	-
	5-15	tansig
hidden	3-10	tansig
output	1	purelin

S: number of neurons in each layer F: activation function

The tansig activation function, pointed out in the above table, was chosen as:

$$F(net) = \frac{2}{1 + exp(-2net)} - 1 \qquad \text{Eq. 5.7}$$

where *net* is calculated from Eq. 5.5. The purelin function is a linear function defined as:

$$F(net) = net \qquad \text{Eq. 5.8}$$

Eventually, after training the designed network, the analytical algorithm to find a mathematical expression describing the relation between inputs and output of the network takes

the following sequence:

$$net_j^k = \sum_{i=1}^{n} W_{ji}^k \cdot O_i^{k-1} + B_j^k \qquad (k=1,2,3),\ (j=1,2,\ldots,n^k) \qquad \text{Eq. 5.9}$$

and:

$$O_j^k = f_j(net_j^k) \qquad (j=1,2,\ldots,n^k),\ (k=1,2,3) \qquad \text{Eq. 5.10}$$

where superscript k represents the number of layers, W_{ji}^k is the final weight connecting the *i*th neuron from *(k-1)*th layer to the *j*th neuron of *k*th layer, O_j^{k-1} is the output of the *j*th neuron from *(k-1)*th layer which in turn is the input for *k*th layer and finally, B_j^k is the bias of the neuron. O_j^0 in Eq. 5.9 is the input vector and O_j^3 may be regarded as the output vector.

For a four layer neural network model, with the input vector of *m* degree and one single output, which is the case in all the experiments, the set of Eq. 5.9 and 5.10 can be summarized in one statement:

$$Y = F_3\left\{\sum_{k=1}^{N^2} W_{1k}^3 \cdot \left\{F_2\left\{\sum_{l=1}^{N^1} W_{kl}^2 \cdot \left\{F_1\left\{\sum_{m=1}^{N^0} W_{lm}^1 \cdot X_m + B_l^1\right\}\right\} + B_k^2\right\}\right\} + B^3\right\} \qquad \text{Eq. 5.11}$$

where N^k is the number of neuron in *k*th layer. Eq. 5.11 is the mathematical expression for a four layer neural network with *m* input and one output. Since some of the coefficients in the mathematical model, such as diffusivity coefficient of the water and the soil particles, appear as the differentiation of the output (for instance soil suction) with respect to one of

the input vectors (such as moisture ratio), Eq. 5.11 should be differentiable with respect to the inputs, X_m. First of all, in order to accomplish this, considering that all the activation functions used in Eq. 5.11 are continuous and differentiable, it can be easily proved that the Eq 5.9 is also a continuous and differentiable function and therefore, can be differentiated respect to each member of the input vector, X_m. Substituting the tansig and the purline functions in Eq. 5.11 from Eqs. 5.7 and 5.8 results in:

$$Y = \sum_{k=1}^{N^2} W_{1k}^3 \cdot \left\{ F\left\{ \sum_{l=1}^{N^1} W_{kl}^2 \cdot \left\{ F\left\{ \sum_{m=1}^{N^0} W_{lm}^1 \cdot X_m + B_l^1 \right\} \right\} + B_k^2 \right\} \right\} + B^3 \qquad \text{Eq. 5.12}$$

In order to differentiate from Eq.5.12, the differentiation of tansig function (Eq. 5.7) must be determined as follows:

$$\frac{dF(net)}{d(net)} = 1 - F^2(net) \qquad \text{Eq. 5.13}$$

Eventually, differentiation of Eq. 5.12 with the help of Eq. 5.13 results in:

$$\frac{dY}{dX_m} = \sum_{k=1}^{N^2} \left\{ W_{1k}^3 \cdot [1 - (F(net_k^2))^2] \cdot \sum_{i=1}^{N^1} \left\{ W_{ki}^2 \cdot [1 - (F(net_k^1))^2] \cdot W_{im}^1 \right\} \right\} \qquad \text{Eq. 5.14}$$

$$(m=1,2,\ldots,n^0)$$

were:

$$net_k^2 = \sum_{j=1}^{N^1} W_{kj}^2 \cdot F(net_j^1) + B_j^j \quad (k=1,2,\ldots,n^2) \qquad \text{Eq. 5.15}$$

$$net_j^I = \sum_{m=1}^{N^0} W_{jm}^I \cdot X_m + B_i^I \quad (j=1,2,\ldots,n^0) \qquad \text{Eq. 5.16}$$

A neural network program was developed in the neural network toolbox of MATLAB software for the training process. In further numerical considerations, Eq. 5.12 and Eq. 5.14 were coded as one of the main program's subroutines for the estimation of the coefficients used in the mathematical model.

5.1.2. Finite difference scheme

From the physical point of view, the problem described by Eq. 5.2 can be categorized as a propagation or initial value problem. Considering the mathematical behavior of the equation, it may be called a parabolic equation since the mixed derivative term is absent and moreover, the second order derivative of only one of the independent variables is presented.

To numerically evaluate this equation, a finite difference approach was developed. Since the equation contains several non-linear terms, one possible solution is to employ an explicit difference scheme. However, this method requires a complete stability analysis as well as investigation of the convergency which indeed are the most important characteristics of the method. To avoid this extreme inconvenience, the implicit method was employed which caries some stability and convergency advantages. After dropping the unnecessary index, Eq. 5.2 may be rewritten as:

$$T_1\vartheta_t = -(D_1\vartheta_z)_z + \vartheta(D_2\vartheta_z)_z - T_2(\vartheta_z)^2 + T_3\vartheta_z \qquad \text{Eq. 5.17}$$

where $T_3 = dK/d\vartheta$, since K is only a function of ϑ. It is assumed that the point ϑ_i^n forms a discrete approximation for Eq. 5.17 with uniform time interval Δt and uniform vertical spacing Δz in each time interval. Using the backward and central difference formula for the first and second order space derivatives respectively, and forward difference formula for the time derivative term, Eq. 5.17 can be discretized in fully implicit form as follows:

$$\frac{1}{\Delta t}(T_1)_i^{n+1}(\vartheta_i^{n+1}-\vartheta_i^n) = -\frac{1}{\Delta z^2}[(D_1)_{i+1/2}^{n+1}(\vartheta_{i+1}^{n+1}-\vartheta_i^{n+1})-(D_1)_{i-1/2}^{n+1}(\vartheta_i^{n+1}-\vartheta_{i-1}^{n+1})]$$
$$+\frac{1}{\Delta z^2}\vartheta_i^{n+1}[(D_2)_{i+1/2}^{n+1}(\vartheta_{i+1}^{n+1}-\vartheta_i^{n+1})-(D_2)_{i-1/2}^{n+1}(\vartheta_i^{n+1}-\vartheta_{i-1}^{n+1})] \quad \text{Eq. 5.18}$$
$$-\frac{1}{\Delta z^2}(T_2)_i^{n+1}(\vartheta_i^{n+1}-\vartheta_{i-1}^{n+1})^2+\frac{1}{\Delta z}(T_3)_i^{n+1}(\vartheta_i^{n+1}-\vartheta_{i-1}^{n+1})$$

The truncation error of such a discretization is: $O(\Delta t, \Delta z^2)$. Considering the following assumptions:

$$\lambda = \frac{\Delta t}{\Delta z^2}\ ,\ d=(T_2)_i^{n+1}\ ,\ g=(T_3)_i^{n+1}\ ,\ b_1=(D_1)_{i+1/2}^{n+1}=\frac{1}{2}[(D_1)_i^{n+1}+(D_1)_{i+1}^{n+1}]$$
$$b_2=(D_1)_{i-1/2}^{n+1}=\frac{1}{2}[(D_1)_{i-1}^{n+1}+(D_1)_i^{n+1}] \quad \text{Eq. 5.19}$$
$$c_1=(D_2)_{i+1/2}^{n+1}=\frac{1}{2}[(D_2)_{i+1}^{n+1}+(D_2)_i^{n+1}]\ ,\ c_2=(D_2)_{i-1/2}^{n+1}=\frac{1}{2}[(D_2)_{i-1}^{n+1}+(D_2)_i^{n+1}]$$

and after some rearrangement, Eq. 5.18 reduces to:

$$(a-\lambda b_1-\lambda b_2-\Delta z\lambda g)\vartheta_i^{n+1}+\lambda b_1\vartheta_{i+1}^{n+1}+(\lambda b_2+\Delta z\lambda g)\vartheta_{i-1}^{n+1}+(\lambda c_1+\lambda c_2-\lambda d)(\vartheta_i^{n+1}$$
$$+\lambda d(\vartheta_{i-1}^{n+1})^2-\lambda c_1(\vartheta_i^{n+1}\vartheta_{i+1}^{n+1})-(\lambda c_2+2\lambda d)(\vartheta_i^{n+1}\vartheta_{i-1}^{n+1})=a\vartheta_i^n \quad \text{Eq. 5.20}$$

This difference equation has two distinct non-linear characteristics. First of all, the coefficients *a, b, c, d* and *g* should be evaluated at time *n+1*; therefore, they are considered the

additional unknowns in each time step. Secondly the fourth, fifth, sixth and seventh terms on the left hand side of the equation count as the non-linear terms in a system of algebraic equations.

The simplest and most common solution to the first type of non-linearity is to linearize the difference equation by evaluating all unknown coefficients at the previous marching time station. To improve this method, one may use a simple iterative updating procedure. To do this, after solving the first set of equations in time $n+1$ by utilizing the coefficients from the previous time, n, the coefficient can be updated by utilizing the solution just obtained at the time $n+1$. This procedure can be repeated iteratively until the desired accuracy is obtained. The second aforementioned non-linearity of the equation may be handled using Newton linearization with more satisfactory convergency. This method is also known as Successive Approximations by Newton linearization.The convergency of this method depends on the accuracy of the initial guess and for this reason the time interval must not be too large. More intensive information regarding this approach and others as well, can be found in Anderson (1992).

The following details denote how Newton linearization was applied to non-linear terms in Eq. 5.20:

fourth and fifth terms: Assuming: $\eta = \hat{\vartheta}_i^{n+1}$, $f(\eta) = \eta^2$, $\Delta\eta = \vartheta_i^{n+1} - \hat{\vartheta}_i^{n+1}$ where the caret ($\hat{}$)denotes an evaluation of the variable from a previous iteration level and $\Delta\eta$ is denoted as the change in ϑ_i^{n+1} between two iterative solutions obtained from the difference equation. Expanding the fourth term about the value at the previous iteration level by

means of Taylor series, it can be written:

$$(\vartheta_i^{n+1})^2 = f(\eta + \Delta\eta) = f(\eta) + \frac{\partial f}{\partial \eta}\Delta\eta + \ldots\ldots \qquad \text{Eq. 5.21}$$

Neglecting the terms with derivative of order two and higher, after substitution the result is:

$$(\vartheta_i^{n+1})^2 = 2\hat{\vartheta}_i^{n+1}\vartheta_i^{n+1} - (\hat{\vartheta}_i^{n+1})^2 \qquad \text{Eq. 5.22}$$

where the only unknown on the right hand side of the equation is ϑ_i^{n+1} and hence, the fourth non-linear term can be replaced by its equivalent linear terms. The same formula might be derived for the fifth term:

$$(\vartheta_{i-1}^{n+1})^2 = 2\hat{\vartheta}_{i-1}^{n+1}\vartheta_{i-1}^{n+1} - (\hat{\vartheta}_{i-1}^{n+1})^2 \qquad \text{Eq. 5.23}$$

To linearize the sixth term, it can be assumed:

$$\eta_1 = \hat{\vartheta}_i^{n+1}\ ,\ \eta_2 = \hat{\vartheta}_{i+1}^{n+1}\ ,\ f(\eta_1, \eta_2) = \eta_1\eta_2\ ,\ \Delta\eta_1 = \vartheta_i^{n+1} - \hat{\vartheta}_i^{n+1}\ ,\ \Delta\eta_2 = \vartheta_{i+1}^{n+1} - \hat{\vartheta}_{i+1}^{n+1}$$

Expanding the sixth term about the value at the previous iteration level using the Taylor series results in:

$$\vartheta_i^{n+1}\vartheta_{i+1}^{n+1} = f(\eta_1 + \Delta\eta_1, \eta_2 + \Delta\eta_2) = f(\eta_1, \eta_2) + \frac{\partial f}{\partial \eta_1}(\Delta\eta_1) + \frac{\partial f}{\partial \eta_2}(\Delta\eta_2) + \ldots\ldots \text{Eq. 5.24}$$

Neglecting the terms with derivative of order two and higher, after substitution:

$$\vartheta_i^{n+1}\vartheta_{i+1}^{n+1} = \hat{\vartheta}_i^{n+1}\hat{\vartheta}_{i+1}^{n+1} + \hat{\vartheta}_i^{n+1}\vartheta_i^{n+1} + \hat{\vartheta}_{i+1}^{n+1}\vartheta_{i+1}^{n+1} - (\hat{\vartheta}_i^{n+1})^2 - (\hat{\vartheta}_{i+1}^{n+1})^2 \qquad \text{Eq. 5.25}$$

with the same algorithm, the last term becomes:

$$\vartheta_i^{n+1}\vartheta_{i-1}^{n+1} = \hat{\vartheta}_i^{n+1}\hat{\vartheta}_{i-1}^{n+1} + \hat{\vartheta}_i^{n+1}\vartheta_i^{n+1} + \hat{\vartheta}_{i-1}^{n+1}\vartheta_{i-1}^{n+1} - (\hat{\vartheta}_i^{n+1})^2 - (\hat{\vartheta}_{i-1}^{n+1})^2 \qquad \text{Eq. 5.26}$$

Substituting Eq 5.22, Eq 5.23, Eq 5.25 and Eq 5.26 into the difference equation, Eq.5.19, results in:

$$A\vartheta_i^{n+1} + B\vartheta_{i+1}^{n+1} + C\vartheta_{i-1}^{n+1} = D \qquad \text{Eq. 5.27}$$

where:

$$A = a - \lambda b_1 - \lambda b_2 - \Delta z \lambda g + (\lambda c_1 + \lambda c_2 - 4\lambda d)\hat{\vartheta}_i^{n+1} \qquad \text{Eq. 5.28}$$

$$B = \lambda b_1 - \lambda c_1 \hat{\vartheta}_{i+1}^{n+1} \qquad \text{Eq. 5.29}$$

$$C = \lambda b_2 + \Delta z \lambda g - \lambda c_2 \hat{\vartheta}_{i-1}^{n+1} \qquad \text{Eq. 5.30}$$

$$D = a\vartheta_i^n - 3\lambda d(\hat{\vartheta}_i^{n+1})^2 - (\lambda c_2 + 3\lambda d)(\hat{\vartheta}_{i-1}^{n+1})^2 - \lambda c_1(\hat{\vartheta}_{i-1}^{n+1})^2 + \lambda c_1 \hat{\vartheta}_i^{n+1}\hat{\vartheta}_{i+1}^{n+1} + (\lambda c_2 + 2\lambda d)\hat{\vartheta}_i^{n+1}\hat{\vartheta}_{i-1}^{n+1} \qquad \text{Eq. 5.31}$$

Equation 5.27 is a tridiagonal algebraic set of equations which may be solved in each time step iteratively until the desired accuracy for the solution is achieved. In order to start the iteration procedure in the first time step, the initial value of ϑ might be used as a first guess to initiate the unknown coefficients in equation 5.27. For the next iteration, the new values of ϑ will be used to evaluate the new coefficients.

Fig. 5.4 (p.illustrates the mesh structure assumed in the development of the computer code in the numerical analysis. The lateral discretization belongs to the time, while the vertical intervals stand for the space. Counter *k*, that is the time interval number, begins from one to the maximum covering the whole infiltration time. Counter *m*, that is the number representing the vertical space discretizations, begins from zero at the upper boundary to *m* at the lower boundary. Three sets of algebraic equations may be extracted from Eq. 5.27 by substituting for *i* from *1* to *m-1*:

$$A_1\vartheta_1^{n+1} + B_1\vartheta_2^{n+1} = D_1 - C_1\vartheta_0^{n+1} \qquad i = 1$$

$$A_i\vartheta_i^{n+1} + B_i\vartheta_{i+1}^{n+1} + C_i\vartheta_{i-1}^{n+1} = D_i \qquad 2 \le i \le m-2 \qquad \text{Eq. 5.32}$$

$$A_{m-1}\vartheta_{m-1}^{n+1} + C_{m-1}\vartheta_{m-2}^{n+1} = D_{m-1} - B_{m-1}\vartheta_m^{n+1} \qquad i = m-1$$

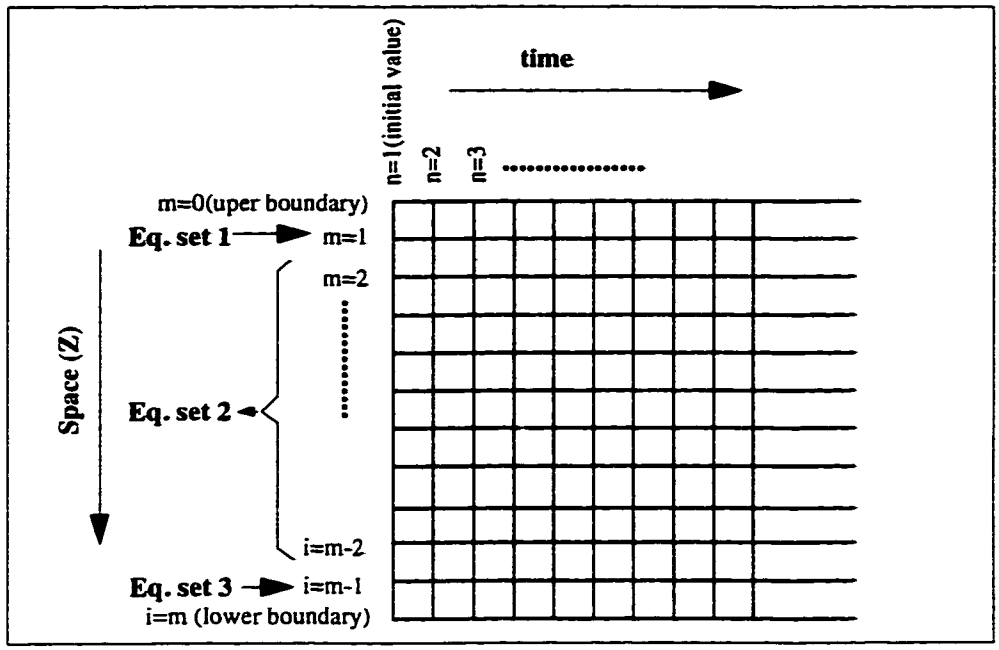

Fig. 5.4) Sketch of designed mesh for computer code algoritme

The set of Eq. 5.32 is iteratively solved in each time step by using a computer program, developed in C++ language. The flowchart of the computer program algoritme has been illustrated in Fig 5.5 (p.137).

5.2. Experimental verification

The results of the numerical analysis of the developed theoretical model were verified through a set of infiltration experiments. Tests were conducted by letting distilled water infiltrate through semi-infinity soil columns in three different confinement condi-

tions: completely confined, semi-confined and free to swell. The goal of these series of tests was to find the moisture profile at different times.

5.2.1. Apparatus and test procedure

An apparatus was designed and set up to be used in the three aforementioned conditions of soil confinement in the infiltration test. Figs. 5.6 (p.138) through 5.8 (p.140) illustrate the different set up of this apparatus. The first set up (Fig. 5.6) deals with the free swelling of the soil column in which the amount of swelling was recorded by a micrometer adjusted over the sample. The sample had access to the water from the top and the water level was kept constant during the experiment. A light cap was placed over and in contact with the soil surface to avoid soil dispersion at the surface. Each soil column, while being removed from the cell by means of a designed sample extruder, was sliced using a cutting device. The thickness of the slice was controlled by reading a micrometer placed over the extruder. After slicing, the weight and moisture content of the slices were determined by conventional methods. Eventually, as a result, a set of moisture profiles, as well as time-swelling curves, were obtained.

The next apparatus set up was related to the sample in the semi-confinement condition (Fig.4.7). In this set up an overload equal to 55 kPa was applied over the sample by hanging the proper weight to both sides of the load arm. Similar to the previous set up, the swelling was recorded by means of a micrometer adjusted over the soil surface. Accessing the distilled water from the top, the soil swelled upward. At a scheduled time, the sample inside the cell was sliced and finally the different moisture profiles were obtained.

In the last verification test, another apparatus was set up to examine the effect of the completely confined soil sample on moisture profiles (Fig.4.8). After fixing the top cap over the soil surface with no free space, water was allowed to infiltrate the sample from the top. The swelling pressure progress was measured by means of a rigid load cell adjusted over the sample. With the procedure explained in the previous tests, after different times, the samples were extruded from the cell, sliced and their water content and other physical properties were determined. As a result, similar information about the moisture profiles of the soil column was obtained.

For the porpuse of Numerical Analysis, the moisture ratio corresponding to three different conditions were experimentally found and summarized in Table 2.1.

Table 5.3: Maximum Moisture Ratio, ϑ_{sat}, for Different Overloading Conditions

Sample	*Overload kPa*	ϑ_{ini} *cm3/cm3*	ϑ_{sat} *cm3/cm3*	ρ_{ini} *cm3/cm3*
Free swelling	0	0.15	4.00	1.75
semi-confined	50	0.15	1.75	1.75
confined	>275	0.15	1.00	1.75

In the upcoming chapter these results and those of the numerical analysis are compared using different criteria.

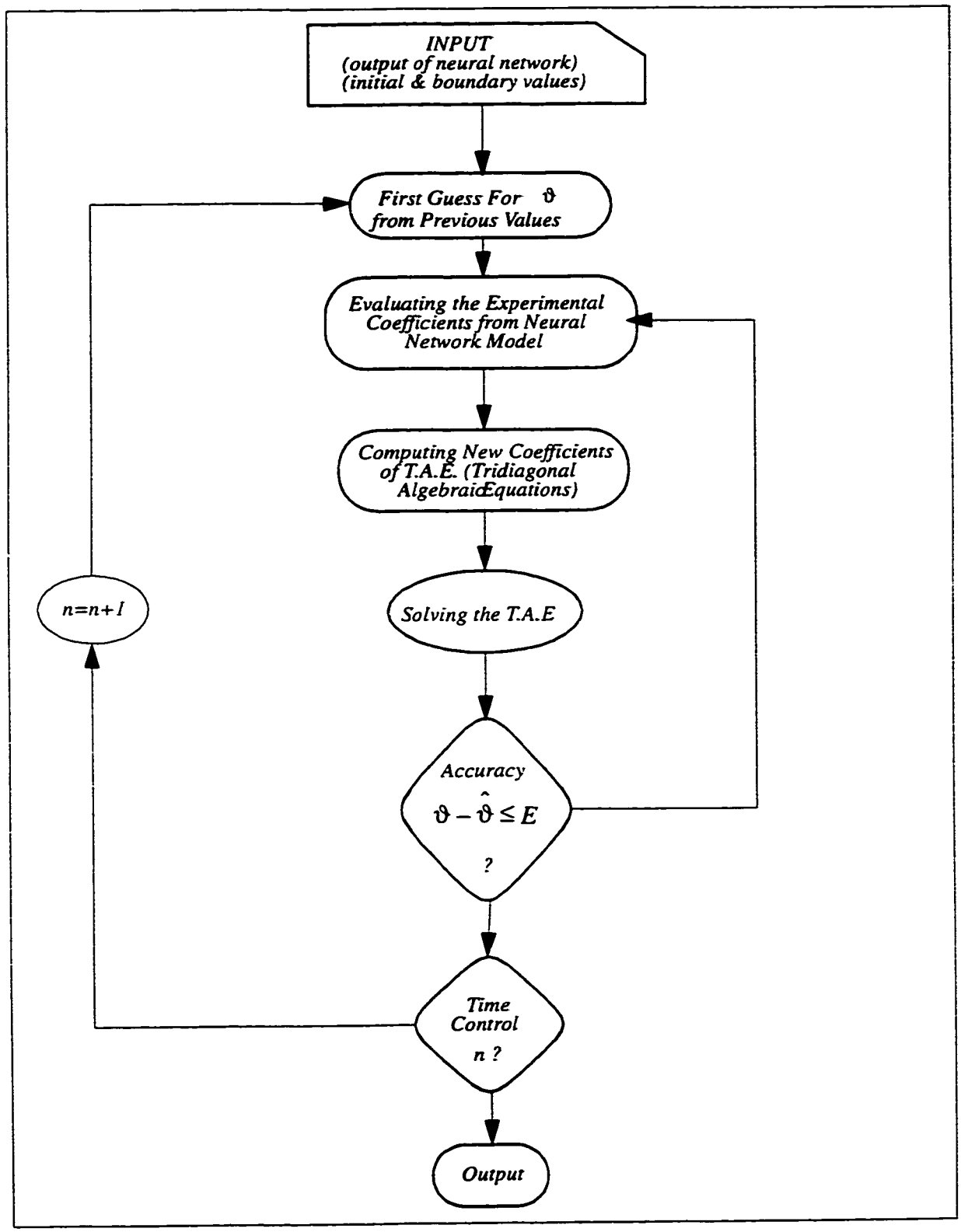

Fig. 5.5) Flowchart of computer program for numerical evaluation of Eq.4.17

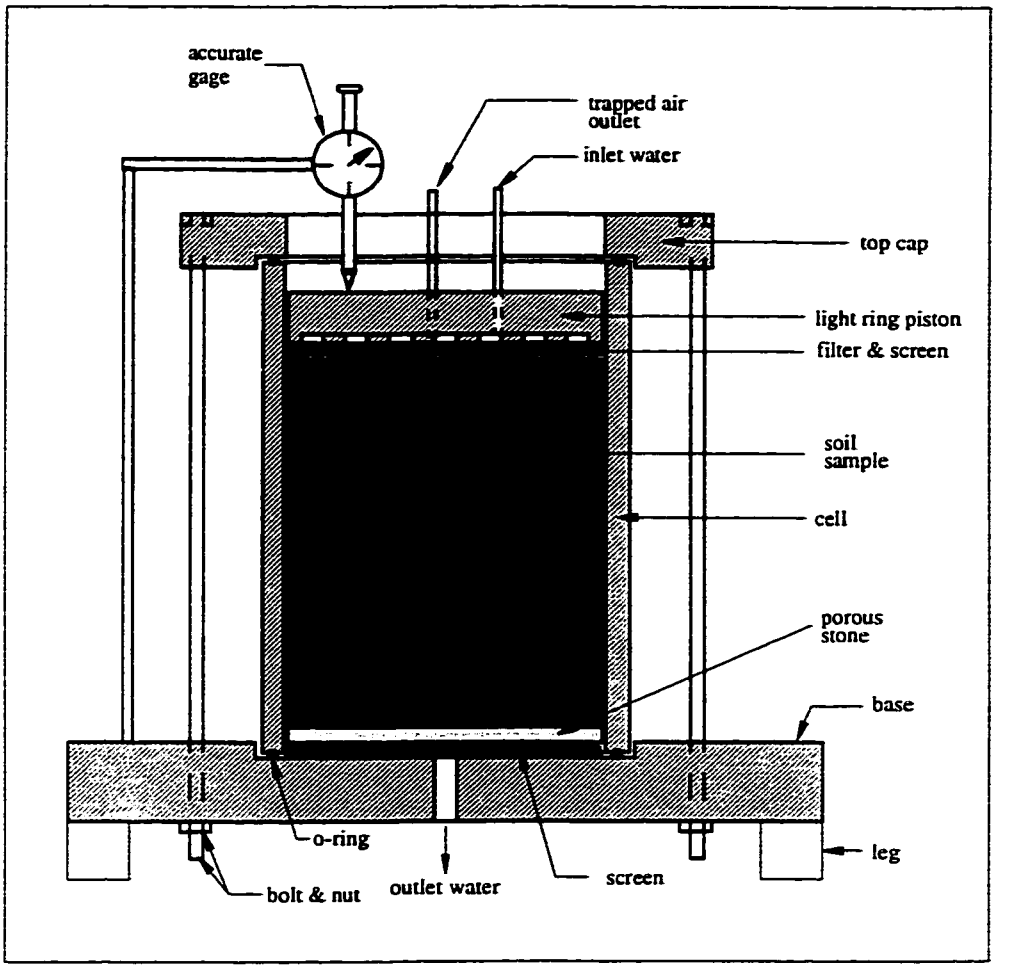

Fig. 5.6) Apparatus set up for free swelling infiltration test (slice method)

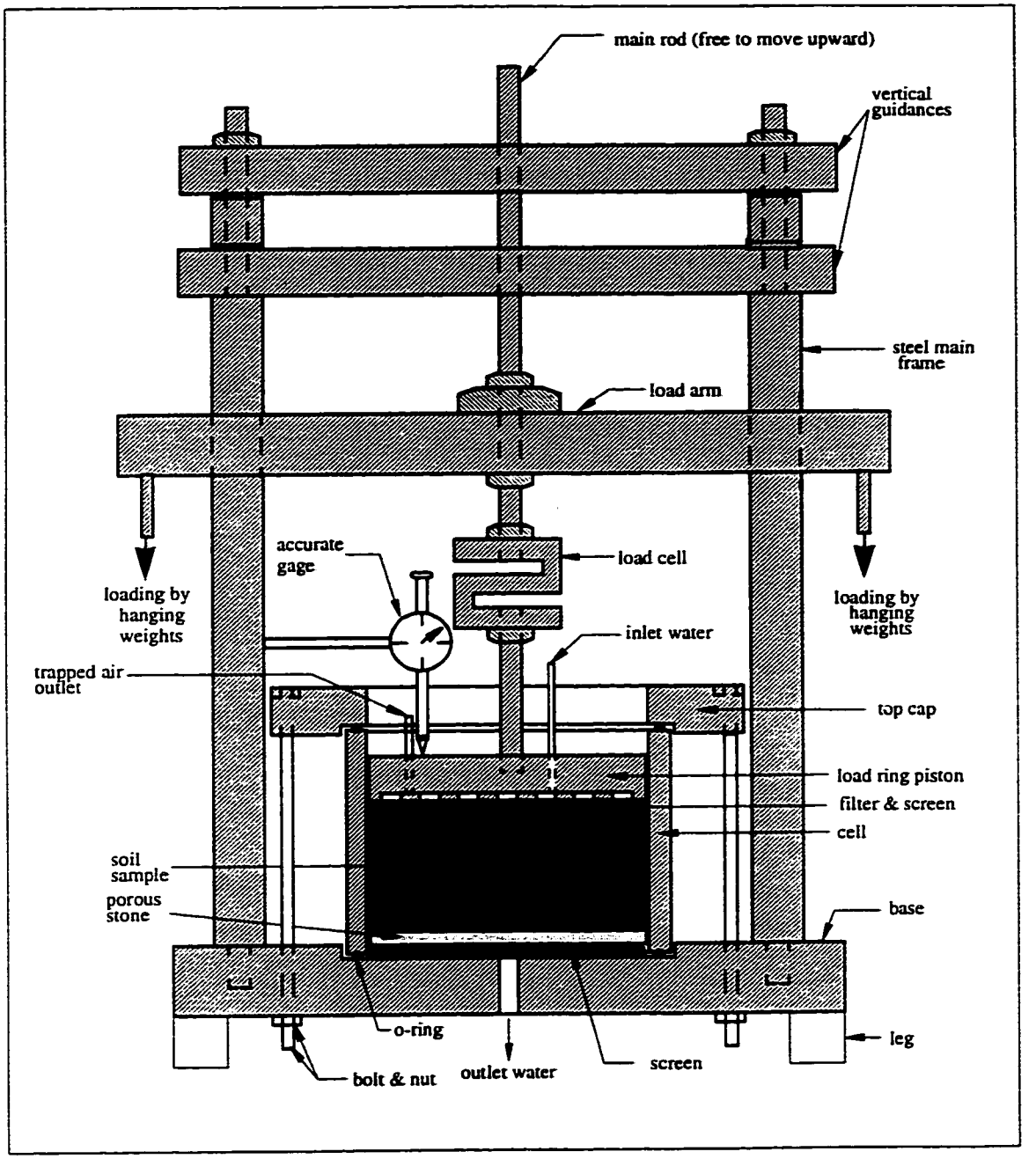

Fig. 5.7) Apparatus set up for semi-confine condition of infiltration test (slice method)

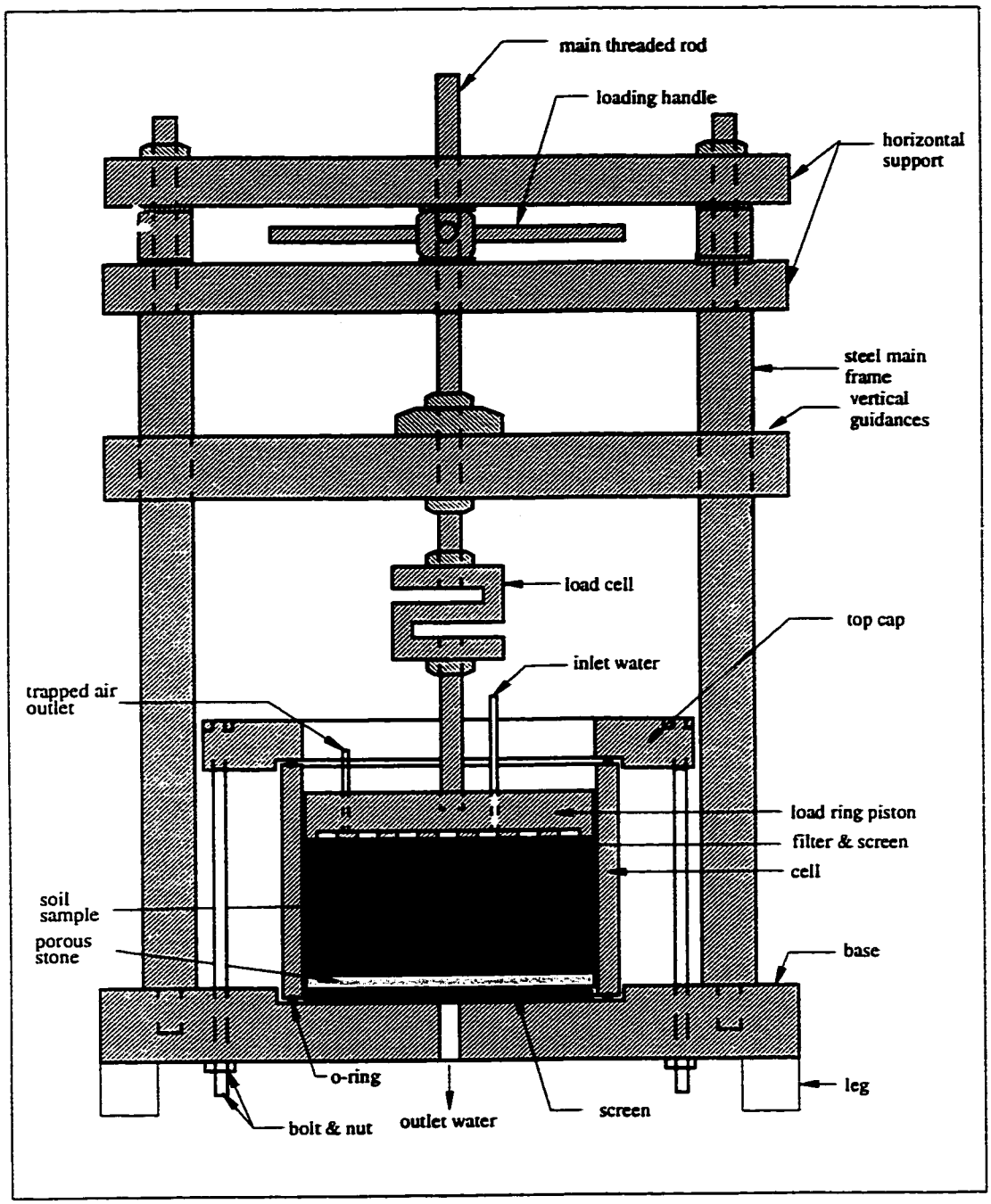

Fig. 5.8) Apparatus set up for completely confine condition of infiltration test (slice method)

CHAPTER

6
Results and Discussion

In the previous chapters, a one dimensional analytical model for the flow of water through swelling soils was developed, and the required coefficients were experimentally determined. Furthermore, a numerical analysis of the developed model was carried out in two parts; to accomplish the first part, a neural network model was established to organize the experimental results for further utilization, and in the second part a finite difference scheme was coded to give an approximate solution to the theoretical model. Eventually, a set of infiltration tests was conducted for model verification.

The experimental results of the hydraulic and swelling properties of the soil implemented in the theoretical model as the linear or nonlinear coefficients, were briefly discussed in chapters 3 and 4. In the following chapter the discussion first focuses on the validity of the proposed neural network model. Then the results of the numerical analysis are compared with the infiltration data. Subsequently an intensive sensitivity analysis of the numerical solution is presented and finally some further works are proposed which are thought to be complementary to the present study.

6.1. Neural Network Model

As discussed earlier in chapter 5, a designed neural network model was applied to the experimental data. In order to assess the ability of the model to approximate the experimental functions, the results of this application are compared with those of other empirical formulas, evaluating hydraulic and swelling properties of an unsaturated, swelling soil. For instance, the results of the soil moisture retention measurement test on sample KA1 discussed in chapter 3 are compared with the results of the empirical and neural network model. The modified Van Genuchten model, Eq. 3.10, with parameters extracted from Table 3.12 is assumed as the empirical model for the moisture retention curve. Fig. 6.1 (p.148) illustrates the comparison between experimental data and two fitted models. By inspection of these graphs it is clear that there is a much better agreement between the initial data and neural network model and that almost a perfect fit by this model was achieved over the entire range of data. For further demonstration of the ability of the neural network model, a second example from the soil shrinkage measurement test was selected. The experimental results of specimen A4 (or B1) from Table 3.15 in chapter 3 and the results obtained from the neural network model were plotted in Fig. 6.2 (p.148). The graph shows an excellent compatibility between the two results. The same agreement is observed in the modeling of other experimental data. Experience with model showed that, for those experimental results having a higher density of data points, the interpolation of the data by the model is more successful. However, the application of the model to the results of the saturated permeability test, which has the lowest data density among all the experimental tests, proved the acceptable accuracy of the model. This is illustrated in Fig. 6.3 (p.149).

6.1.1. Model Sensitivity

The developed neural network model was found to be sensitive to a number of factors each of which was optimized by testing different model results. For instance, it was found that the number of neurons in either layer (hidden or intermediate) influences the nature of the model's interpolation. In other words, choosing a higher number of neurons in the hidden layers may result in faster convergency of the learning process and significantly increases the accuracy for the exact input points, but the number of local minimizations in each layer may increase which in turn causes much more difficulty for the model to minimize the error in accordance with the desired error. Furthermore, nonlinear interpolation of the points between the exact input data may fail if a higher number of neurons is chosen. The optimized number of neurons were found to be between 5 and 15 for the first layer, and 3 to 10 for the second layer depending on the complexity of the curve shape and the density of data. As discussed in chapter 4, multiple presentation of the data set will also improve the learning process. Following this procedure may consume more computer time but produces more satisfactory results.

6.2. Infiltration Test Results

As discussed in chapter 5, to verify the results of the numerical analysis of the developed mathematical model, infiltration tests in three different conditions were conducted. The results of the first test (free to swell in upward direction) are illustrated in Figs. 6.4 (p.149) and 6.5 (p.150). In the first figure (6.4), soil moisture profiles in depth are graphed at different times. The horizontal line, Z=0, represents the initial soil surface. As

the infiltration of water into the soil progresses, the soil swells and its surface moves up to the maximum of 25 mm during 30 days. The rate of soil expansion is high at the beginning of the infiltration (60% in 7 days) and gradually decreases. During the infiltration, the expanded layer (0-2.5 cm.) has a relatively higher degree of water content which significantly drops along a very short length of depth. This result shows that the infiltration of water is highly dependent on the amount of free water which is limited in the higher depth as a result of less expansion and higher bulk density. However, the slope of the transition part of the curve gradually increases. From the figure, the smallest transition part is 7 mm after 5 hours, and the biggest is about 5 cm after 30 days. Fig. 6.5 shows the same results but from a different point of view, that is, the assessment of moisture ratio variation at a certain spatial point. Rapid saturation is observed at the depth close to the surface, but there is significantly slower saturation in the higher depth. The maximum saturation point for each curve depends on the soil bulk density at the corresponding depth, i.e., the higher the depth the smaller the maximum saturation.

The results of the second test, water infiltration through an unsaturated, overloaded (50 kPa), swelling soil sample, are shown in Figs. 6.6 (p.150) and 6.7. Inspecting the figures, a similar trend, with respect to the unloaded test, is observed. However, as a result of overloading, relatively less soil expansion occurred and the maximum swelling was recorded as 6.5 mm during 20 days. The maximum moisture ratio measured at the surface was 1.8 cm^3/cm^3, while the unloaded sample measured more than 4 cm^3/cm^3.

The results of the third infiltration test, under completely confined condition, have been illustrated in Figs. 6.8 (p.151) and 6.9 (p.152). In this test, as a result of confinement,

no overall change in the soil porosity was observed. The maximum moisture ratio at the top of the sample was measured at $1cm^3/cm^3$ within 30 days, which was lower with respect to that of previous tests. This maximum drops in depth (Fig. 6.9); however, it is relatively lower than that of the other two tests. This interesting result confirms the important role of the overloading which restricts the infiltration. Inspecting Fig. 6.9, one may find a significantly rapid increase in the moisture ratio at the depth close to the surface (H=0 to .3 cm). Development of the swelling pressure versus logarithm of time is illustrated in Fig. 6.10 (p.152). According to the figure, the swelling pressure reaches its maximum value (275 kPa) after 7 days; thereafter, there is no significant change in the swelling pressure.

The set of graphs shown in Fig. 6.11 (p.153) together with Fig. 6.12 (p.154) compare the results of three infiltration tests. First (Fig. 6.11), the variation of moisture ratio at eight different depths is compared. It is concluded that the maximum saturation at any depth is at its highest for the free swelling condition and is at its lowest for the completely confined. If, according to the highest swelling pressure recorded, the completely confined condition is assumed to be virtually similar to a sample overloaded by 275 kPa pressure, a highly nonlinear distribution of maximum moisture ratio is observed at each depth. In other words, samples one and two, with a difference of 50 kPa in their overload, have a difference of 2.5 cm^3/cm^3 in their maximum saturation, while samples two and three, with a difference of 225 kPa in their overload, have a difference of 1 cm^3/cm^3 in their maximum saturation. Three 7 day moisture profiles, belonging to the three different infiltration tests, are tipically chosen and graphed in Fig. 6.12. After evaluating this and the other corresponding figures (not illustrated here), it is found that at any specific time, there is a depth at which all the three profiles becomes unique, measured with respect to the initial surface

level. This depth is called *Effective Infiltration Depth (EID)* and only depends on the type of soil and the time of measurement. Different effective infiltration depths at different times were determined and graphed in Fig. 6.13 (p.154). A linear relationship is observed between EID and time, which is formulated as: H_I =0.15 T (H_I in cm and T in day). Observing this interesting result, by having the time-EID curve, correspond to an arbitrary time, one may find a depth after which any moisture profile for an overloading pressure value in the infiltration test may be approximately constructed using just one moisture profile of the same time. Obviously a soil with no swelling activity does not have any EDI; i.e., obtaining only one moisture profile of any overloaded sample is sufficient to predict those of others.

6.3. Numerical Result Verification

This section verifies the results of the numerical analysis using those of infiltration tests. Depending on the initial soil condition in terms of the confinement, verification can be classified in three groups. The computer program input for all the conditions is summarized in Table 6.1. Other input such as moisture retention characteristics, saturated and unsaturated permeability, shrinkage and swelling characteristics, and particle permeability are accessible by the program through the results of the neural network model.

Table 6.1: General input parameters of soil for computer program

Sample	*Overload kPa*	β *cm3/cm3*	ϑ_{ini} *cm3/cm3*	ϑ_{sat} *cm3/cm3*	ρ_{ini} *g/cm3*
Free swelling	0	0.53	0.15	4.00	1.75
semi-confined	50	0.38	0.15	1.75	1.75
confined	>275	0.30	0.15	1.00	1.75

Figs. 6.14 (p.155) through 6.16 (p.156) show the comparison between the different moisture profiles obtained from the numerical and experimental results. As the figures show the results of the numerical analysis agree with those of the infiltration experiments. However, overall, little disagreement exists between the results from the very beginning and the end of the moisture profiles. This disagreement may be considered a result of discontinuity at the boundary and initial conditions. In the case of the completely confined condition (Fig. 6.16), the general flow equation (Eq. 2.51) is reduced to the following, considering $D_s=0$ and $\frac{\rho_s}{\rho_b} = a$:

$$a(1 + exp(-\beta\vartheta_w))\left(\frac{\partial\vartheta_w}{\partial t}\right)_{Z_R} = \frac{\partial}{\partial Z_R}\left(D_w\frac{\partial\vartheta_w}{\partial Z_R}\right) + \frac{\partial K_w}{\partial Z_R} \qquad \text{Eq. 6.1}$$

One may refer to this equation as a one dimensional flow equation characterizing the moisture distribution through an unsaturated, confined swelling soil.

In the numerical analysis, the amount of swelling can also be estimated from the relative shrinkage curve having the soil moisture ratio. Figs. 6.17 and 18 (p.157) illustrate the measured and estimated soil surface expansion during the time. Inspecting the curves, an overestimation is observed in the results of the numerical analysis. This overestimation can be due to the ignored hysteresis in the theoretical model development and experimental simulation. However, the results may be successfully used to predict the soil expansion upon wetting.

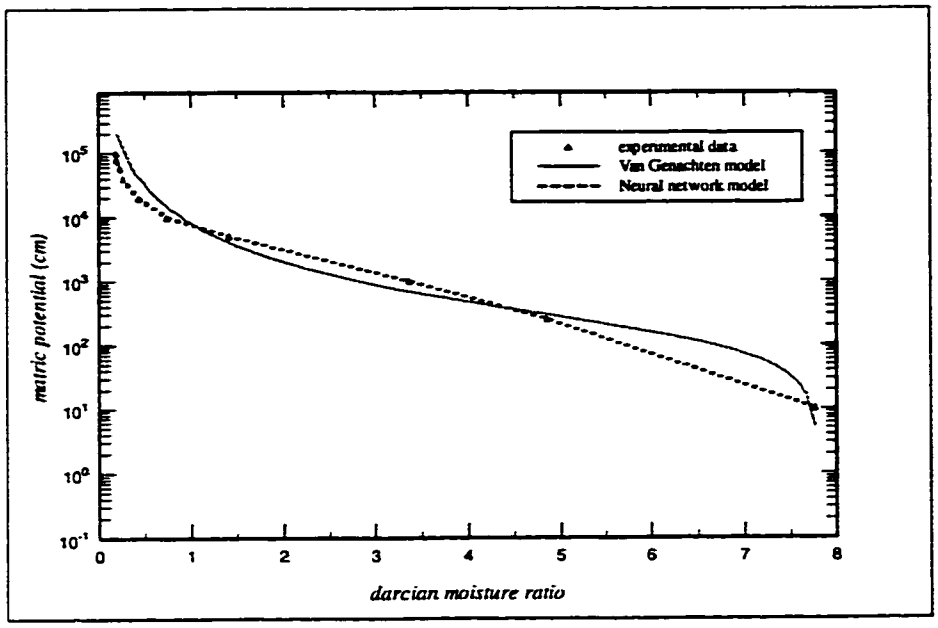

Fig. 6.1) Comparison between the experimental data and two model of empirical and neural network for sample A1 in soil moisture retention measurement test.

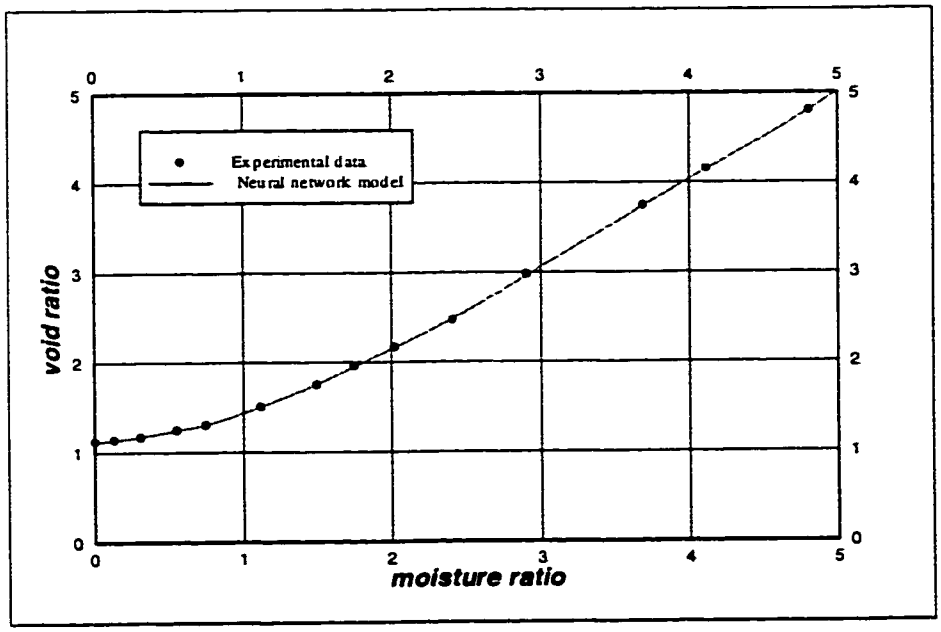

Fig. 6.2) Comparison between the experimental data and neural network model for sample A4 or B1 in soil shrinkage measurement test.

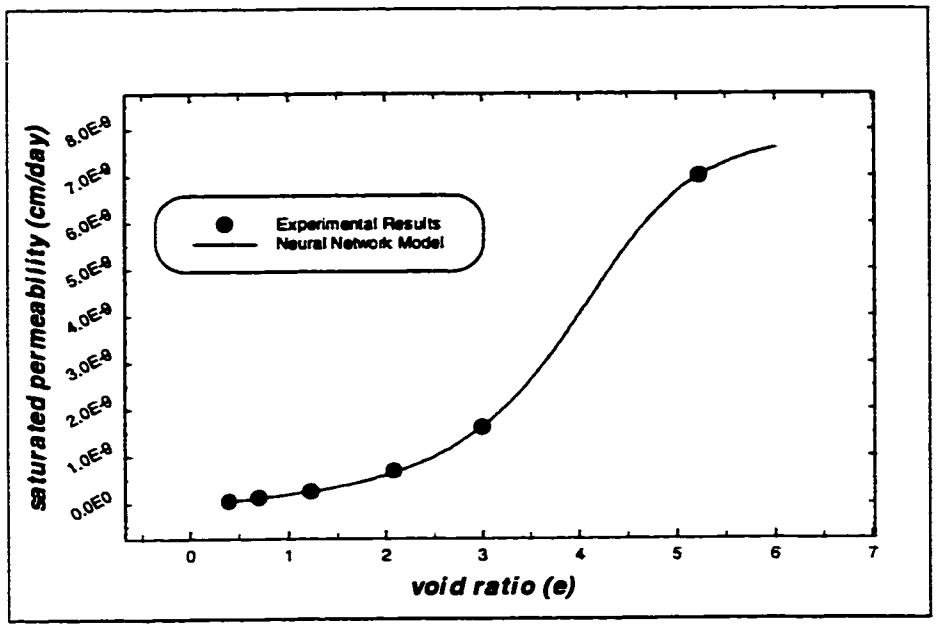

Fig. 6.3) Comparison between the experimental data and neural network model in saturated hydraulic conductivity versus void ratio test

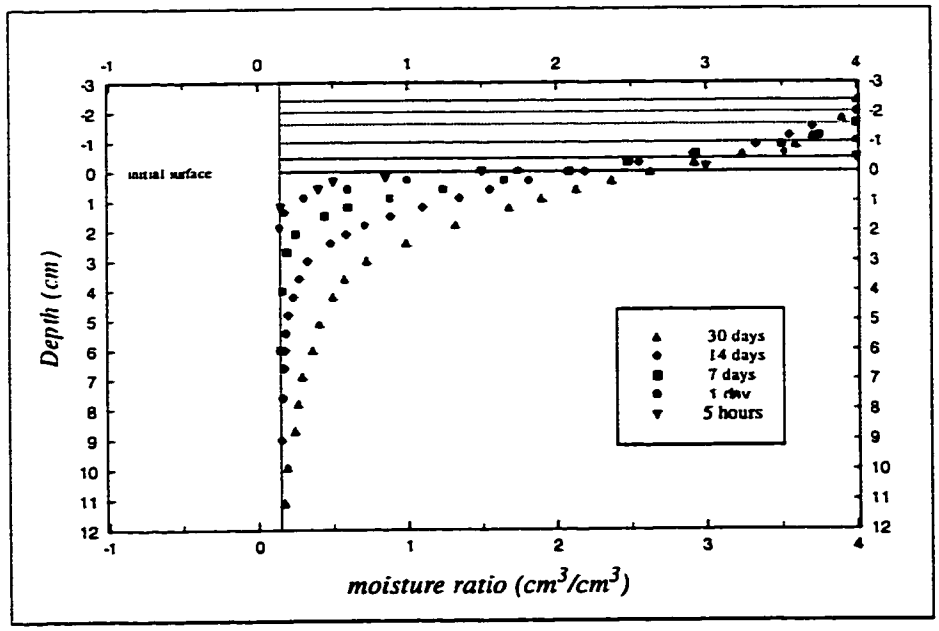

Fig. 6.4) Water profile in infiltration test at different time (condition: free to swell upward)

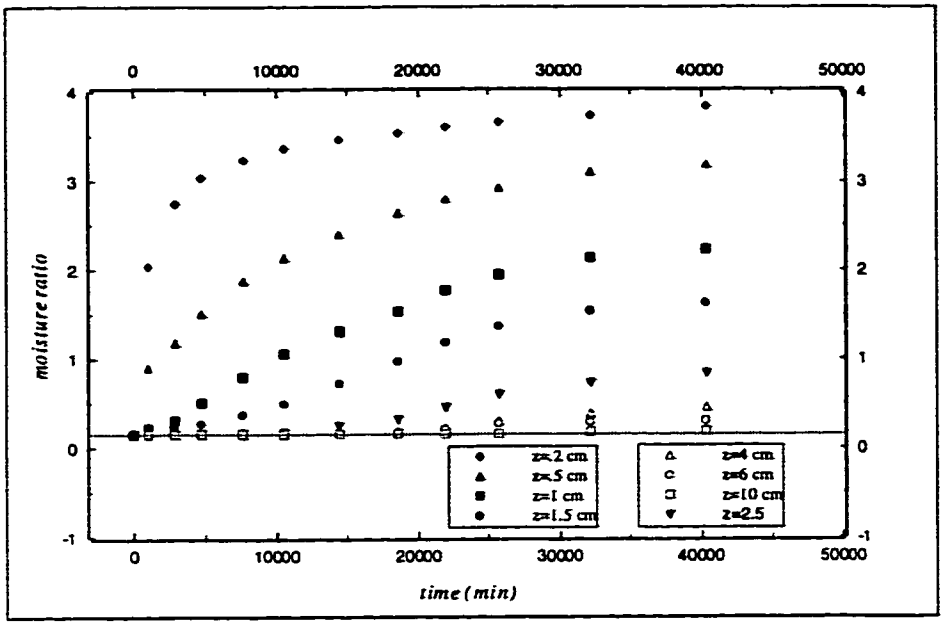

Fig. 6.5) Variation of soil moisture ratio with time at different specific depths (sample condition: free to swell upward)

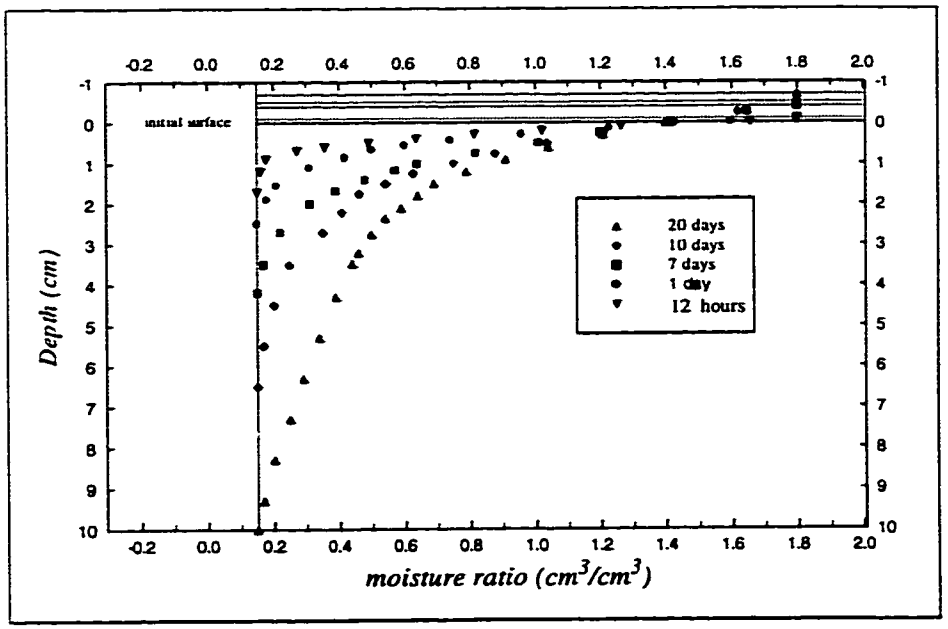

Fig. 6.6) Water profile in infiltration test at different time (condition: semi-confined overload = 50 kPa)

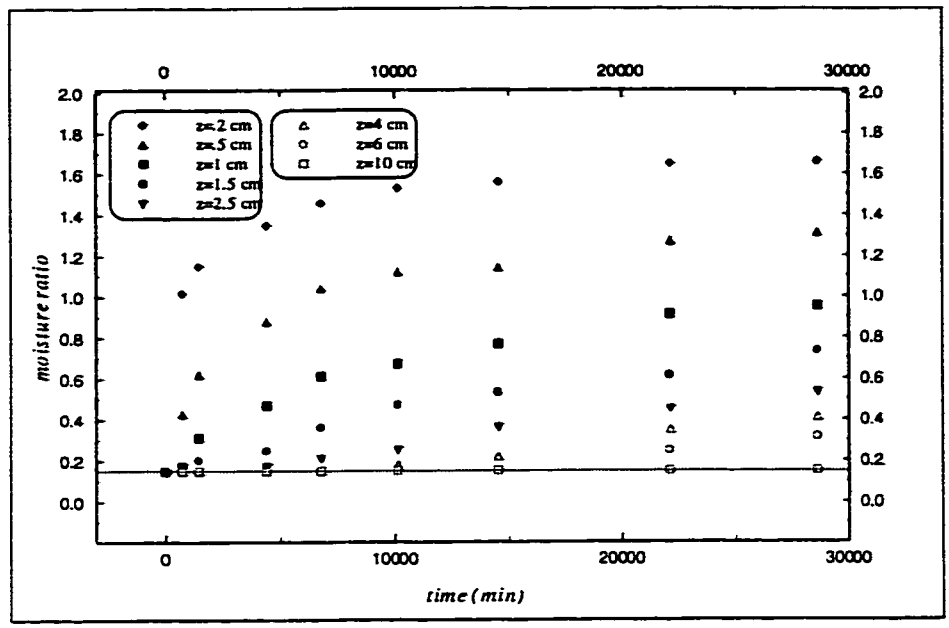

Fig. 6.7) Variation of soil moisture ratio with time at different specific depths (condition: semi-confined overload = 50KPA)

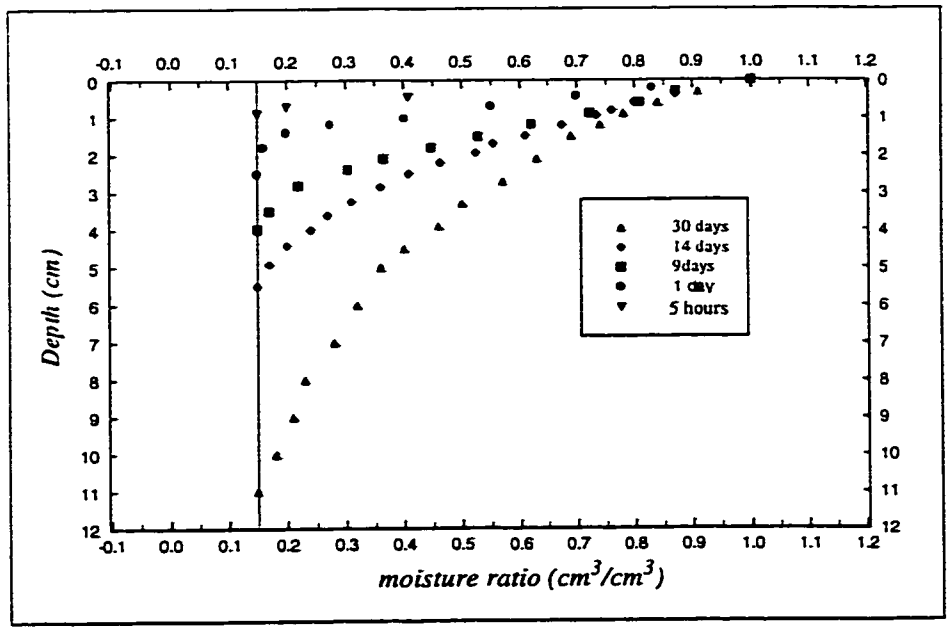

Fig. 6.8) Water profile in infiltration test at different time (condition: completely confined)

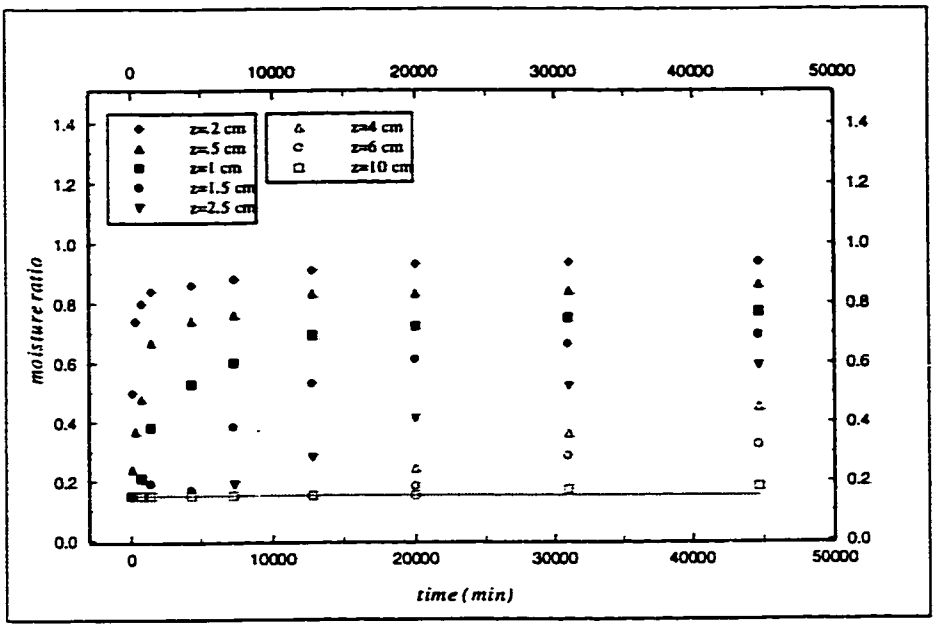

Fig. 6.9) Variation of soil moisture ratio with time at different specific depths (condition: completely confined)

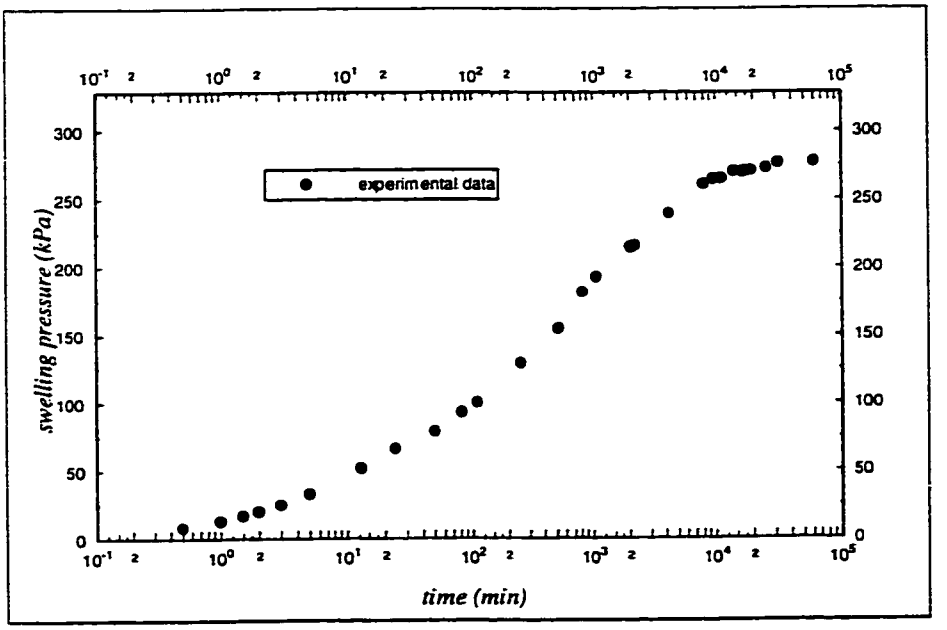

Fig. 6.10) Swelling Pressure Versus Time Curve for Completely Confined Condition

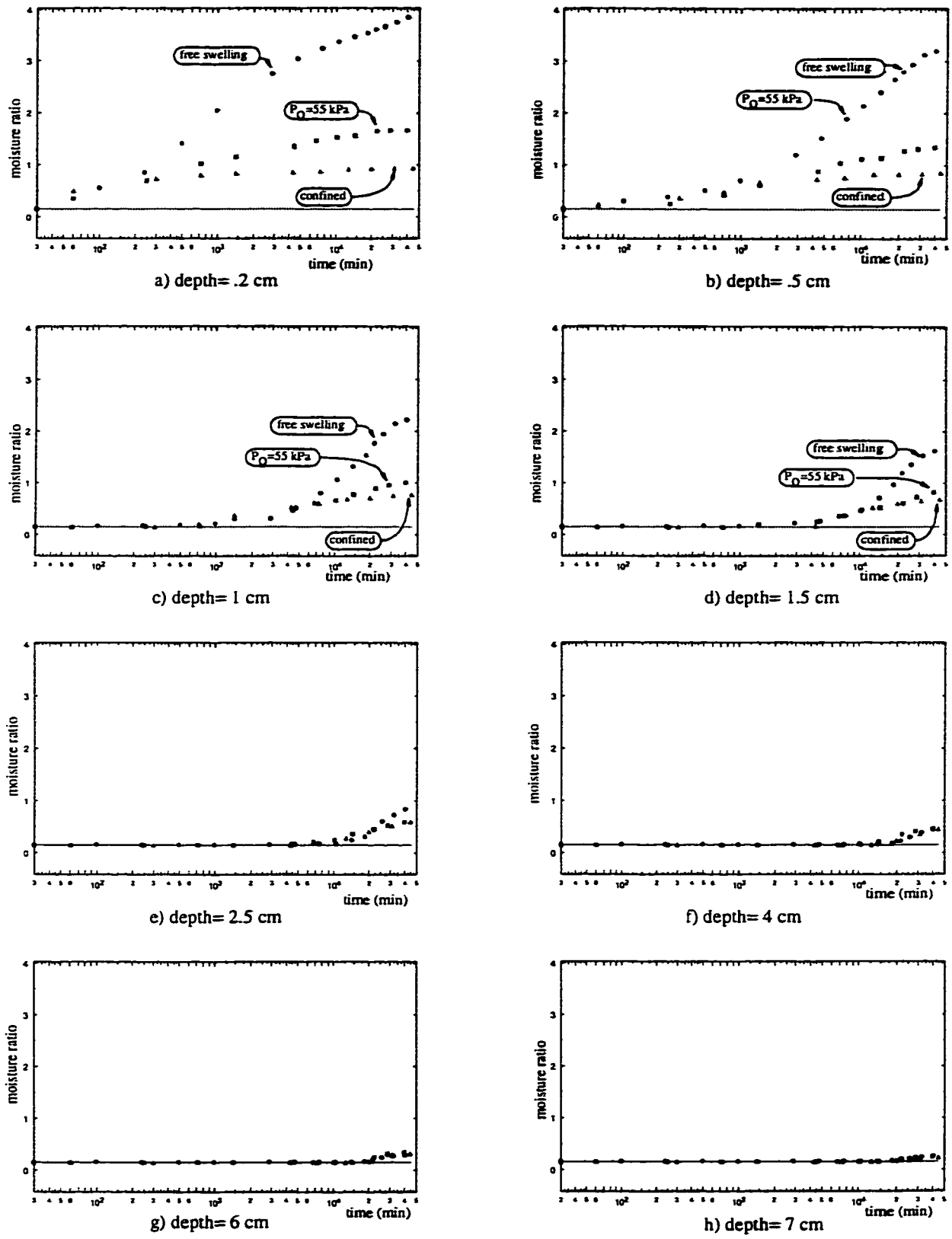

a) depth= .2 cm

b) depth= .5 cm

c) depth= 1 cm

d) depth= 1.5 cm

e) depth= 2.5 cm

f) depth= 4 cm

g) depth= 6 cm

h) depth= 7 cm

Fig. 6.11) Moisture content variation with time for three different confinement conditions of soil column (in all figures the horizontal axes represents time in minute in logarithmic scale and the vertical axes stands for the soil moisture ratio)

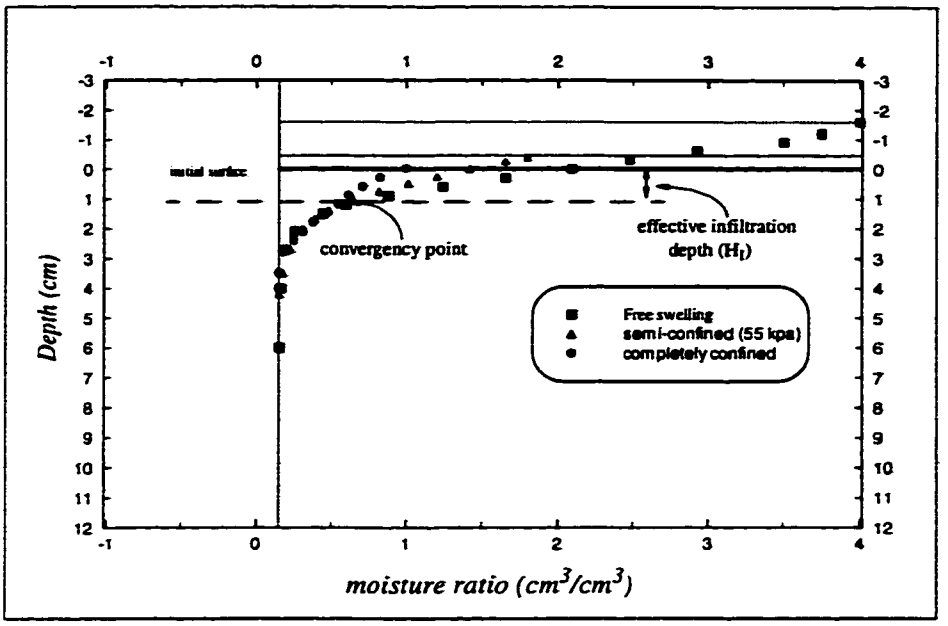

Fig. 6.12) Comparison between 7 days soil moisture profiles of different confinement conditions and effective infiltration depth (H_I)

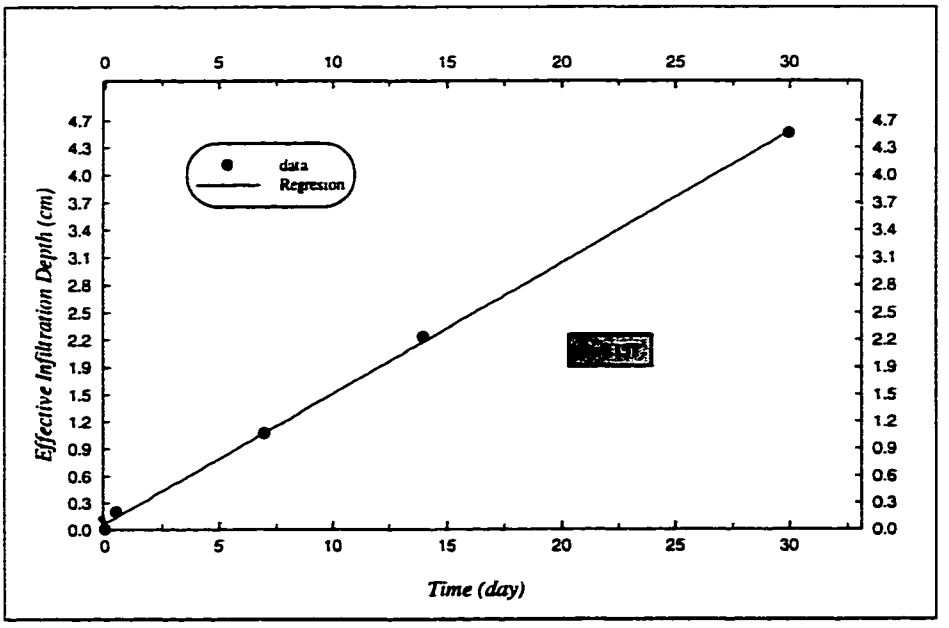

Fig. 6.13) Variation of Effective Infiltration Depth (H_I) with respect to time

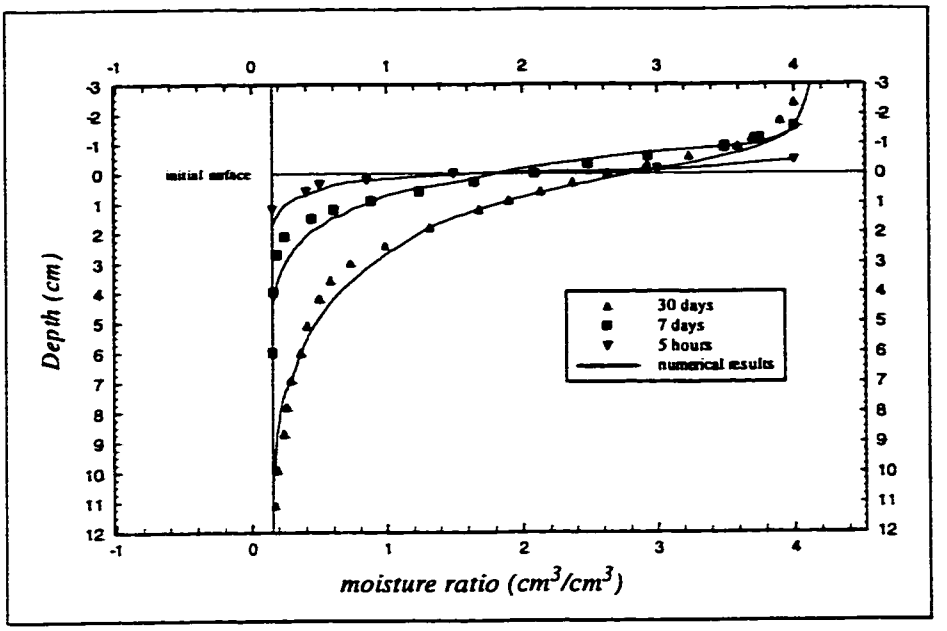

Fig. 6.14) Comparison between the soil moisture profiles, calculated from numerical analysis and measured in infiltration test (soil condition: free to swell upward)

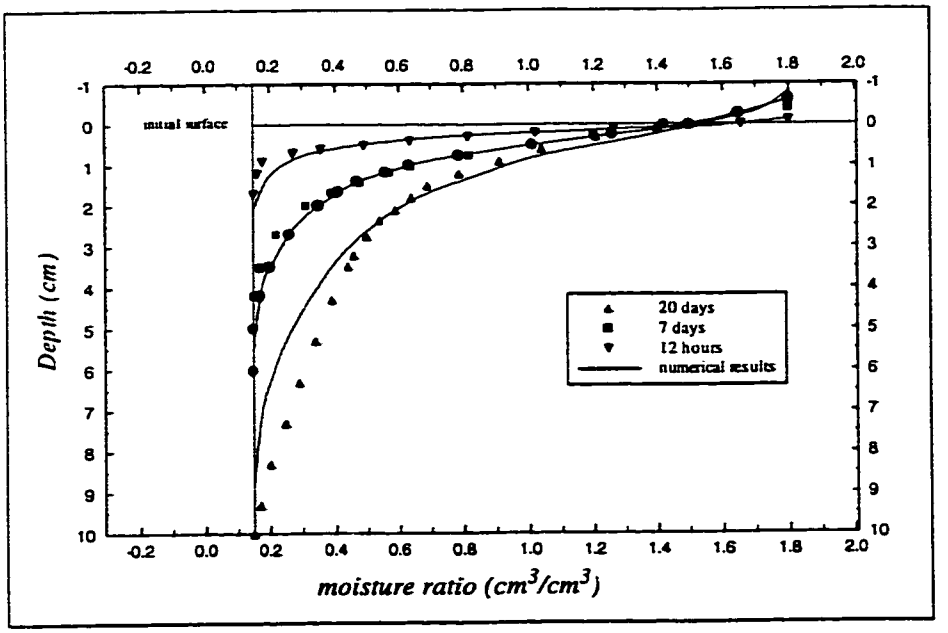

Fig. 6.15) Comparison between the soil moisture profiles, calculated from numerical analysis and measured in infiltration test (soil condition: semi-confined with over-load= 50 kPa)

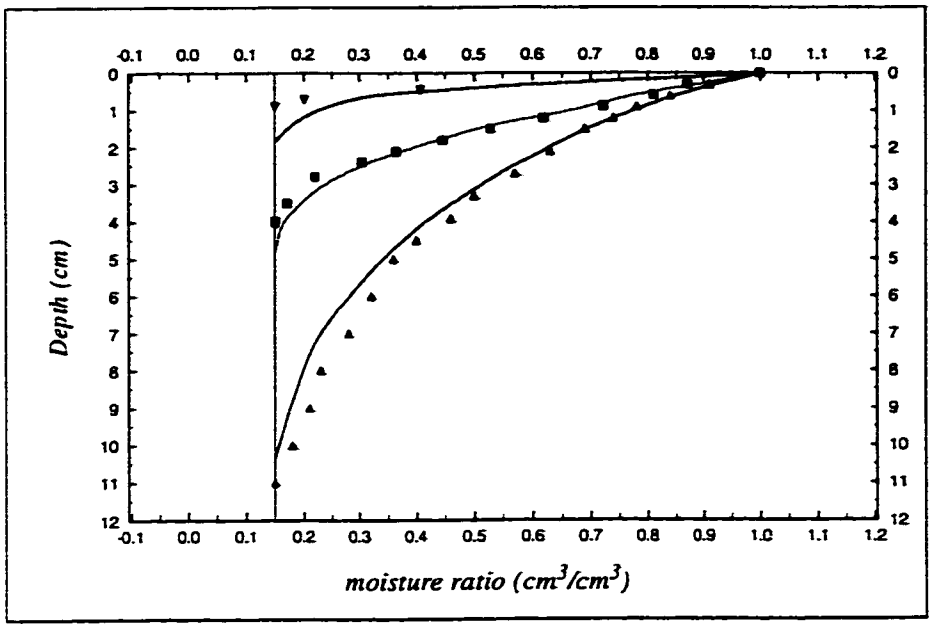

Fig. 6.16) Comparison between the soil moisture profiles, calculated from numerical analysis and measured in infiltration test (soil condition: completely confined)

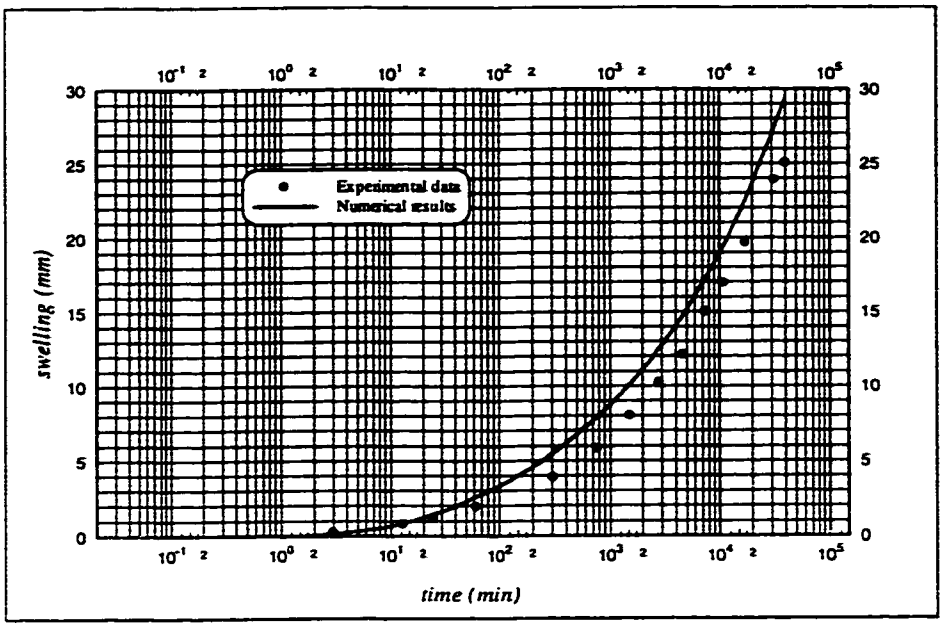

Fig. 6.17) Comparison between amount of swelling measured and that of numerical analysis (soil condition: free to swell upward)

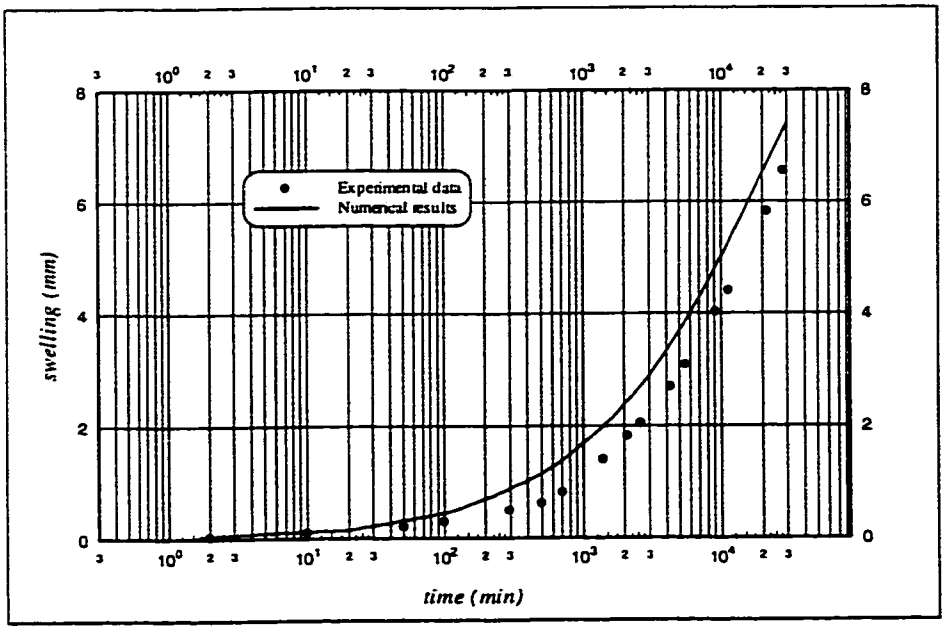

Fig. 6.18) Comparison between amount of swelling measured and that of numerical analysis (soil condition: semi-confined with overload= 50 kPa)

CHAPTER

7

Summary, Conclusion and Recommendations

7.1. Summary and Conclusion

The following conclusions can be drawn on the basis of the present study.

7.1.1. Mathematical and Numerical Modeling

A generalized three dimensional mathematical model was developed based on time dependent water adsorbtion by the soil particles. The model includes the effect of swelling or shrinkage of the soil as well as overloading. A maximum water adsorption value, β,was introduced using the moisture retention curve. This term acts as a time-dependent source/sink in the model and its exponential function denotes the simultaneous amount of adsorbed water by soil particles. The coefficient $\widehat{\nabla R}$ represents the effect of the soil body deformation on the soil moisture profile and can change from infinity for a porous medium undergoing a very large amount of deformation, to unity for non-deformable medium.

The three dimensional model was then simplified to a one dimensional model expressing the vertical water movement through swelling soils. In chapter 4 a numerical procedure was established with the help of a neural network model for parameter estimation and a finite difference scheme to solve the one dimensional flow equation. The results showed that the neural network model is capable of characterizing any experimental function with as many soil parameters as are included. In most of the model evaluations, a perfect compatibility through the entire range of data was observed. The finite difference method illustrated an excellent performance in numerically solving the flow equation to predict the soil moisture profiles. The results of the numerical analysis were presented in three soil confinement conditions.

7.1.2. Preliminary Experiments

7.1.2.1. Hydraulic Properties

A series of experiments was conducted to characterize the moisture dependent parameters involved in the model. As a first step, saturated hydraulic permeability versus void ratio was measured by means of a very simple procedure. It was observed that as the soil void ratio increases, the saturated hydraulic conductivity rises more rapidly. Different empirical models were then compared and a new model was introduced. The logaritmic-power model was perfectly fitted over the saturated permeability-void ratio data. The second step was to characterize the moisture retention curve. Using a high pressure plate apparatus, soil suction versus moisture ratio was measured under different soil initial conditions and different overload pressure. The adsorbtion limit was estimated from each curve and the van Genuchten model was verified to express the parametric relationship

between suction and moisture ratio. To do this, RETC computer program was modified to estimate the fitting parameters of the model. However, in order to include as many soil parameters as possible in estimating the soil moisture retention curve, a neural network model was developed (chapter 5). In the next part a complete review of the history of the unsaturated hydraulic conductivity measurements for non-deformable soils was carried out and with the use of the pressure plate test data, a new methodology was proposed to measure this property for deformable soils. Furthermore, an empirical model was developed based on the model of van Genuchten. The proposed model was successfully fitted over the experimental results.

7.1.2.2. Swelling and Shrinkage Properties

The shrinkage characteristic of a swelling soil was measured in two conditions depending on the overload condition. The air dry method was used for an unloaded sample and the soil volume changes versus soil moisture ratio was measured in different conditions depending on the initial soil moisture ratio and the percentage of the swelling constituent. It was concluded that the best empirical model to characterize the relation between four important soil parameters (overload pressure, void ratio, suction and moisture ratio) through which the state of the soil is unambiguously defined, is the neural network model. In the case of the overloaded samples, an adapted methodology was used for the purpose of shrinkage characterization. Two different amounts of overload pressure were examined and the effect of cracks was corrected on the curves.

Swelling pressure is another important property of swelling soils which is included in the flow equation as a nonlinear coefficient. The variation of this pressure

against moisture ratio was measured employing a new experimental method. The method was a combination of the constant volume and different pressure methods. The results show that the proposed model is much more reliable, since only one specimen was used in the test and as well, it enjoys the benefit of the "constant volume" method in measuring the swelling pressure.

The coefficient of soil particle permeability, introduced in the theoretical formulation, was the next property measured. An attempt was made to establish a simple definition and an experimental procedure to quantify this parameter. The experimental results indicate that the values of the soil particle permeability vary from 10^{-9}m/s to 10^{-7}m/s, while for the same range of the moisture ratio, the values of unsaturated hydraulic permeability vary from 10^{-14}m/s to 10^{-8}m/s. This comparison shows the significance of soil particle movement with respect to the water movement in unsaturated swelling soils.

7.1.3. Infiltration Experiments

Three sets of infiltration tests depending on the sample confinement condition were conducted. The purpose of these tests was to verify the results of the numerical model. The slice method was employed in order to measure the different properties of the soil in depth. Maximum infiltration time was 30 days and the results were illustrated in two forms: variation of the moisture profile through time and local moisture changes through time. Investigating the results, a new parameter called Effective Infiltration Depth (EID) was defined as one of the properties of water infiltration through overloaded swelling soils. EID can simply be determined using at least two moisture profiles of the same time but of unequally overloaded samples.

7.2. Conclusion

The results of the numerical analysis confirmed that the developed mathematical model can successfully predict the state of the water inside the unsaturated, expansive soil due to water infiltration. The study also indicated that the static neural network model, as a promising model, can precisely characterize any experimental function related to the soil properties and cooperates with other numerical approaches such as finite difference method to solve a highly nonlinear partial differential equation such as unsaturated flow equation. A fully implicit finite difference method was successfully developed to solve the flow equation. Another significance of the present research was to propose the new experimental methods to measure the hydraulic and swelling properties of unsaturated, expansive soils. Accompanying each discussion, a comprehensive history of the problem was presented.

Using the developed model, the moisture profile through swelling soils can be predicted. This prediction, in geotechnical engineering, helps engineers to avoid subsequent problems, such as differential settlements of the structure, by taking into the account the amount of the soil swelling. Regarding the applications of the model in agricultural engineering, the plant growth and synchronizing the irrigation time can be better investigated having the correct knowledge of soil water state. One of the most important application of this research is in evaluating the water and contaminant transportation through the vadose zone by some modification in governing the mathematical equation. Furthermore, employing the new developed experimental methods in the present research, one can determine and employ the different hydraulic and swelling properties of swelling soils, which

are very important in geotechnical, agricultural and geoenvironmental engineering. Introducing the application of the neural network modeling in treating the experimental data was also another feature of this research by which not only the civil and geoenvironmental engineers, but also any other expertise, who deals with a significant number of experimentally measured variables, could benefit.

7.3. Future Work

Based on the present study, the following works can be suggested as complimentary research:

1- The mathematical model could be extended to the solute and contaminant transport through unsaturated, swelling soils. To do this, one may develop and add the proper diffusion, advection and decay terms to the equation. However, special attention should be paid to the extra swelling or shrinkage caused by the effect of additional substances and also the adsorption coefficient must be reevaluated.

2- An alternative dynamic neural network model can be developed based on the adaptive learning rules to directly characterize the moisture profile inside the soil. Unlike the mathematical model, there is no limitation in choosing the number of coefficients (different soil properties). Such a model can unambiguously define not only the soil-water interaction, but also can predict any other required properties as a set of model outputs. The effect of nonuniform infiltration, nonhomogenous soil, temperature, fluid viscosity, presence of other substances, fluid-fluid interface, and any other variable properties which can be measured and be presented to the model as a set of inputs, can be included in the model.

REFERENCES

Agarwal et al. (1989). A method for measuring swelling pressure of an expansive soil. *Proceedings of 4th international conference on expansive soils.* p155-159.

Ahuja, L.R. (1973). Anumerical and similarity analysis of infiltration into crusted soils. *Water resour. Res.* v9, p987-994.

Alonso, E.E., A. Gens, and A. Josa. (1992). A unified model for expansive soil behaviour. *Proceedings of 7th international conference on expansive soils.* p24-29.

Anderson (1992). Computational fluid dynamicsAn introduction. *Book* Springer-Verlag, New York, 291p.

Baver, L. D. (1940). Soil Physics. *John Wiley & Sons Inc., New York.*

Bouma,J., C. Belmans, L.W. Dekker, W.J.M. Jeuressen (1983). Assessing the suitability of soils with macropores for subsurface liquid waste disposal. *J. Environ. Qual.* v12, p305-311.

Brackley, I.J. (1973). Swell pressure and free swell in a compacted clay. *Proc. of 3th Int. conf. on expansive soils. Haifa.* v1, p169-176.

Brackley, I.J. (1975). Swell under load. *Proceedings of 6th Reg. Conf. for Africa on SMFE, Durban.* v1, p65-70.

Bronswijk, J.J.B. (1988). Modeling of water balance, cracking and subsidence of clay soils. *Journal of Hydrology.* v97, p199-212.

Bronswijk, J.J.B. (1991). Drying, cracking and subsidence of a clay soil in a lysimeter. *Soil Sci.* v152, p92-99.

Brooks, R. and A. Corey. (1964). Hydraulic properties of porous media. *Hydro. Paper No. 3* Civ. Engrg. Dept., Colorado state Univ., Fort Collins, Colo.

Brooks, R. and A. Corey. (1966). Properties of porous media affecting fluid flow. *J. Irrig. and Drain. Div.* ASCE, v92, n2, p61-88.

Buckingham (1907). The measurement of soil moisture diffusivity. *U.S. Dep. Agr. Bul. soils.* Bull 38

Burdine, N.T. (1953). Relative permeability calculation from pore size distribution data. *Trans. Am. Inst. Min. Metall. Pet Eng.* v198, p7-77

Childs E.C.(1936). The transport of water through heavy clay soils. *J. Agric. Sci.* 26, 114-127

Dirksen , C. (1991). Unsaturated hydraulic conductivity. *In K.A. Smith and C.E. Mullins (ed.) Soil analysis, physical methods.* Marcel Dekker, New York.

Eching, S.O., J.W. Hoomans, and O. Wendroth. (1994). Unsaturated hydraulic conductivity from transient multistep outflow and soil water pressure data. *Soil Sci. Soc. Am. J.* v58 p687-695.

Feddes, R. A. and P. Kabat, P. J. T. Van Bakel, J. J. B. Bronswijk and J. Halbertsma (1988). Modelling soil water dynamics in the unsaturated zone-state of the art. *Journal Of Hydrology.* 100, p69.

Fox, W. E. (1964). A study o bulk density and water in a swelling soil. *Soil Sci.* v4, p301 .

Fredlund, D. G. (1993) Soil mechanics for unsaturated soils. John Wiley & Sons, inc. New York.

Fredlund, D., A. Xing, and S. Huang. (1994). Predicting the permeability function for unsaturated soils using the soil-water characteristic curve. *Can. Geotech. J.* v32, p533-546.

Fredlund, D., A. Xing. (1994). Equation for the soil-water characteristic curve. *Can. Geotech. J.* v31, n4, p521.

Freeman and Skapura (1992). Neural Networks, algoritms, Applications, and programing techniques. Addison-Wesley Publishing company, New York.

Giraldez J. V. and G. Sposito (1985). Infiltration in swelling soils. *Water Resources Research.* v21 n1 p33-44.

Giraldez, J.V. (1976) The theory of infiltration and drainage in swelling soils. *Ph. D. dissertation.* University of California, Riverside, CA.

Giraldez, J.V., G. Sposito, and C. Delgodo. (1983). A general soil volume change equation, I. The two parameter model. *Soil Sci. Am. J.* v47, p419-422.

Groenevelt, P.H. and G.H. Bolt (1972). Water retention in soil. *Soil Science.* v113 (4), 238-245

Gupta, S.C., D.A. Farrell, and W.E. Larson. (1974). Determining Effective Soil Water Diffusivities from One-Step Outflow Experiments. *Soil Sci. Soc. Am. Proc.* v38, p710-716.

Haines, W. B. (1923). The volumetric changes associated with variations of water content in soil. *J. Agric. Sci.* v13, p296-310.

Hayashi, M., G. van der Kamp, D. L. Rudolph. (1997). Use of Tensiometer Response Time to determine the hydraulic conductivity of unsaturated soil . *Soil Science.* v162 n8, p566.

Hopmans, J.W., T. Vogel, and P.D. Koblik. (1992). X-ray tomogaphy of soil water distribution in one-step outflow experiments. *Soil Sci. Soc. Am. J.* v56, p365-362.

Huerta, A., G.A. Kriegsmann and R.J. Krizek. (1988). Permeability and compressibility of slurries from seepage induced consolidation. *J, Geotech. Eng. ASCE.*v114(5), p614-641.

Khaddaj, S., L. Lancelot, and I. Shahrour. (1992). Experimental study of the swelling behaviour of heavily overconsolidated flandres clays. *Proc. of 7th Int. conf. on expan. soils.* p239-244

Klute, A. (1986). Water retention, Laboratory methods. *method of soil analysis, part 1. 2nd edition.* Agron. Monorg. 9. ASA and SSSA, Madison, WI. p635-662.

Kool, J.B., J.C. Parker, and M. Th. Van Genuchten. (1985). Determining Soil hydrauic properties from one-step outflow experiments by parameter estimation, I. Theory and numerical studies. Soil Sci. Soc. Am. J. v49, p1348-1354.

Lauritzen C. W. and A. J. Stwart (1941). Soil volume change and accompanying moisture

and pore space relationships. *Soil Sci. Soc. Am. Proc.* 6, p113-116.

Leon, E. C., H. Rahardjo, (1997). Permeability functions for unsaturated soils. *J. Geotechnical and Geoenvironmental Engineering.* v123, n12, p1118.

McGarry, D., and K.W.J. Malafant. (1987). The analysis of volume change in unconfined unit of soil. *Soil Sci. Am. J.* v51 p290-297.

McIntyre, D.S, and G.B. Stirk. (1954). A method for determination of apparent density of soil aggregates. *Aust. J. Agri. Research.* v5, p291-296.

Meerdin J.S., C.H. Benson, and M.V. Khire. (1996) Unsaturated hydraulic conductivity of two compacted barrier soils. *J. of Geotech. Eng.* v122, n7, p565-576.

Messing, I. and N.J. Jarvis (1990). Seasonal variations in field saturated hydraulic conductivity in two swelling caly soils in Sweden. *J. Soil Sci.*.v41, 229-266

Mohrath, D., L. Bruckler, M. Bourlet, (1997). Errore analysis of an evaporation method for determining hydrodynamic properties in unsaturated soil . *Soil Sci. Soc. Am. J.* v61 n3, p725.

Mualem, Y. (1976). A new model for prediction the hydraulic conductivy of unsaturatad porous media. *Water Resour. Res.* v12, p513-522

Nakano, M. , Amemiya, Y. and Fujii K. (1986). Saturated and unsaturated hydraulic conductivity of swelling soil. *Soil Sci.* v141 p1-6.

Nofziger, D. L. and Swartzendruber. (1974). Water content and bulk density during wetting of a bentonite- silt column. *Soil Sci. Am. J.* v40, p345-348.

Ohtsubo, M., K. Egashira and M. Takayama. (1985). Properties of a low swelling smectitic clay of interest in soil engineering. *Canad. Geotech. J.* v22 p241-245.

Parker, J.C., J.B. Kool, and M. Th. Van Genuchten. Determining Soil hydraulic properties from one-step outflow experiments by parameter estimation, II. Experimental studies. Soil Sci. Soc. Am. J. v49, p1354-1359.

Passioura, J.B. (1976). Determining soil water diffusivities from one-step outflow experiments. *Aust. J. Soil Res.* v7, p79-90.

Philip, J. R. (1957). The theory of infiltration, 1. The infiltration equation and its solution. *J. Soil Res.* 6, p249-267.

Philip, J. R. (1968). Kinetics of sorption and volum change in clay-clloid pastes. *Aust. J. Soil Res.* v6, p249-267.

Philip, J. R. (1970). Hydrostatics in swelling soils and suspension, Unification of concepts. *Soil Science.* v109(5) p294-298.

Philip, J. R. and Smiles, D. E. (1969). kinetics of sorption and volume change in three-component systems. *Aust. J. Soil Res.* v7, p1-19.

Philip, J.R. (1969). Moisture equilibrium in the vertical in swelling soils, Basic theory. *Aust. J. Soil Res.* v7, p90-120.

Raats, P. A. C. and A. Klute (1969). One-dimensional, simultaneous motion of the aqueous phase and the soil phase of saturated and partially saturated porous media. *Soil Sci.* v107, 329-333.

Raats, P. A. C. and Klute, A. (1968a). Transport in soils, The balance of mass. *Soil Sci. Am. Proc.* v32, 161-166.

Raats, P. A. C. and Klute, A. (1968b). Transport in soils, The balance of momentum. *Soil Sci. Am. Proc.* v32, p452-456.

Raats, P.A.C. (1965). Development of equations describing transport of mass and momentum in porous media, with special reference to soils. Ph.D. dissertation Univ. of Illinois, Urbana-Champaign.

Reeve, M.J., and D.G.M. Hall. (1987). Shrinkage in clayey subsoils of contrasting structure. *J. Soil Sci.* v29, p315-323.

Richards (1931). The measurement of soil moisture diffusivity. *Physics.* 1, page 318-333.

Ross P.J. and J.Y. Paralange.(1994). Comparing exact and numerical solutions of richards' equation for one-dimensional infiltration and drainage. *Soil Sci. Soc. Am. J.* v15 N6 P341

Ross P.J. and J.Y. Parlange (1994). Investigation of a method for deriving unsaturated soil hydraulic properties from water content profiles. *Soil Sci. Soc. Am. J.* v57 n6 p335..

Ross Peter J. and K. R. J. Smettem(1993). Describing soil hydraulic properties with sums of simple functions. *Soil Sci. Soc. Am. J.* v57 p26.

Rossic. and J. R. Nimmo.(1994). Modeling of soil water retention from saturation to oven dryness. *Soil Sci. Soc. Am. J.* v57 p26.

Salas, J.A.J.,and J.M. Sarratosa. (1957). Foundations on expansive clays. *Proceedings of 4th Int. Conf. on Soil Mech. and Found. Engg.* v1, p424-428.

Salehzadeh A. and A. H. Demond.(1994). Apparatus for the rapid automated measurement of unsaturated soil transport properties. *Soil Water Resource Research.* v30 n10 p2679.

Simune, J. M. T. van Genuchten, (1997). Estimating unsaturated soil hydraulic properties from multiple tension disc infiltrometer data . *Soil Science.* v162 n6, p383.

Slichter (1898). Theoretical investigation of the motion of groundwater. *????*

Smiles, D. E. (1974). Infiltration into a swelling material. *Soil Sci.* v117, p140-147

Smiles, D. E. and Rosenthal M. J. (1968). The movement of water in swelling materials. *Aust. J. Soil Res.* v6, 237-248.

Smiles D.E. (1976). On the validity of the theory of flow in saturated swelling materials. *Aust. J. Soil Res.* 14, 389-395

Snethen, D. R. (1981). Characteristics of expansive soils using soil suction data. *Soil Sci.* 115, p315-320.

Sposito, G. and Giraldez J. V. (1976). On the theory of infiltration in swelling soils. *Water in heavy soils proceeding of symposium.* Sept. 8-10, 1976.

Stolte, J., G.J. Veerman, and M.C.S. Wopereis. (1992). Manual soil physical measure-

ments. *Version 2.0. Tech. Doc. 2.* DLO Winand Staring center, Wageningen, the Netherlands.

Stolte, J., J.I. Freijer, W. Bouten, C. Dirksen, J.M. Halbertsma, J.C. Van Dam, J.A. Van den Berg, G.J. Veerman, and J.H.M. Wosten (1994). Comparison of six methods to determine unsaturated soil hydraulic conductivity. Soil Sci. Soc. Am. J. v58, p1596-1603.

Stroosnijder, L. and G.H. Bolt (1984). Moisture characteristics of heavy clay soils. Proceedings of the ISSS symposium on water and solut movement in heavy soils. ILRI publication 37, Wageningen, the Netherlands p324-329.

Talsma, T. (1977). Measurement of the overburden component of total potential in swelling field soils. *Aust. J. Soil Res.* v15, p95-102.

Tamari, S., L. Bruckler, J.M Halbertsma, and J. Chadoeuf. (1993). A simple method for determining soil hydraulic properties in the laboratory. *Soil Sci. Soc. Am. J.* v57, p642-651.

Tariq, A., and D.S. Durnford (1993). Soil volume shrinkage measurements, a simple method. *Soil Sci.* v155, p325-330.

Tomasella, J., H. G. Hodnett, (1997). Estimating Unsaturated Hydraulic Conductivity of Brazilian Soils Using Soil-Water Retention Data. *Soil Science.* v162, n10, p703

Touma, J. and Vauclin, M. (1986). Experimental and numerical analysis of two-phase infiltration in a partially saturated soil. *Transport in porous Media.* V1 P27

Townsend, F.C. and M.C. McWay. (1990). Larg strain consolidation prediction. *J, Geotech. Eng. ASCE.*v116(2), p222-243.

Van Dam J. C. and J. N. M. Stricker and P. Droogers.(1994). Inverse Method to determine soil hydraulic functions from multistep outflow experiment. *Soil Sci. Soc. Am. J.* v58 p647.

Van Dam, J.C., N.M. Stricker, and P. Droogers. (1992). Evaluation of the inverse method for determining soil hydraulic functions from one-step outflow experiments. *Soil Sci. Soc. Am. J.* v56, p1042-1050.

Van Genuchten (1980). A close form Equation Predicting the Hydraulic Conductivity of Unsaturated. *Soil Sci. Soc. Am. J.* v44 p892.

Vereecken, H., R. Kaiser, T. Putz. (1997). Evaluation of the multistep outflow method for the determination of unsaturated hydraulic properties of soils . *Soil Science.* v162 n9, p618

Warrick A. W. (1993). Inverse estimation of soil hydraulic properties with scaling, One-dimensional infiltration. *Soil Sci. Soc. Am. J.* v57 p631.

Warrick A. W. and A.A. Hussen(1993). Scaling of Richrds' equation for infiltration and drainage. *Soil Sci. Soc. Am. J.* v57 p15

Wendroth, O., W. Ehlers, J.W. Hopmans, H. Kage, J. Halbertsma, and J.H.M. Wosten. (1993). Reevaluation of the evaporation method for determining hydraulic functions in unsaturated soils. Soil Sci. Soc. Am. J. v57, p1436-1443.

Wildenschil, D., K. Hogh Jensen, (1997). A two-stage procedure for determinating unsaturated hydraulic characteristics using a syringe pump and outflow observation. Soil Sci. Soc. Am. J. v61 n2, p347.

Wind, G.P. (1968). Capillary conductivity data estimated by a simple method. *In Symp. on"water in the unsaturated zone".* v1 Proc. Wageningen, the Netherlands. June 1996.

Wosten J. H. M. and M. Th. Van Genuchten (1988). Using texture and other soil properties to predict the unsaturated soil hydraulic functions. *Soil Sci. Soc. Am. J.* v52 p1762.

Yazdizadeh et al.(1997). Identification of class of Nonlinear Systems Using dynamic Neural Network Structures. *International Confrence on Neural Networks, Huston. Tx.*

Yong, R.N. and B.P. Warkentin. (1969). Flow of water in partially saturated expansive soils. *Proc. of 2th Int. conf. on expansive soils. Texas A&M press.* p85-97.

Youngs E. G.(1991). Infiltration measurements--A review. *Hyd. Processes.* v5 p309.

Zachmann, D.W., P.C. Duchateau, and A Klute. (1981). The calibration of the Richards' flow equation for a draining column by parameter identification. *Soil Sci. Soc. Am. J.* v45, p1012-1015.

Zaslavsky, D. (1964). Saturated and unsaturated flow equation in an unstable porous medium. *Soil Sci.* v98, p317-321.

Zurada (1992). Introduction to Artificial Neural Systems. West Publishing Company, New York 683 page.